The Impact of Oscillator Phase Noise on the Design of Millimetre-Wave Continuous Wave Radar Systems

Siddiq, Kashif

Award date:
2017

Awarding institution:
University of Bath

The Impact of Oscillator Phase Noise on the Design of Millimetre-Wave Continuous-Wave Radar Systems

Kashif Siddiq

A thesis submitted for the degree of Doctor of Philosophy

University of Bath
Department of Electronic & Electrical Engineering

April 2017

Abstract

This PhD thesis focuses on quantifying the impact of oscillator phase noise on the design of MMW CW radar systems with the goal of optimising the system to achieve better target detection and tracking. Phase noise in the transmitters of radar systems is known to distort the target response by broadening the linewidth and raising the noise floor of radar systems when a strong scatterer is present in the scene, hence degrading the detection and tracking performance. The situation is worse when multiple large scatterers are present, as the noise sidebands of all scatterers superimpose causing small targets, like pedestrians, to disappear in the phase noise sidebands. Some of the phase noise is cancelled at short ranges in coherent radars but the cancellation is not effective at long ranges.

This research presents the design of phase noise reduction techniques. Phase noise modelling at the system level is presented to elaborate the methods of minimising the impact of phase noise. After developing a phase noise theory, practical measurements from a triangular corner reflector and a moving vehicle are presented to validate the theory. It will be shown that the frequency synthesiser is the most significant phase noise contributor. The design and implementation of a low phase noise signal source is presented. Both linear and non-linear phase noise models are used and developed further in order to meet the radar optimisation goals. An elaborate relationship of the phase spectrum with the RF spectrum of an oscillator is presented. The idea of *coherence time* is used as a tool for the selection of radar signal sources, and a novel derivation of the minimum bound on the transmitter phase noise level presented to prevent excessive distortion of target spectra.

A new phase noise model is developed for the analog-to-digital conversion process using an independent sampling clock. The case of a sampling clock derived from the transmitter's reference oscillator will also be discussed. The models aid the selection of an appropriate sampling clock for a given radar application. A novel method of characterising the phase noise statistics using the integer and the fractional Brownian motion models will be presented. Models for the lineshape and the linewidth of the RF spectrum are dealt with in detail by reviewing the existing models in the literature. These analyses aid in assessing the fundamental resolution capability of radar systems in terms of the phase noise processes. A novel analysis of the RF spectrum of a signal impaired with random-walk phase noise is detailed, and it is shown that the RF spectrum exhibits time-dispersion and *satellite peaks*.

It is shown that the success of the proposed work depends on techniques for careful measurement, analysis, and mitigation of the various noise processes.

Contents

List of Symbols

c : Speed of light (m/s)

λ : Carrier Wavelength (m)

f : Offset frequency (Hz)

ν : RF frequency (Hz)

ω : Radian RF frequency (rad/s)

R : Range of a Target

τ_d : Delay Time (s)

τ_m : Measurement Time (s)

τ_c : Coherence Time (s)

$\mathcal{N}$: Normal Probability Density

μ : mean (average) value

σ^2 : Variance

N : Frequency Multiplication Factor

m : The discrete sample index

M : Number of samples acquired

B_S : Swept Bandwidth (Hz)

T_S : Sweep Time (s)

B_L : Loop Bandwidth (Hz)

B_n : Noise Bandwidth (Hz)

σ_t : RMS time jitter (s)

σ_{ti} : RMS jitter at the input

σ_{to} : RMS jitter at the output

σ_{t_clk} : RMS jitter in sampling clock

Tx : Transmitter

Rx : Receiver

W_β : RF Linewidth due to β-th phase noise process

$\widehat{W}_\beta$: Frequency Multiplied RF Linewidth due to β-th phase noise process

σ_ϕ^2 : Variance of the phase noise process

$\sigma_{\phi i}^2$: Variance of the phase noise process at the input

$\sigma_{\phi o}^2$: Variance of the phase noise process at the output

f_c : Coherence Frequency (Hz)

f_α : Least low-phase noise frequency point (Hz)

L_p : Phase Noise Pedestal Height (dBc/Hz)

W_p : Phase Noise Pedestal Width (Hz)

θ_{az} : Azimuth 3-dB Beamwidth

θ_{el} : Elevation 3-dB Beamwidth

f_D : Doppler Frequency Shift (Hz)

P_t : Transmitted Power

P_r : Received Power

G_t : Transmitting Antenna Gain

G_r : Receiving Antenna Gain

σ_{tgt} : Radar Cross-section (RCS)

$x(t)$: A general random process

$r_x(\tau)$: Autocorrelation function of $x(t)$

B_{FFT} : The FFT Bandwidth (Hz)

$\phi(t)$: The phase noise process

$\phi_\beta(t)$: The β-th phase noise process

$\mathcal{L}(f)$: Phase Noise (dBc/Hz)

$\mathcal{L}_X(f)$: Phase Noise at point X

$S_\phi(f)$: Spectral Density of Phase Fluctuations (rad^2/Hz)

$R_\phi(\tau)$: Autocorrelation Function of the phase noise process $\phi(t)$

$S_{RF}(f)$: RF spectral density (W/Hz)

$S^b_{RF}(f)$: Baseband RF spectral density

$S^c_{RF}(f)$: Baseband Carrier RF spectral density

$S^p_{RF}(f)$: Baseband RF spectral density of the Phase Noise Pedestal

$S_\beta(\omega)$: Signal Spectral Density containing the β-th phase noise process

$R_\beta(\tau)$: Signal Autocorrelation Function containing the β-th phase noise process

$R_{\phi_\beta}(\tau)$: Autocorrelation Function of the β-th phase noise process

$R_{\phi_4}(t_1, t_2)$: Non-stationary autocorrelation function of the random-walk frequency noise process

$R_{\hat{x}_4}(t, \tau)$: Non-stationary autocorrelation function of the signal $x(t)$ impaired with random-walk frequency noise

List of Acronyms

ADC Analog-to-Digital Converter

AGS Advanced Guard System

AM Amplitude Modulation

CLK Clock

CP Charge Pump

CTS Compact Traffic Sensor

DDS Direct Digital Synthesiser

EM Electromagnetic

EMI Electromagnetic Interference

ETSI European Telecommunications Standards Institute

FFT Fast Fourier Transform

FM Frequency Modulation

FMCW Frequency Modulated Continuous Wave

HDR High-Definition Radar

I/Q In-phase/Quadrature

IC Integrated Circuit

IEEE Institute of Electrical and Electronics Engineers

IF Intermediate Frequency

LO Local Oscillator

LRS Long-Range Sensor

MMW Millimetre Wave

NASA National Aeronautics and Space Administration

PCB Printed Circuit Board

PFD Phase-Frequency Detector

PLL Phase Lock Loop

PM Phase Modulation

PPI Plan Position Indicator

RBW Resolution Bandwidth

RMS Root Mean Square

RF Radio Frequency

SCR Signal-to-Clutter Ratio

SCV Sub-Clutter Visibility

SNR Signal-to-Noise Ratio

TCXO Temperature Compensated Crystal Oscillator

VCO Voltage Controlled Oscillator

List of Figures

List of Tables

(55:3) He has created man:
(55:4) He has imparted unto him articulate thought and speech.

Al-Qur'an

ACKNOWLEDGEMENTS

I wish to thank my PhD advisers Dr Robert J. Watson and Dr Stephen R. Pennock for their support and guidance in this research. I also wish to thank Prof Cathryn Mitchell and Dr Peter Shepherd of the University of Bath, and Prof Paul Brennan of the University College London for their helpful review of this Thesis and their suggestions for improvement.

Special thanks to Mr Mervyn Hobden, Hon. Fellow BHI, for a clear introduction to the phase noise problem in radars, and for his continued guidance in this research and beyond. His work in the John Harrison Research Group has been a source of inspiration and guidance.

The author wishes to thank Innovate UK and Navtech Radar Ltd. for their partial support in this work. The support of the members of staff at Navtech Radar Ltd. during this work is gratefully acknowledged. In particular I thank Mr Richard Poulton, Mr Guy Avery, and Mr John Shear for their support and guidance in the development project linked with this research.

In the end I would like to thank my parents, family and friends for their continued support and encouragement. Special thanks to my wife and kids for their patience during the evenings spent on this work.

DEDICATION

To my family and friends

List of Author's Publications

The following research papers have been published during the course of this PhD work and form a part of this Thesis :

- K. Siddiq, M. K. Hobden, S. R. Pennock, R. J. Watson, "Phase noise in FMCW radar systems," *in IEEE Transaction on Aerospace and Electronic Systems,* 2017. (Accepted subject to review)

- K. Siddiq, M. K. Hobden, S. R. Pennock, R. J. Watson, "The linewidth of oscillators with power-law phase noise," *in IEEE Transaction on Circuits & systems II: Express Briefs,* 2017. (Submitted)

- K. Siddiq, R. J. Watson, S. R. Pennock, "A generalised Brownian motion model of RF spectral dispersion due to phase noise," *2017 European Radar Conference (EuRAD),* Nuremberg, 2017. (Accepted)

- K. Siddiq, M. K. Hobden, R. J. Watson, S. R. Pennock, S. Martins, "On phase measurement in FMCW radar systems," *Sensor Signal Processing for Defence (SSPD),* Dec. 2017. (Submitted)

- K. Siddiq, R. J. Watson, S. R. Pennock, P. Avery, R. Poulton and S. Martins, "Analysis of sampling clock phase noise in homodyne FMCW radar systems," *2016 IEEE Radar Conference (RadarConf),* Philadelphia, PA, 2016.

- K. Siddiq, R. J. Watson, S. R. Pennock, P. Avery, R. Poulton and B. Dakin-Norris, "Phase noise analysis in FMCW radar systems," *2015 European Radar Conference (EuRAD),* Paris, 2015, pp. 501-504.

Chapter 1

Introduction

Radar systems, originally developed for the detection and tracking of *targets*, have found a wide variety of applications in the past few decades. These include Security/Surveillance, Industrial Automation, Level measuring systems, Automatic Cruise Control (ACC), highways traffic monitoring, traffic incident detection, and debris detection on airport runways, just to mention a few. Millimetre wave (MMW) radars have gained popularity in recent years, with the legislation permitting the use of the MMW band for radar applications in all of the above-mentioned areas. Automotive radars and fixed roadside radars (for the purposes of speed monitoring and automatic incident detection (AID), among others) have also occupied primarily the 76-77 GHz frequency band. Due to this shared use of the radio spectrum, all 76-77 GHz technology is licensed by the European Telecommunications Standards Institute (ETSI) and mandated to coexist safely (ETSI standard 301-091 [1]).

1.1 The Long-Range Sensor Project

The research work in the present thesis is based on a Knowledge Transfer Partnership (KTP) project between the University of Bath and Navtech Radar Ltd., UK. Navtech's radar systems operate in the 76-77 GHz frequency band, and have applications in Industrial Automation, highways monitoring, and perimeter/infrastructure security. Prior to the KTP project, Navtech's security sensors were limited in range for the detection of pedestrians up to 1 km in relatively light clutter environments (like on tarmac). For heavily cluttered environments like grass and vegetation, the maximum detection range was reduced to 750 m. The goal of the KTP project was to design a long-range radar sensor (*LRS*) with the capability to detect pedestrians up to 2 km in strongly cluttered environments. This type of radar has applications in security/surveillance, drone detection, foreign object debris (FOD) detection, and

airport surface movement applications.

The design of the LRS required a full system optimisation to be carried out. The integration of a higher power transmitter, the design of a more complex data processing unit and a larger bandwidth data transfer unit were central to the success of the LRS project. All of the above features were to be designed in a pragmatic and cost-effective way to achieve a commercial solution. At the time of writing, the project has concluded successfully and the performance goals have been met. The project has resulted in a new line of radar systems for Navtech, known as the HDR300 series of radars. Further details of the LRS project can be found in Appendix B.

One of the main problems in using high-power signals for detection at longer ranges is that the phase noise sidebands around any strong reflector (like a road-sign, a wall of a large building, or even a windsock on an airfield) lead to a raised noise floor, which in turn leads to very poor detection performance in the masked region. Phase noise shows up as a streaking effect in radar displays, which leads to a loss of definition in the scene. To solve this problem, the fundamental limits on the detection performance under phase noise need to be studied. Another effect of phase noise (actually *frequency* noise) is that the target peaks (or *linewidths*) broaden, leading to the degradation of the resolution of radars. Incorrect selection of the transmitting source in terms of phase noise can worsen these problems. Various subsystems of a radar contribute phase noise that a designer needs to be aware of to mitigate their effect. The basis of the present PhD Thesis lies in the scientific work carried out in the context of Phase Noise.

1.2 Types of Noise

Electronic noise limits the performance of most modern electronic systems including, but not limited to, communication systems, radar systems, spectroscopic system, meteorological systems, and electronic warfare systems. In order to design any high-performance electronic system, the internal and the external noise mechanisms must be understood and minimised.

Noise in electronic systems can be classified as follows:

- **Natural (random) Noises**
  - Additive amplitude noise

    Includes Thermal noise and Shot noise. Also known as *White-Phase Noise* as their frequency spectrum is flat.

  - Multiplicative amplitude noise

    Also called Amplitude Modulation (AM) Noise

  - Phase noise

    Also called Phase Modulation (PM) Noise, or *coloured-noise* as explained below.

- **Man-Made (Systematic) Interference**

  - Internal System Interference
    * Conducted Noise, e.g. Switch-mode power-supply noise
    * Capacitively or Magnetically Coupled Noise
    * Radiative Noise (EMI)
    * Noise due to inappropriate grounding.
  - External Interference
    * Power-line noise
    * Conducted or Radiated Interference from nearby systems.

- **Radar-Specific External Interference**

  - Interference from other radar systems operating in the same frequency band, which can lead to the appearance of ghost targets [2].
  - Clutter from the operating environment, including land clutter (e.g. vegetation, trees, hedges), sea clutter, and atmospheric clutter (e.g. precipitation, rain, fog) [3–6].

For the design under consideration, an engineer may face any or all of the above-mentioned noises. An understanding of the noise mechanisms is key to adopt design methods to combat them. These noises can couple onto the desired signal at any point in the circuits and systems, and care should be taken in the design process to minimise their effect. Phase noise is arguably the most important source of noise at present, and appears in various forms in electronic and non-electronic systems. Noise processes similar to phase noise have also been observed in many natural phenomena [7]. As mentioned earlier, the present Thesis focuses exclusively on combating the internal phase noise in radar systems.

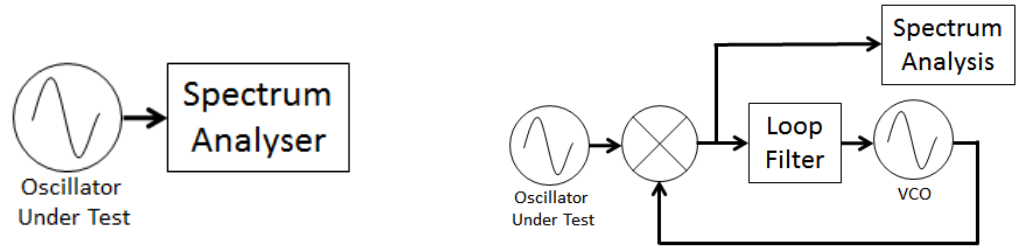

(a) Measurement of $S_{RF}(f)$

(b) Measurement setup for $S_\phi(f)$

Figure 1.1: Measurement setups for (a) the RF Spectrum and (b) the spectral density of phase fluctuations of an Oscillator.

1.3 Phase Noise

In the following, a basic model of phase noise will be presented. Consider a general signal $x(t)$ produced by an oscillator,

$$x(t) = A(t)\cos(\omega_0 t + \phi(t)), \tag{1.1}$$

where $\omega_0 = 2\pi\nu_0$ represents the steady-state radian oscillation frequency of the oscillator, and $A(t)$ and $\phi(t)$ represent respectively the amplitude modulation (AM) and the phase modulation (PM) of the cosinusoidal *carrier* signal. The AM and PM can be intentional or due to instabilities and thermal noise phenomena in the system. When the PM is due to random noise phenomena, $\phi(t)$ is called the *Phase Noise Process* or simply Phase Noise. Phase noise causes a random modulation of the phase of a noiseless signal. In the following discussion on phase noise the AM noise will be considered negligible.

It is well-known that phase noise appears as phase-modulation sidebands around a carrier's spectrum when the spectrum is measured *directly* using, for example, a spectrum analyser or a Fabry-Perot Interferometer. Fig. 1.1a shows the measurement setup for direct spectrum measurement, while Fig. 1.2 shows the measured spectrum which we will term $S_{RF}(f)$. Mathematically,

$$S_{RF}(f) = |\mathcal{F}[x(t)]|^2 = \mathcal{F}[R_x(\tau)], \tag{1.2}$$

where $\mathcal{F}$ denotes the Fourier Transform and $R_x(\tau)$ is the autocorrelation function of $x(t)$. The central carrier peak can be noticed in Fig. 1.2, along with the phase noise sidebands. Phase noise around the carrier signal is measured as a ratio of the power in the noise sidebands, per Hz, relative to the power in the carrier, and is specified in dBc/Hz (decibels relative to the carrier per Hertz). The 3-dB linewidth of the carrier peak has been marked in Fig. 1.2 and the sidebands have been divided into

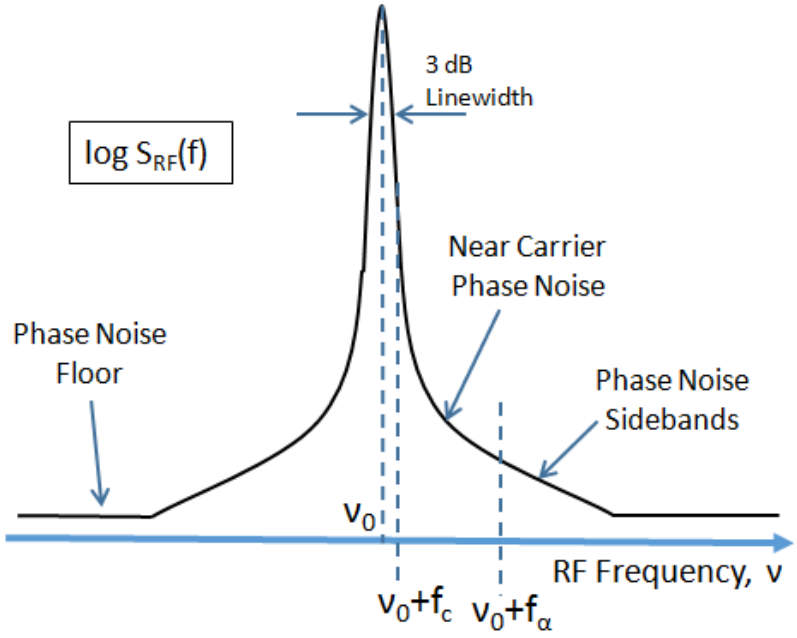

Figure 1.2: Illustration of the RF Spectrum of an oscillator

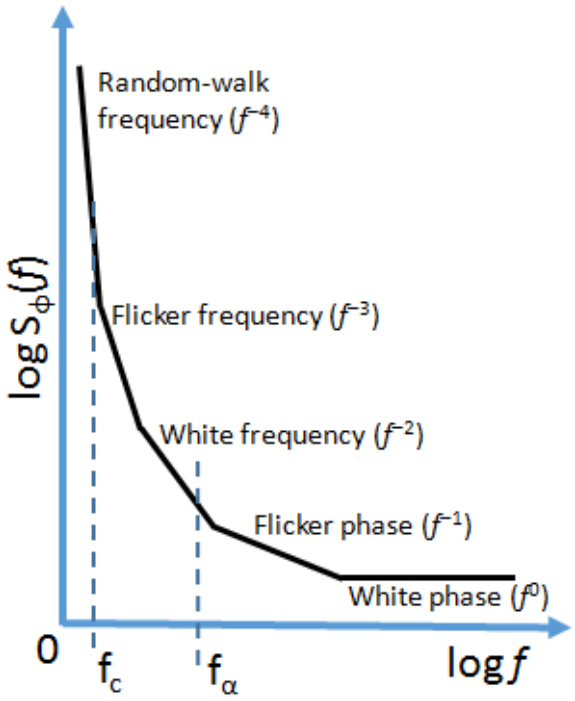

Figure 1.3: A generic plot of the Spectral Density of Phase Fluctuations [8].

the *near-carrier* phase noise and the *far-from-carrier* phase noise regions: these will be explained in a later chapter.

One problem in using the RF spectrum is that it is not possible to distinguish between the phase noise and the AM noise in the carrier signal, as both appear as sidebands in the RF spectrum. Therefore, phase noise is most popularly characterised using the Spectral Density of Phase Fluctuation $S_\phi(f)$, also called the *baseband spectrum of phase fluctuation*. It has been noted that $S_\phi(f)$ is a complete model of phase noise: in particular $S_{RF}(f)$ is not useful in characterising low-frequency phase noise processes [9] (also called the *frequency noise processes*). The complete relationship between $S_\phi(f)$ and $S_{RF}(f)$ will be discussed later under the discussion on oscillator linewidth where the frequency points f_α and f_c will also be clarified. Fig. 1.1b shows the measurement setup to measure $S_\phi(f)$: the idea is to use a phase-lock loop (PLL) to keep in step with the frequency variations in the oscillator under test (OUT) while measuring the baseband phase process $\phi(t)$. This setup has the inherent capability to reject AM noise. Mathematically,

$$S_\phi(f) = |\mathcal{F}[\phi(t)]|^2 = \mathcal{F}[R_\phi(\tau)], \tag{1.3}$$

where $R_\phi(\tau)$ is the autocorrelation function of $\phi(t)$. While using the measurement setup of Fig. 1.1b, the imperfections introduced by the VCO and the filtering stages need to be calibrated out for the reliable measurement of $S_\phi(f)$.

Fig. 1.3 shows a generic plot of $S_\phi(f)$ [8, 10], where the power-law nature is apparent. The power-law components of phase noise are classified as follows:

- Random Phase Noise
  - White Phase ($1/f^0$) noise
  - Flicker Phase ($1/f$) noise
  - White frequency ($1/f^2$) noise
  - Flicker Frequency ($1/f^3$) noise
  - Random-Walk Frequency ($1/f^4$) noise
  - Flicker-Walk Frequency ($1/f^5$) noise

Conventionally a colour is associated with each of the power-law components of phase noise as shown in Table 1.1. The term *coloured noise* is used for Phase noise because it has a non-flat frequency spectrum as shown in Fig. 1.3.

In addition to the random phase noise, systematic phase noise components can also be present in an oscillator that are classified as follows:

Table 1.1: Random Phase Noise Processes

Type of Noise	**Power Law**	**Colour**
White Phase	$1/f^0$	Purple/Violet
Flicker Phase	$1/f$	Blue
White frequency (or Random-Walk Phase)	$1/f^2$	White
Flicker Frequency (or Flicker Walk Phase)	$1/f^3$	Pink
Random-Walk Frequency	$1/f^4$	Brown/Red
Flicker Walk (Random Run) Frequency	$1/f^5$	Infrared

- Systematic Phase Noise
  - Linear Frequency Drift
  - Quadratic Frequency Drift
  - Cubic Frequency Drift.

We will not deal with systematic phase noise in this Thesis.

The phase noise processes $\phi_\beta(t)$ corresponding to each power-law component are usually treated as being independent of each other [11,12] although some researchers have pointed out that the underlying mechanisms may be related. In the present analysis $\phi_\beta(t)$ will be assumed to be independent, so that the phase noise process $\phi(t)$ having K power-law components can be written as,

$$\phi(t) = \sum_{i=0}^{K} \phi_\beta(t). \tag{1.4}$$

Therefore, $R_{\phi\phi}(\tau)$ can be written as,

$$R_{\phi\phi}(\tau) = \sum_{i=0}^{K} R_{\phi_\beta}(\tau), \tag{1.5}$$

where $R_{\phi_\beta}(\tau)$ is the autocorrelation function of $\phi_\beta(t)$. Finally, $S_\phi(f)$ can be written as,

$$S_\phi(f) = \sum_{i=0}^{K} S_{\phi_\beta}(f). \tag{1.6}$$

1.4 The Radar Noise Problem: Reduce the noise sidebands

The Fourier Transform of an ideal finite-duration sinewave is a narrow peak of width inversely proportional to the observation time, and having a sideband structure that

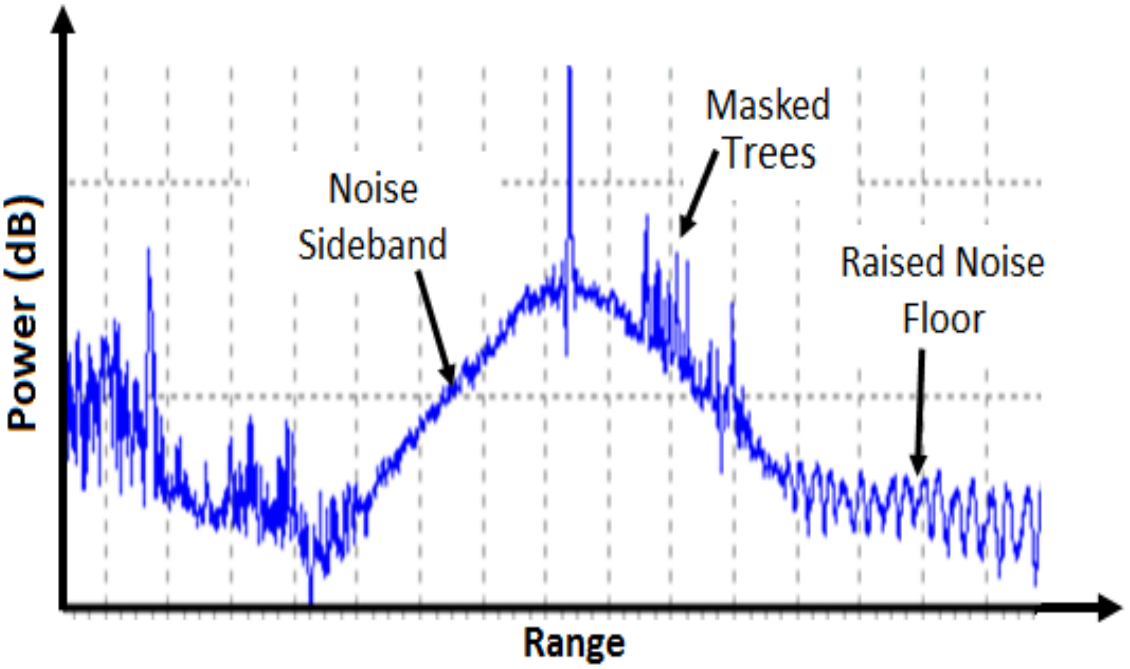

Figure 1.4: Illustration of the phase-noise sidebands around a strong target that make weaker targets difficult to detect.

depends on the type of window/weighting function used. Phase noise causes the energy of sinewaves to spread, and gives rise to broader spectral peaks and sideband spectra defined by the phase noise shaping in the signal generator circuits. As such the weighting function no longer defines the sideband spectra.

Fig. 1.4 shows the Fourier Transform of the IF signal of a real FMCW[1] radar system when the radar scene contains a large triangular corner reflector target in the scene. The narrow peak can be observed at the target's range along with noise sidebands due to phase instabilities in the transmitter. Thus, phase noise appears as phase-modulation sidebands around a carrier's spectrum. For radar systems having a high dynamic range this causes the noise-floor to increase around large targets making the detection and tracking of small targets difficult if not impossible in the region of the raised noise-floor. Large targets are said to *mask* small targets nearby. This effect is only visible in high-performance radars where thermal noise has been reduced to a level where the phase noise can show up. This problem has been reported in earlier works as well [13].

Reduction of phase noise, therefore, is a prime challenge to improve the detection and tracking performance of radars. Phase Noise reduction techniques will be presented in this Thesis. In addition to a reduction in tracking performance, the energy from the main spike is being wasted in the noise sidebands. Reduction in phase

[1]Frequency Modulated Continuous Wave

noise, therefore, would make the target response sharper resulting in an increase in the SNR.

Almost every component in the radar transmitter chain contributes to the total phase noise in the transmitted signal. The success in achieving low phase-noise lies in identifying the subsystems and components having the largest contribution to the overall phase noise. Additional effects, like the cancellation of phase noise at shorter ranges in coherent radars, will also taken up in this work. Phase noise can also be visualised as *phase jitter*, i.e. the random fluctuations of the zero-crossings of a periodic waveform [14]. The idea of phase jitter is useful to analyse the transfer of phase noise from a sampling clock to the sampled signal.

1.5 Objectives of the research

The objective of the present Thesis is to study the fundamental phase noise limitations of millimetre wave (MMW) continuous wave (CW) radar systems and to design generalised methods to optimise their performance by reducing the phase noise. The mechanisms of Phase Noise will be studied throughout this work and methods to optimise the *SNR* (signal-to-noise ratio) performance will be detailed. Optimising the performance of radars on these lines results in better target tracking performance, better discrimination of targets from clutter, an increased dynamic range resulting in the detection of weak targets nearby strong targets, and a potential increase in the detection range.

Some of the results presented in this Thesis have direct applications in commercial requirements analysis. For example, while it is apparent that using low-phase noise circuits and techniques results in low-noise system performance, what is generally not known is *how low* the phase noise needs to be to achieve the desired performance. Not knowing ones requirement can lead to a design that solves the problem but is not commercially viable due to the high cost. As will be seen in the next chapters, quantitative bounds for the required noise performance have been derived where appropriate.

The methods for high-performance and low-noise circuits and systems design are scattered over various sources in the literature as evidenced by the references at the end of this Thesis. In this work these methods will collected and specialised for the phase noise optimisation of radar system. Numerous examples will be given in the forthcoming chapters.

Phase noise is known to have a profound effect on the performance of modern electronic systems. Yet some of the most fundamental problems in phase noise remain unsolved. While a large body of work on oscillator phase noise is available,

there is a dearth of work on how to accurately relate phase noise processes to the spectral dispersion in RF signal sources. Phase noise on the system-level in the context of FMCW radars has not received much attention. Phase noise analysis of analog-to-digital converters (ADC) with a focus on radars is not available, including how the phase noise transfer-function of ADCs compares with that of frequency mixers and frequency multipliers. The idea of oscillator linewidth is important to define the fundamental resolution capability of FMCW radar systems, but has received less attention in this context, although some work has been done on oscillator linewidths in the other areas of science, including Quantum electronics, lasers, and time metrology. The present Thesis will address these problems.

1.5.1 Summary of Objectives

The following list summarises the objectives of this research:

1. Development of phase noise models of the sub-systems inside an FMCW radar.
    - Optimisation of the important parts of the system including frequency multipliers, amplifiers, filters, frequency mixers, etc., to achieve low-phase noise performance.
    - Design of low-noise frequency synthesisers: architecture selection, stability, and phase-noise requirements.
    - Demonstration of the reductions in phase noise through practical design implementation and measurements.
    - Decorrelation of phase noise in coherent radar systems resulting in a non-linear range-dependence of the observed noise sidebands.
    - Derivation of a new fundamental limit on the maximum allowable phase noise level in radar sources to prevent incoherent spectral broadening.
    - Derivation of an equation to estimate the *coherence time* in radars.
2. Development of a model for the phase noise introduced by the analog-to-digital conversion process.
    - Development of a model relating the phase noise in the sampled signal to the phase noise in the demodulated radar signals and the jitter in the sampling clock.
3. Development of the quantitative bounds on the phase measurement process in FMCW radar systems.

- A demonstration that dual I/Q channels are not necessarily needed for phase measurement in FMCW radar systems.

4. Analyse the idea of Oscillator Linewidth, its relationship with the phase noise processes, and its application to radar systems.

5. Development of a Generalised Brownian Motion model of phase noise to relate the phase and frequency noise processes to the integer and fractional Brownian processes, in order to model the RF spectral dispersion in oscillator signal.

As mentioned before, the central theme behind these objectives is to optimise the performance of MMW CW radar systems.

1.6 Original Contributions of This Work

The following are the original contributions of this work:

1. A new maximum bound on the frequency synthesiser's phase noise to preserve coherence in radar systems.

   This bound leads to a selection criterion for radar signal sources. The troubles caused by non-conformity to this bound show up at either very long-ranges or for very high frequency radars (e.g. sub-millimetre wave radars).

2. Development of the relationship between the phase noise spectrum and the RF spectrum of oscillators

   - Graphical illustration of the relationship

   - Integer and fractional Brownian motion based model of phase noise

   - Oscillator linewidth model

3. Derivation of a new equation for an optimistic estimate of the coherence time of radar systems based on the integrated phase noise in the transmitter.

4. A new proof comparing the phase noise in the baseband FMCW signal and the phase noise in the sampling clock.

   This leads a radar designer to make an informed decision on the selection of a sampling clock for the radar design at hand.

These contributions have led to the publication of the journal and conference papers mentioned at the start of this Thesis.

1.7 Organisation of the Thesis

The present Thesis has been written in a way to integrate the research papers written by the Author in a coherent fashion with the flow of the material presented. A list of the Author's research papers appears at the beginning of this Thesis, along with their stage of publication at the time of writing. The papers have been referenced at the start of the relevant chapters. The research papers already published by the Author have been included in this Thesis with the permission of the IEEE.

The Thesis is organised as follows. Chapter 2 will give the broad background to the present research, as well as the general literature survey. The relevant and important works related to phase noise have been highlighted, and the gaps in the literature have been pointed out that will be filled in by this work. Phase noise modelling of FMCW radar subsystems is presented in Chapter 3 which leads to the design of an alternative low-phase noise frequency synthesiser. Chapter 4 extends the system-level phase noise analysis to derive a new bound on the maximum allowable phase noise sideband level in radar transmitter to preserve *phase coherence*. Also derived is a new equation to estimate the *coherence time* of radar systems. The reduction in the phase noise sidebands is demonstrated through the practical measurement results of a low-phase noise signal source. Chapter 5 details the development of models of the phase noise transfer from a sampling clock to the sampled radar signal under the process of analog-to-digital conversion. The quantitative design equations have been worked out to select a sampling clock of the appropriate phase noise/jitter for the design at hand.

Chapter 6 demonstrates that a single-channel phase measurement system could be used reliably under certain widely met conditions, instead of a dual I/Q receiver. This information can be used to decide whether or not a dual I/Q receiver systems is needed for an application at hand, and leads to a simplified receiver design for FMCW radar systems. Chapter 7 pulls together our works on phase noise and RF spectra presented in the previous chapters, and presents the unifying role of the integer and the fractional Brownian motion processes to describe the RF spectral dispersion due to phase noise. Chapter 8 reviews the relationship between an oscillator's RF spectrum and its phase noise spectrum. A detailed review of the works from other branches of science on the oscillator *linewidth* is included. Chapter 9 presents the Conclusion to the Thesis and the proposed future work.

In Appendix A a relation for the covariance of integral Brownian motion has been derived. Appendix B presents the highlights of some of the development work done in the long-range sensor (LRS) project. Appendix C introduces some alternative phase noise modelling methods. The references are included at the end of the Thesis.

Chapter 2

Background and Literature Survey

2.1 Radars

Historically the word RADAR was used as an acronym for *Radio Detection and Ranging*. A radar is an electronic system that transmits an electromagnetic (EM) wave (or *signal*) in a desired region, receives the waves reflected off objects, and processes the received waves to extract useful information about those objects. The desired return signals are called *target echoes* and the undesired signals are called clutter. It can be aptly said that "One man's clutter is another man's target" [15].

Radars have long been classified based on the type of waveform being used in the transmitters. Pulsed radar use modulated pulses (generally having a defined pulse repetition frequency or *PRF*) as the transmit waveform. Continuous-wave (CW) radars use continuously modulated signals (generally having a defined sweep repetition frequency or *SRF*). Similarly, Noise Radars use pseudo-random (PN) coded sequences of pulses or continuous waveforms, and so on. Radars have been designed all over the Electromagnetic frequency spectrum in different forms. In this work the major focus is on Frequency Modulated Continuous Wave (FMCW) radars designed in the millimetre-wave (MMW) frequency band. FMCW radar systems have some specific feature that will be explained shortly.

The *Radar Range Equation* (2.1) calculates the maximum detection range achievable by a radar for a given level of transmit power P_t, antenna gains G_t, G_r, the carrier wavelength λ, the target's radar cross-section σ_{tgt}, and the minimum power detectable by the radar $P_{r(min)}$:

$$R_{max} = \sqrt[4]{\frac{P_t G_t \sigma_{tgt} \lambda^2 G_r}{(4\pi)^3 P_{r(min)}}}. \tag{2.1}$$

An inspection of (2.1) reveals that to double the detection range, one needs to

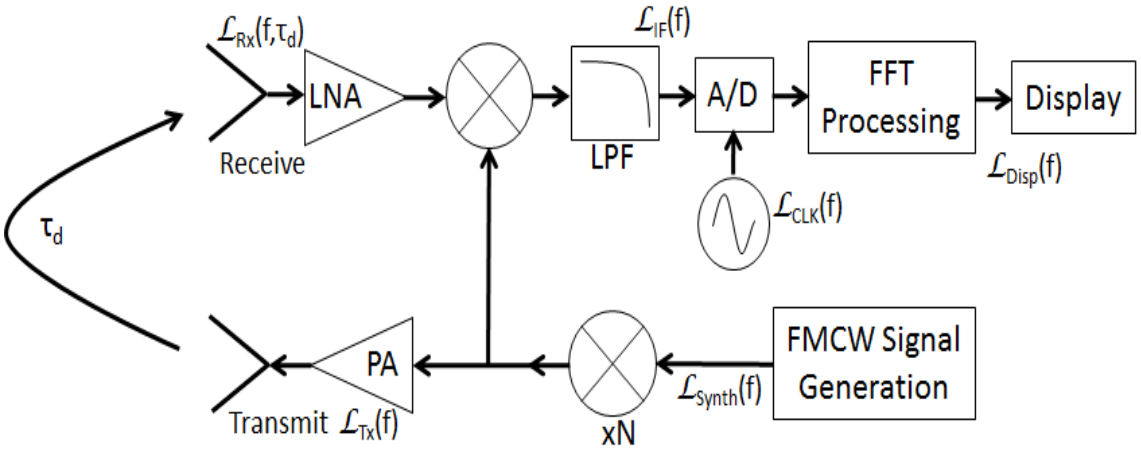

Figure 2.1: Block diagram of a generic FMCW radar system

increase the transmit power 16 times (or 12 dB). Increasing the power by 6 dB increases the range by 41%. One should note, however, that increased power has its associated challenges.

2.2 FMCW Radars

Fig. 2.1 shows a block diagram of a MMW FMCW radar[1]. The *FMCW Generator* generates a linear FMCW waveform: shown in Fig. 2.2 are the in-phase (I) and the quadrature (Q) channel linear FMCW signals. Some radars use only one of these waveforms while others use dual I/Q waveforms for transmission. It is interesting to note that the RMS value (or average power) of an LFM waveform is exactly the same as a single sinewave: however the energy is spread over the swept frequency band. The generated LFM waveform is then either frequency mixed or frequency multiplied up to the transmit frequency (the latter case is shown in Fig. 2.1). A portion of the transmitted signal makes up the local oscillator (LO) signal which demodulates the received signal to the IF (intermediate frequency). The demodulated signal is digitised after filtering and amplification.

The filter stage in Fig. 2.1 serves a few purposes. First of all, it is a low-pass anti-aliasing stage for the A/D converter. Secondly, it usually incorporates a DC block stage to filter out the very close-in reflections from the leakage paths inside an FMCW radar. Third, the filter can have a shaped profile according to the R^4 power law in (2.1): in this case it is called a *Sensitivity Time Control* (STC) filter. The in-band gain of this filter must be optimised for the best linear dynamic range.

As the transmitted signal's frequency increases linearly with time, it can be

[1]PA=Power Amplifier, LNA=Low Noise Amplifier, A/D=Analog-to-Digital Converter, IF=Intermediate Frequency, $\mathcal{L}_X$=Phase Noise at point X

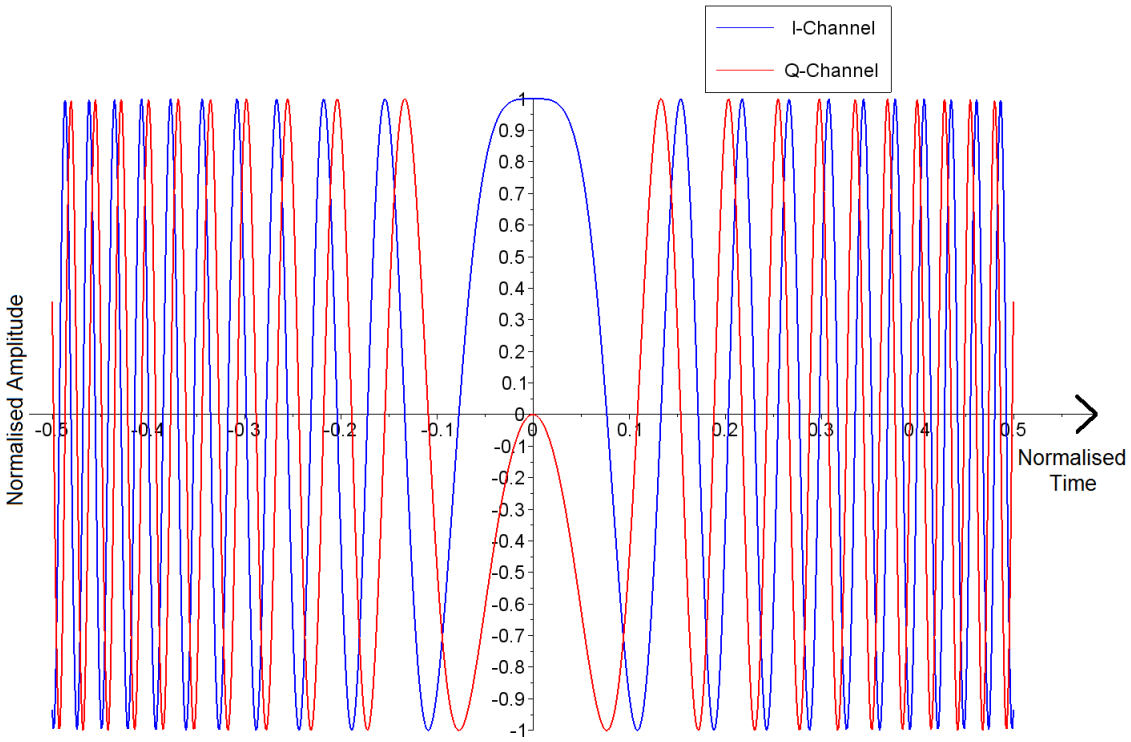

Figure 2.2: The Linear FMCW Waveform

represented conveniently on a frequency vs. time plot as shown in Fig. 2.3. The transmitted signal sweeps a bandwidth of B_S Hz in sweep time T_S. There is a time difference as well as an instantaneous frequency difference between the transmit (Tx) & receive (Rx) signals proportional to the target's range as illustrated. The homodyne mixer in Fig. 2.1, therefore, produces a sinewave corresponding to the frequency difference ΔF between the Tx & the Rx,

$$\Delta F = B_S \times \frac{\tau_d}{T_S}, \tag{2.2}$$

where τ_d is the round-trip delay time of the Tx signal given by $\tau_d = 2R/c$, R being the target's range and c being the speed of light. The Fourier Transform of this sinewave is normally expected to be a narrow peak at the frequency ΔF corresponding to the target's range, with a sideband structure defined by the type of window/weighting function used for spectral estimation. However, in reality the situation is complicated due to the presence of phase noise in the transmitted signal.

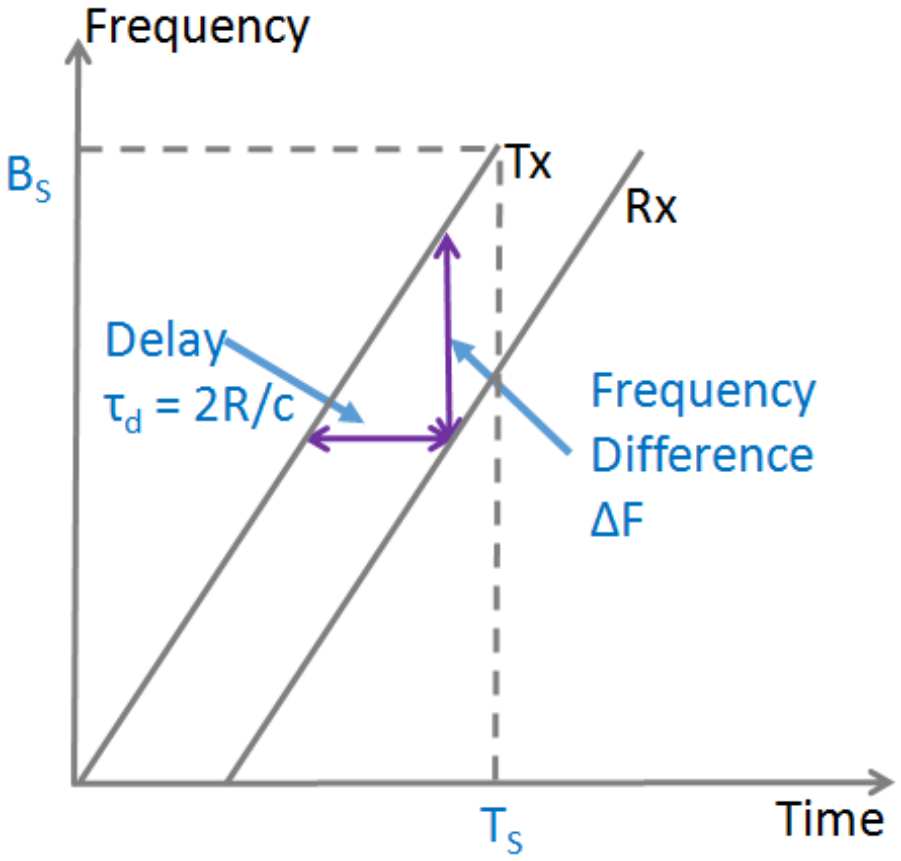

Figure 2.3: Time Vs. Frequency plot of a linear frequency modulated (LFM) waveform.

2.3 Features of FMCW Radars

FMCW radars have some benefits that make them suitable for commercial applications. Some of the major benefits are mentioned below.

Smaller Component Dimensions

Occupying the frequency band between the Microwave and the far-infra-red bands, MMW circuits and components make use of the design knowledge from both Microwave Engineering and Optics. It is known from Microwave Engineering that the physical dimensions of circuits shrink according to the wavelength of electromagnetic signals. MMW signals have frequencies roughly 10 times larger than Microwave signals. So the circuits are roughly 10 times smaller than Microwave circuits.

Finer Angular-Resolution

One of the performance metrics of high-performance radars is their *resolution* defined as the ability of a radar to discriminate between two targets close by in *range* and *azimuth* for ground- and sea-based radars (and also *elevation* for airborne radars). While the *range-resolution* is independent of the radar's carrier frequency (and depends solely on the waveform *bandwidth*), the *azimuth-* and *elevation-resolutions*, collectively called *angular-resolution*, depend directly on the carrier's wavelength and the dimensions of the antenna being used.

$$\theta_{az(el)} = \frac{k_a \lambda}{D_{az(el)}}, \tag{2.3}$$

where $\theta_{az(el)}$ is the *beamwidth* or the 3 dB angular width of the antenna's beam, λ is the carrier's wavelength, $D_{az(el)}$ is the length of the antenna in the azimuth (or elevation) dimension, and k_a is a parameter depending on the antenna's design. Equation (2.3) shows that for the same antenna dimensions a MMW radar's beamwidth will be a fraction of a Microwave radar and, therefore, will achieve finer angular resolution. This is a significant advantage of MMW antennas.

Lower Clutter

Area clutter, like ground and sea clutter, occupy the full antenna beam compared with other targets like humans that in general occupy only a fraction of the beam. Finer resolution also means that the clutter power decreases proportionally to the decrease in beamwidths. This idea can be used to increase the *signal-to-clutter ratio*

(SCR) which is the ultimate performance metric for ground- and sea-based radars. MMW radars benefit from the high transmit frequency again.

Finer Doppler Measurement

Finer Doppler measurements are possible with MMW radars as the Doppler frequency induced in the carrier signals due to the motion of targets is proportional to the carrier's frequency,

$$f_{Doppler} = \frac{2 f_c V_r}{c}, \tag{2.4}$$

where f_c is the carrier frequency, V_r is the radial velocity of the target with respect to the radar, and c is the speed of light.

Lower Peak Transmit Power

One advantage of using CW radars over pulsed radars is that CW radars can use a lower peak transmit power to achieve the same maximum detection range. This is because CW radars spread the power over the complete sweep instead of concentrating them in narrow pulses. This simplifies the design of radar transmitters as lower power levels can be handled easily by solid-state transmitters and the linearity of the power amplifier stages in the transmitter is less of an issue.

Lower IF/Baseband Bandwidth

FMCW radars have a lower IF bandwidth than pulsed radar systems. One way of looking at this is that in pulsed radars, the range resolution is defined by the pulse width, which stays almost the same at RF or baseband. On the other hand, in FMCW radars the range resolution is defined by the swept bandwidth, while the range is defined by the difference frequency between the transmitted and the received signal. Depending on the transmitted power and the desired maximum range, the IF signal can be low-pass filtered to limit the bandwidth.

As an example, consider a pulsed radar with a range resolution of 15 cm. The pulsed width has to be 1 ns (ignoring any broadening), and so a baseband bandwidth of 1 GHz is needed even for short ranges. Sampling this signal at above 2 GHz will require a costly ADC. The FMCW counterpart will also need to sweep 1 GHz of bandwidth to achieve 15 cm range resolution. However, if the sweep time is, say, 1 ms and the desired maximum range is 5 km, then using (2.2) the maximum beat frequency is 33.3 MHz. So the ADC needs to sample at above 66.6 MHz - a huge saving compared with pulsed radars.

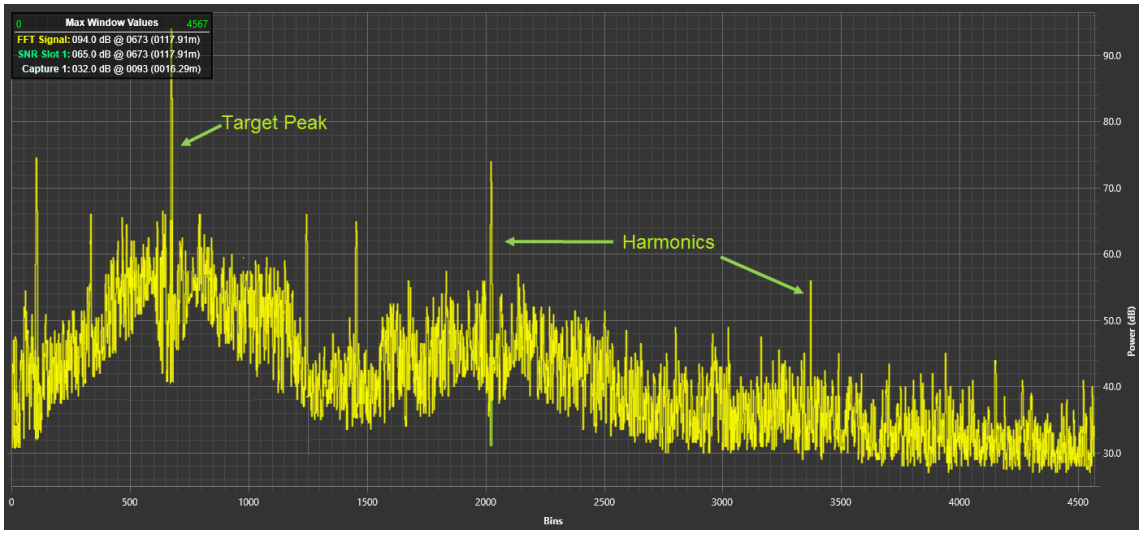

Figure 2.4: Illustration of the harmonics of the beat frequency of a target. The odd harmonics are prominent due to saturation in the IF/baseband chain.

Range Harmonics Under Saturation

If the mixer diodes or the IF/baseband chain in an FMCW radar saturates due to large return power from a target, the harmonics of the beat frequency are produced. This effect is illustrated in Fig. 2.4. This feature of FMCW radar systems does not have a counterpart in pulsed radars, and is a cause of false target indications. The same target will indeed saturate an equivalent pulsed radar too, however the baseband pulse saturation does not cause any harmonics.

Transmit/Receive Isolation

In CW/FMCW systems, the transmitter is on all the time, so special measures are needed to minimise the leakage power coupling from the transmitter to the receiver when they are co-located (e.g. in monostatic radars). The leakage power couples through the receive mixer, directly from the transmit antenna to the receive antenna, or through reflections from the metal work and the radome. As a design guideline, the total leakage power must be less than the thermal noise figure of a designed radar (which should also be low).

In pulsed radar systems, once the pulse is transmitted the transmitter is turned off. So there is no leakage power to combat. However, the transmitted pulses have a much larger peak power than FMCW systems, so the receiver has to be turned off for that duration. This means that pulsed radars in most cases come with a mandatory blind spot around the radar. For a 100 ns pulse, the blind spot will be 15 m. Properly calibrated FMCW systems do not have such a blind spot.

2.4 Literature Survey

This section gives a brief literature survey related to the area of the present work and the gaps therein. The specific literature review for each topic taken up in the forthcoming chapters can be found in the respective chapters.

2.4.1 General Overview

Noise in engineering systems is an old subject. The long-term drift phenomenon (modelled as *Random-Walks* in modern systems), for example, was known to horologists in the 18th Century. The landmark development of John Harrison's precision marine chronometer in the early 18th Century can be viewed as the development of a *system* to combat the natural forces causing frequency drifts in pendulum clocks.

The history of electrical circuits can be traced back to the experiments by Michael Faraday and his contemporaries. The development of modern electronic circuits and systems can be traced back to the development of transistor in 1947 by John Bardeen, Walter Brattain, and William Shockley, followed by Jack Kilby's development of the first integrated circuit at Texas Instruments in 1958.

Electronic amplitude and phase noises have been studied since early 20th Century, notably by Walter Schottky at Siemens Research Labs and J. B. Johnson at Bell Labs. Thermal noise was originally reported by Schottky in [16, 17] where he measured a flat (white) noise spectrum. In an attempt to reproduce Schottky's experimental results, Johnson found that the noise was not white at low frequencies and reported his measurements in [18]. Schottky studied this *Flicker Effect* further and came up with a Lorentzian spectrum (not named so in his paper) for the observed noise [19]. Thermal noise was studied further in [20–22], and set the foundation of noise theory as we know it today. It is interesting to note that the *Boltzmann Constant* from Gas Laws also describes thermal electronic noise phenomena.

2.4.2 Phase noise in Radar Systems

The *IEEE Proceedings* of 1966, vol. 54, no. 2, appears to be the first issue where the whole issue is dedicated to phase noise in oscillators and systems. This issue followed the NASA-IEEE Symposium on Short-Term Stability in 1964. Phase noise has received a lot of attention ever since. It is still an active area of research. In the present thesis, some of the fundamental problems related to phase noise in FMCW radar systems will be addressed. Phase (1/f) noise is also recognised by one school of thought (led by Dr Peter Handel, at the University of Missouri) as a fundamental Quantum-Mechanical phenomenon [23].

From the perspective of phase noise in radar systems, the NASA-IEEE Symposium on Short-Term Stability (in 1964) included foundational papers by Leeson [24] and Raven [25] among others. One significant work in understanding the effects on phase noise in radar systems is the book by Goldman [26]. The book details a system-level phase noise analysis methodology which has been successfully applied by us, with some extensions, to analysing phase noise in FMCW radar system [27] where the phase noise contribution of various building blocks in radar systems have been detailed. This leads to a method of estimating the total phase noise in radar displays. However, in the above-mentioned works the focus has generally been on the white-phase and flicker-phase noise processes. This thesis will also discuss the effects of the frequency noise processes (i.e. the white-frequency, the flicker-frequency, and the random walk-frequency noise processes).

2.4.3 Jitter Transfer in ADCs

How does the sampling clock's phase jitter affect the overall phase noise in radar systems? There are two aspects of this question:

- What factors affect the noise floor of the radar, and what is the contribution of the sampling clock to the noise floor?
- What is the contribution of the clock's phase jitter to the phase noise sidebands in the digitised radar returns?

The effect of phase jitter in sampling clocks has been addressed before as contributing to the overall system noise floor [28–30], and as the clock's noise spectrum being transferred to a noise-less signal under the sampling process [29,31]. However, the case of sampling a signal corrupted with phase noise by a clock having its own phase jitter, and their relative contribution to the total phase noise in the sampled signal has not yet been taken up. In [32] the total phase noise in the sampled signal is accurately estimated using an iterative optimisation-based approach. In [33] the problem of the transfer of the sampling clock's noise to a generic input signal has been addressed. However these approaches do not give insight into the phase jitter requirements of the ADC clock or how the clock jitter compares with the received signal's phase noise. Ultra-low phase noise oscillators and sampling clocks are expensive, so an estimation of the phase noise requirement is imperative to select the oscillator meeting the phase noise requirement with the lowest cost.

2.4.4 Frequency synthesiser architectures for radar systems

Frequency synthesisers have been studied extensively and numerous books are available on the subject. Recent works on the subject include [34–37]. Choosing the right architecture for the frequency synthesiser is important for the following reasons:

- It must be capable of generating the desired signals for the application at hand.
- It governs the phase noise generated at source: reducing phase noise in the frequency synthesiser means a dB-for-dB reduction in phase noise in the radar display.

Following are the major frequency synthesisers being studied in the present work:

1. Phase-lock loops (PLL), including conventional PLLs and the charge-pump (CP)/phase-frequency detector (PFD) based PLLs [38]:
    - Pros: The CP/PFD-based PLLs have been very popular recently. Their prime advantage is the automatic phase and frequency acquisition feature inside a single IC. They can be used to generate a wide range of waveforms with high precisions.
    - Cons: The downside of these PLLs, as pointed out in later chapters, is that the in-band phase noise in these PLLs is limited by the PFD noise and not the reference oscillator [27]. In high dynamic-range applications like radar systems this causes the phase noise sidebands to raise the noise floor around large targets as will be seen in Chapter 3. This makes the optimisation process difficult because selecting a lower-noise reference oscillator does not help reduce the in-band noise due to the added PFD noise. Alternative synthesisers need to be explored for the design of low-noise radars.
2. Direct Digital Synthesisers (DDS) [35, 36]:
    - Pros: Modern DDS have ultra-low phase noise and can be used to design a lower-noise radar solution. The phase noise in DDS synthesisers is lower than in PLLs.
    - Cons: One downside is that the DDS chips cost much more than TCXOs and PLL Chips. Another downside is that the DDS chips, and the mixers used in the frequency synthesisers, generate spurii which can cause significant *intermodulation distortion* if the analysis and design is not carried

out carefully. The spurious-free dynamic range is limited (e.g. 80 dB) compared with PLLs. Finally, their power consumption is much higher than PLLs.

3. Some other synthesiser architectures based on extensions of the above two are as follows:

   - Heterodyne Phase Locking [37].
   - Frequency lock loops (FLL) [38].
   - Offset Phase Lock Loops [39, 40].
   - Super-Nyquist frequency synthesis [41].

2.4.5 Signal processing techniques to reduce phase noise

Signal processing techniques have also been used to reduce the effects of phase noise in radars and FMCW radars. In this work, Signal Processing techniques will be used as a secondary phase noise reduction method, the primary being low-noise electronic design as detailed above. Signal processing techniques become the major focus if the desired improvements in noise and phase noise cannot be achieved using low-noise electronics alone.

Averaging

Signal averaging is known to improve the SNR in radars [3], [5]. In the presence of phase noise one question is the effectiveness of coherent and non-coherent averaging techniques in radars. Non-coherent averaging operates on the *detected signal* $|y[m]|$ that does not contain phase information. It can be written as $\frac{1}{M}\Sigma_M|y[m]|^2$, where $|y[m]|^2 = |y_I[m]|^2$ for a single channel radar and $|y[m]|^2 = y_I^2[m] + y_Q^2[m]$ for an I/Q based radar receiver. Coherent averaging on the other hand takes the phase information into account as well. Usually coherent averaging is performed using the Fast Fourier Transform (FFT). The detected (displayed) signal after coherent integration can be written as $|\frac{1}{M}\Sigma_M y[m]|^2$. Note that $y[m]$ also contains additive thermal noise.

As noted in [42], the phase noise in FMCW radars is uncorrelated from one sweep to the next. This effect can be used to improve the signal-to-noise sideband ratio (SNSR) through averaging. Statistical modelling of the phase noise and taking into account the radar signal processing operations allows us to model the statistics of the phase noise in the radar's display. Afterwards the effects of coherent and non-coherent averaging can be studied as a post-processing operation.

Following are the models for coherent and non-coherent averaging.

Non-coherent averaging model

First of all, notice that the non-coherent averaging statistic of the *noise* $V[m]$ in the sampled signal $y[m]$ can be written as $\frac{\sigma^2}{M}\Sigma_M\frac{|V|^2}{\sigma^2}$ for convenience. Suppose $V[m]$ follows the Normal Distribution as $\mathcal{N}(0,\sigma^2)$. Then $|V[m]|^2/\sigma^2$ follows the Exponential Distribution as $Exp(1/2)$. Now $\Sigma_M|V[m]|^2/\sigma^2$ follows the Erlang Distribution $Erlang(k,\lambda)$ having $mean = k/\lambda = 2M$ and $variance = k/\lambda^2 = 4M$. Finally, the non-coherent average statistic $z[m] = \frac{\sigma^2}{M}\Sigma_M|V[m]|^2/\sigma^2$ follows the Erlang Distribution with $mean = 2\sigma^2$ and $variance = \frac{4}{M}(\sigma^2)^2$.

The effect of non-coherent averaging is apparent immediately from this result. As M increases the mean stays the same while the variance goes down by M.

Coherent averaging model

Suppose again that $V[m]$ follows the Normal Distribution as $\mathcal{N}(0,\sigma^2)$. Then $\frac{1}{M}\Sigma_M V[m]$ follows the Normal Distribution as $\mathcal{N}(0,\sigma^2/M)$. Finally, the coherent average statistic $z[m] = |\frac{1}{M}\Sigma_M V[m]|^2$ follows the Exponential Distribution with $mean = 2\sigma^2/M$ and $variance = \frac{4}{M^2}(\sigma^2)^2$.

From this result it can be seen that coherent averaging reduces the mean as well as the variance of the noise sidebands. This result has been verified later in this Thesis.

2.5 Conclusion

This chapter presented some general background knowledge on FMCW radar systems, followed by a broad literature survey for the present Thesis. The section on the features of FMCW radars draws a contrast with pulsed radars and highlights areas where FMCW radars gives superior performance. The literature review started with a review of noise and phase noise, and then discussed some previous works on phase noise in radar systems, sampling clocks, and frequency synthesisers. The research problems to be taken up in this Thesis were also highlighted. The chapter ended with the signal processing models of non-coherent and coherent averaging techniques, that are helpful to reduce thermal noise and thermal plus phase noise respectively.

The next chapters detail the research carried out in this work. The specific literature review for each subsequent chapter will be included at the start of each chapter.

Chapter 3

Phase Noise Analysis in FMCW Radar Systems[1]

3.1 Summary

Phase noise in radar transmitters is known to raise the noise floor around large targets, making impossible the detection & tracking of small targets nearby. This chapter presents phase-noise modelling techniques, with a focus on homodyne FMCW radars, to accurately predict the level of phase noise expected in the radar display. Phase noise models of the sub-systems inside a typical radar are presented. We also discuss the cancellation of phase noise in coherent radar systems for short-ranges and analyse the situation for longer ranges. Practical measurements from a millimetre-wave radar system are presented to validate the theoretical modelling.

3.2 Introduction

Almost every component in the radar transmitter chain contributes to the total phase noise in the transmitted signal. The success in achieving low phase-noise lies in identifying the subsystems and components having the largest contribution to the overall phase noise. Phase noise is defined as one half of the spectral density of phase fluctuations [8]. Phase noise around a carrier signal is measured as a ratio of the power in the noise sidebands, per Hz, relative to the power in the carrier, and is specified in dBc/Hz. Phase noise appears as phase-modulation sidebands around a carrier's spectrum. For radar systems having a high dynamic range this causes

[1]Some of the contents of this chapter have been published in [27].

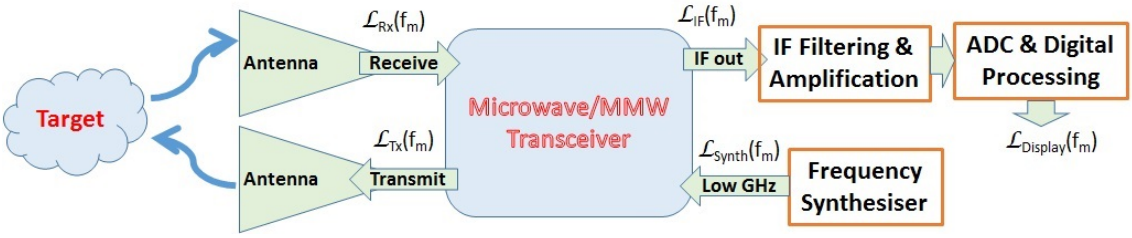

Figure 3.1: Block diagram showing phase noise propagation in a radar system.

the clutter-floor to increase around large targets making the detection and tracking of small targets impossible in the region of raised clutter-floor [13]. Decreasing the overall phase-noise, therefore, is a prime challenge in high-performance radars. In FMCW radars the phase noise appears as noise-sidebands in range around each target [43], unlike pulse Doppler radars where the phase noise sidebands appear in the velocity spectrum. In coherent radars the phase noise is cancelled for short ranges but the cancellation is not effective for long ranges.

This chapter will present our research on achieving low phase-noise in homodyne FMCW radar systems. The chapter will start by presenting phase-noise analysis of all the major parts of a general radar system to enable the designer to select the appropriate components and system architecture to design a low-noise radar suitable for a given application. Afterwards the analysis will be specialised to homodyne FMCW radars. Finally, practical results and measurements from a millimetre-wave (MMW) FMCW radar system are presented to support the modelling.

3.3 System description

Fig. 3.1 shows a block diagram of a general radar system. The *Frequency Synthesiser* block generates a signal synthesised using a suitable frequency synthesis scheme. The synthesised signal is up-converted or frequency-multiplied to the transmit frequency by the *Transceiver* block. The backscatter from the target is received by the receive-antenna and passed on to the transceiver which down-converts or demodulates the signal to an intermediate-frequency (IF). The IF signal is digitised after filtering and amplification. Digital processing follows and makes up what is displayed on the radar screen. Although two antennas as in a bistatic radar are shown in the figure, the analysis presented applies equally to monostatic radars.

Fig. 3.1 is labelled to represent the phase noise at various points in the system using the standard symbol $\mathcal{L}_{sub}(f_m)$, where *sub* is the subscript showing the phase noise measurement point in the system, and f_m is the frequency offset from the carrier frequency at which the phase noise is being measured.

3.4 Modelling the phase noise in radar systems

In the following, the steps to systematically model the phase noise in a given radar system are presented. Although phase noise is usually measured in dBc/Hz, it should be noted that the equations in this chapter are presented in the linear format (not logarithmic). We have chosen so to keep the equations compact with no loss of the insight given by the equations.

3.4.1 Phase noise in the frequency synthesiser

The first step in modelling the phase noise of a radar is to model the phase noise in the primary frequency synthesiser taking into account the phase noise contributions of all components of the synthesiser [44]. We will denote the phase noise in the synthesiser's output as $\mathcal{L}_{Synth}(f_m)$. The overall phase noise can be modelled using a simulation software tool that models the phase noise of all the components in the synthesiser. An example is presented in Section 3.5. Another methods is to measure the phase noise at the output of a frequency synthesiser using a suitable instrument like a signal source analyser.

3.4.2 Phase noise under frequency translation

The synthesiser's output can be translated to the desired transmit frequency band using frequency-multiplication or frequency-mixing.

Frequency Multiplication

For MMW radars, the synthesiser output is usually multiplied up to the desired MMW transmit frequency as shown in Fig. 3.2a (The coherent receiver part is also shown which will be explained in Section 3.4.3). During frequency multiplication two phenomena happen:

i) The bandwidth of the MMW signal is N times the bandwidth of the synthesiser output, where N is the ratio of the transmit frequency to the synthesiser's output frequency. This has a benefit that the bandwidth requirement on the synthesised source is N times less than the bandwidth actually needed for the transmitted signal.

ii) The phase noise sidebands increase by a factor of N^2. So the phase noise sidebands measured at the synthesiser's output will increase by $20\log_{10} N$ dB [26].

Thus, the phase noise in the transmitted signal, $\mathcal{L}_{Tx}(f_m)$ under frequency multiplication is computed as,

$$\mathcal{L}_{Tx}(f_m) = N^2 \times \mathcal{L}_{Synth}(f_m). \tag{3.1}$$

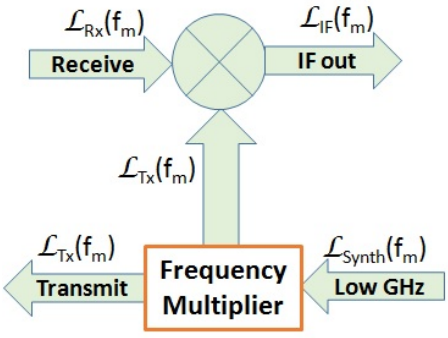

(a) Frequency multiplication. The coherent receiver is also shown.

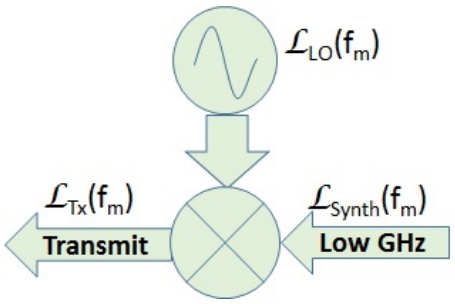

(b) Frequency mixing.

Figure 3.2: Illustration of the two popular methods of generating the transmitted signal.

Frequency Mixing

Frequency mixing is illustrated in Fig. 3.2b. Unlike frequency multiplication, the phase noise on the synthesised source is not increased by the any *factor* in frequency mixing. Instead the phase noise power in the two signals being mixed add up [38]. Therefore, if the two signals have the same phase noise, the output signal's phase noise will be 3 dB higher than the inputs. If one of the inputs has a phase noise 10 dB higher than the other, the output signal's phase noise will roughly be the same as the input having higher phase noise. There are two important considerations in frequency mixing:

i) A highly stable and clean local oscillator (LO) should be used to mix the synthesised signal up to the desired frequency band. If this is not the case, the phase noise on the LO will dominate the output phase noise.

ii) The bandwidth requirement for synthesised sources is the same as the bandwidth needed for the transmitted signal. This means that, in general, the bandwidth requirements on mixed sources are more stringent than on multiplied sources. This is especially true for radar applications where the range resolution ΔR is inversely proportional to the waveform bandwidth B_S, the exact relation being $\Delta R = c/2B_S$, where c is the speed of light.

Thus, for the case of frequency mixing, the phase noise in the transmitted signal is computed according to,

$$\mathcal{L}_{Tx}(f_m) = \mathcal{L}_{Synth}(f_m) + \mathcal{L}_{LO_{Tx}}(f_m). \tag{3.2}$$

If more than one mixing stage is used in the transmit chain then (3.2) should be applied to every stage. Using the guidelines presented in this section a designer can

select whether to use frequency multiplication or frequency mixing for a given radar design to minimise the overall phase noise.

3.4.3 Phase noise in the received and the down-converted signal

The target scatter measured by a radar is a delayed and attenuated replica of the transmitted signal. So the phase noise in the received signal, $\mathcal{L}_{Rx}(f_m)$, is simply a delayed version of the phase noise in the transmitter. Let τ_d represent the delay time where $\tau_d = 2R/c$, R being the target's range.

All radar receivers use a mixer on the receiver side to down-convert and demodulate the received signal to produce the IF signal. In coherent radars the oscillator signal used for down-converting/ demodulating the received signal is derived from the transmitted signal, as shown in Fig. 3.2a. The phase noise in the output of the mixer in this case is given by [26],

$$\begin{aligned} \mathcal{L}_{IF}(f_m) &= \mathcal{L}_{Tx}(f_m) \times 2(1 - \cos(2\pi f_m \tau_d)) \\ \mathcal{L}_{IF}(f_m) &= \mathcal{L}_{Tx}(f_m) \times 4\sin^2(\pi f_m \tau_d). \end{aligned} \tag{3.3}$$

An inspection of the above equations reveals for closer ranges (smaller τ_d) a coherent radar receiver cancels the phase noise at a rate of 20 dB/decade - the shorter the range the larger the cancellation for a given f_m. However, this is not true for longer ranges (larger τ_d). Detailed analysis of phase noise cancellation can be found in [26].

For non-coherent receivers the local oscillator signal used for down-converting/ demodulating the received signal is independent of the transmitted signal. The IF phase noise in this case is given by,

$$\mathcal{L}_{IF}(f_m) = \mathcal{L}_{Tx}(f_m) + \mathcal{L}_{LO_{Rx}}(f_m). \tag{3.4}$$

Therefore, there is no phase-noise cancellation, resulting in noise sidebands independent of range. The actual level of the sidebands can be found using (3.4).

3.4.4 Phase noise in the processed signal

The final step in phase-noise modelling is to compute the effect of analog-to-digital conversion and signal processing on the IF signal. Some effects of the jitter transfer characteristics of analog-to-digital converters (ADC) can be found in [30]. A plethora of signal processing schemes is employed to extract useful information from radar signals, and their effect on the display phase-noise must be computed individually.

Some signal processing techniques are actually used to reduce the effects of phase noise. Here we only consider the effect of the Fast Fourier Transform (FFT) which is a common method of spectrum estimation. The resolution of the FFT is set by the time for which the signal is observed, T_{Obs} (for example, in FMCW radars this will be the sweep interval). If the ADC produces M samples during T_{Obs} at a sampling rate F_S, then $T_{Obs} = M/F_S$. The FFT integrates the spectral data in the "FFT bandwidth", B_{FFT}, to compute one FFT point, where,

$$B_{FFT} = \frac{1}{T_{Obs}} = \frac{F_S}{M}. \tag{3.5}$$

So the FFT bandwidth should be multiplied (added in dB-Hz) to the sidebands to get the final level of phase noise on the radar display.

$$\mathcal{L}_{Display}(f_m) = \mathcal{L}_{IF}(f_m) \times B_{FFT}. \tag{3.6}$$

The units of $\mathcal{L}_{Display}(f_m)$ are dBc (the /Hz drops due to multiplication with B_{FFT}). Equation (3.6) shows that lowering B_{FFT} (increasing T_{Obs}) reduces the integrated phase-noise sidebands.

Equations (3.3), (3.4) and (3.6) are valid for computing the noise-sidebands on a single target. They can be extended to generate the response of multiple targets by adding the IF response of each target after scaling and shifting according to the corresponding target cross-sections and ranges.

3.4.5 Noise Analysis

Once the phase noise has been modelled for the complete radar, one can perform phase-noise measurements at various points in the system. Mismatches between theory and measurements will give an idea of the additional noise produced by different sections of the system. If the noise level in any section is too high than predicted by the simulations, the design of that section should be investigated.

Filters and amplifiers also degrade the phase noise of the signal. However the effect of well designed filters and amplifiers is usually far less than the other stages mentioned above. If phase noise measurements don't conform to the theoretical prediction then the added phase-noise of filters and amplifiers should also be considered. AM noise and noise due to AM-PM conversion also appear as noise sidebands and must be measured and modelled if needed.

Once the phase noise inside a radar system has been characterised, the additional phase modulations introduced by the outside world (targets, atmosphere, etc.) can be measured and studied.

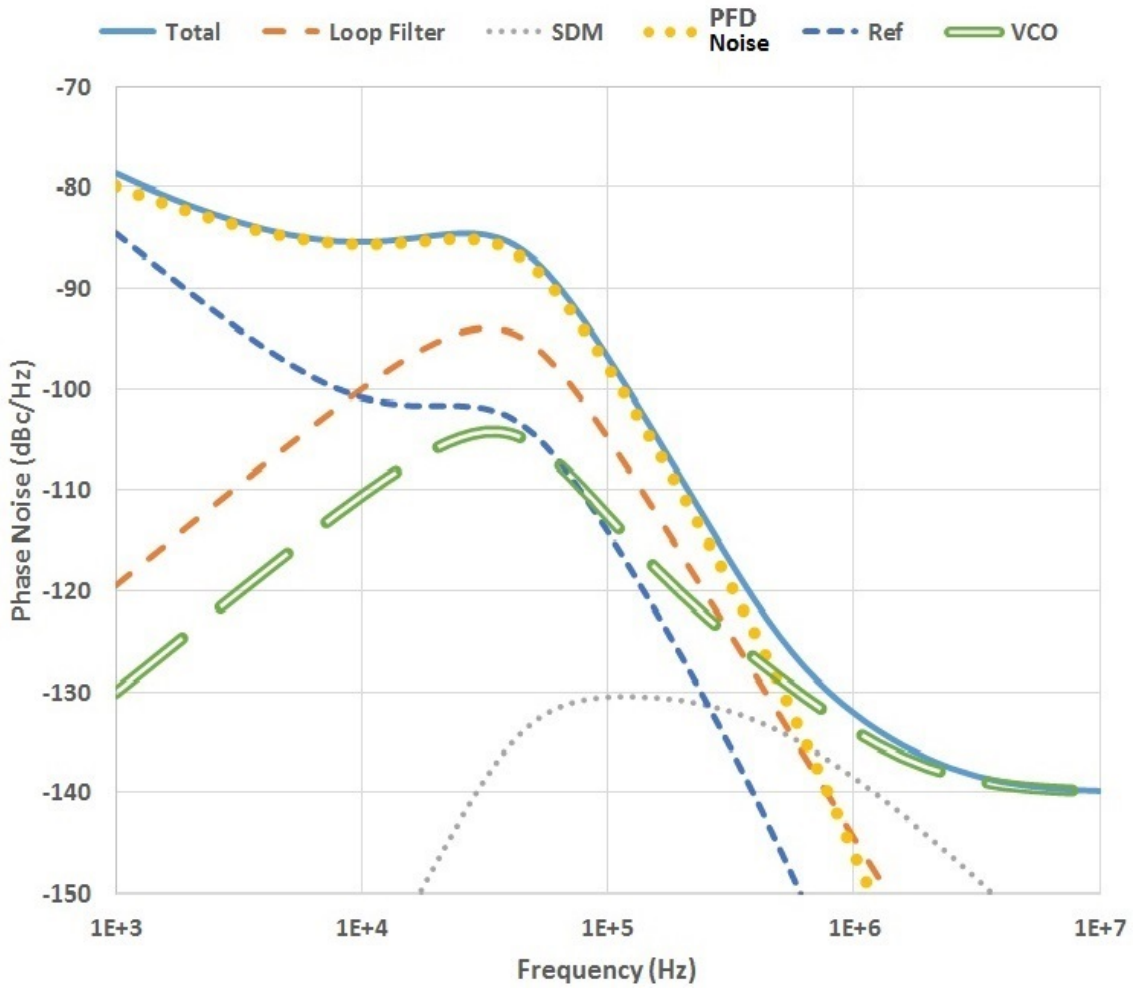

Figure 3.3: Phase noise modelling of the PLL showing contribution of the PLL's components, and the overall synthesiser phase noise $\mathcal{L}_{Synth}(f_m)$ (simulated using ADISimPLL software [45]).

3.5 Application of phase noise modelling to a MMW FMCW radar

We have applied the phase noise modelling method presented above successfully to model the phase noise on a 77 GHz MMW FMCW radar system for security applications. The synthesised radar signal is frequency multiplied to the transmit band, causing an increase in the transmitter's noise sidebands. A coherent receiver is implemented and FFT bin-size corresponding to 25 cm resolution.

3.5.1 Phase noise modelling for the frequency synthesiser

The radar system under consideration employed a phase-frequency detector (PFD) based phase-lock loop (PLL) synthesiser. Fig. 3.3 shows a phase-noise plot of a 9.5

GHz synthesiser produced using Analog Devices' ADISimPLL software [45]. The phase noise curves of the reference crystal oscillator, the voltage controlled oscillator (VCO), the loop filter, and the synthesiser chip are plotted (all multiplied up to 9.5 GHz). It can be noted from Fig. 3.3 that the PFD chip's phase noise is higher than both the multiplied-up crystal oscillator and the VCO, and, therefore, dominates a large portion of the in-band as well as the out-of-band phase noise causing an increase in the noise sidebands. From this modelling process we can see that, unlike a conventional PLL where the in-band noise is limited by the reference oscillator, the in-band noise in this case is limited by the PFD noise. Using a cleaner reference will not help to get better noise performance. Another thing to note with regard to the actual sidebands as measured on a spectrum analyser is that thermal noise will add to the phase noise.

3.5.2 Relation for phase noise sidebands versus target range

An interesting relationship can be derived for the ratio of the close-in phase noise-sidebands on two targets at ranges R_1 and R_2, corresponding to time delays τ_{d1} and τ_{d2}, with phase noises $\mathcal{L}_{Display}(f_m)|_{\tau_{d1}}$ and $\mathcal{L}_{Display}(f_m)|_{\tau_{d2}}$ respectively. Using (3.6) and (3.3), and cancelling the common terms, we can write,

$$\frac{\mathcal{L}_{Display}(f_m)|_{\tau_{d1}}}{\mathcal{L}_{Display}(f_m)|_{\tau_{d2}}} = \frac{\mathcal{L}_{IF}(f_m)|_{\tau_{d1}}}{\mathcal{L}_{IF}(f_m)|_{\tau_{d2}}} = \frac{\sin^2(\pi f_m \tau_{d1})}{\sin^2(\pi f_m \tau_{d2})}. \tag{3.7}$$

For close-to-carrier offsets, f_m is small and the approximation $\sin(\theta) \approx \theta$ can be used. For example, a target at 600 m has $\tau_d = 4\mu s$, and an offset as large as f_m=50 kHz will make $\pi f_m \tau_d = 0.2\pi$, making the approximation valid. Therefore,

$$\frac{\mathcal{L}_{Display}(f_m)|_{\tau_{d1}}}{\mathcal{L}_{Display}(f_m)|_{\tau_{d2}}} = \frac{(\pi f_m \tau_{d1})^2}{(\pi f_m \tau_{d2})^2} = \left(\frac{\tau_{d1}}{\tau_{d2}}\right)^2 = \left(\frac{R_1}{R_2}\right)^2. \tag{3.8}$$

For example, for two point targets at 170 m and 770 m respectively, computing (3.8) we get,

$$\left(\frac{R_1}{R_2}\right)^2 = \left(\frac{170}{770}\right)^2 = 0.05 = -13\ dB. \tag{3.9}$$

Reading in context, the noise sidebands on the 170 m target will be approximately 13 dB *lower* than the sidebands on the 770 m target. Although (3.8) is an approximation, it conforms to the measurements presented in the next section.

3.5.3 Coherent cancellation of phase noise

The equations shown in the previous section were modelled for a 77 GHz MMW radar system employing the frequency synthesiser modelled in Fig. 3.3. Fig. 3.4 shows the modelled phase noise response curves for point targets at ranges from 10 m up to 200 m. The main highlight of this figure is the level of phase noise cancellation due to coherent mixing in the receiver. At 10 m, the cancellation results in a peak sideband level of -68 dBc, which results in a huge improvement in detection and tracking. At 100 m, the peak sideband level is around -48 dBc, which degrades to -42 dBc for a target at 200 m. Phase noise cancellation happens only to the left of the dotted vertical line shown in the figure. It can thus be seen that the region of phase noise cancellation shrinks with increasing range.

Fig. 3.5 plots the peak level of phase noise from Fig. 3.4 versus target range. It can be noticed that phase noise level at 50 m is 12 dB better than at 200 m. This definitely helps with target detection. However, we note that this level of improvement does not solve the phase noise problem entirely for, say, a radar having 100 dB of dynamic range. Beyond 200 m the phase noise cancellation starts levelling off. The phase noise level at 200 m is only 3 dB better than at 300 m. In practical terms this does not represent a significant improvement. The horizontal dashed line in Fig. 3.5 shows the phase noise level at the transmitter. Therefore, a target at 300 m will be expected to have the same peak phase noise level as the in-band phase noise level at the transmitter.

3.6 Practical Measurements of Phase Noise Sidebands using a Triangular Corner Reflector

The theoretical results of the previous section were validated using practical measurements presented in this section. Fig. 3.6 shows a 25 m^2 triangular corner reflector (referred to as the *corner cube*) on a tripod stand that was used for these measurements. As evident from Fig. 3.6, grass and hedges etc. are also present in the scene and cause unwanted backscatter.

Fig. 3.7 to Fig. 3.12 show the measured responses of the corner cube placed at distances of 35 m, 85 m, 101 m, 120 m, 173 m, and 203 m from the radar. 50 averages were used to reduce the thermal noise in the display. The remaining variations in the scene are due to the clutter response. The peak phase noise sideband response of the corner cube can be estimated from these figures as -50 dBc, -45 dBc, -44 dBc, -44 dBc, -41 dBc and -38 dBc respectively.

It can be noted that the measured results are not exactly equal to the theoretical

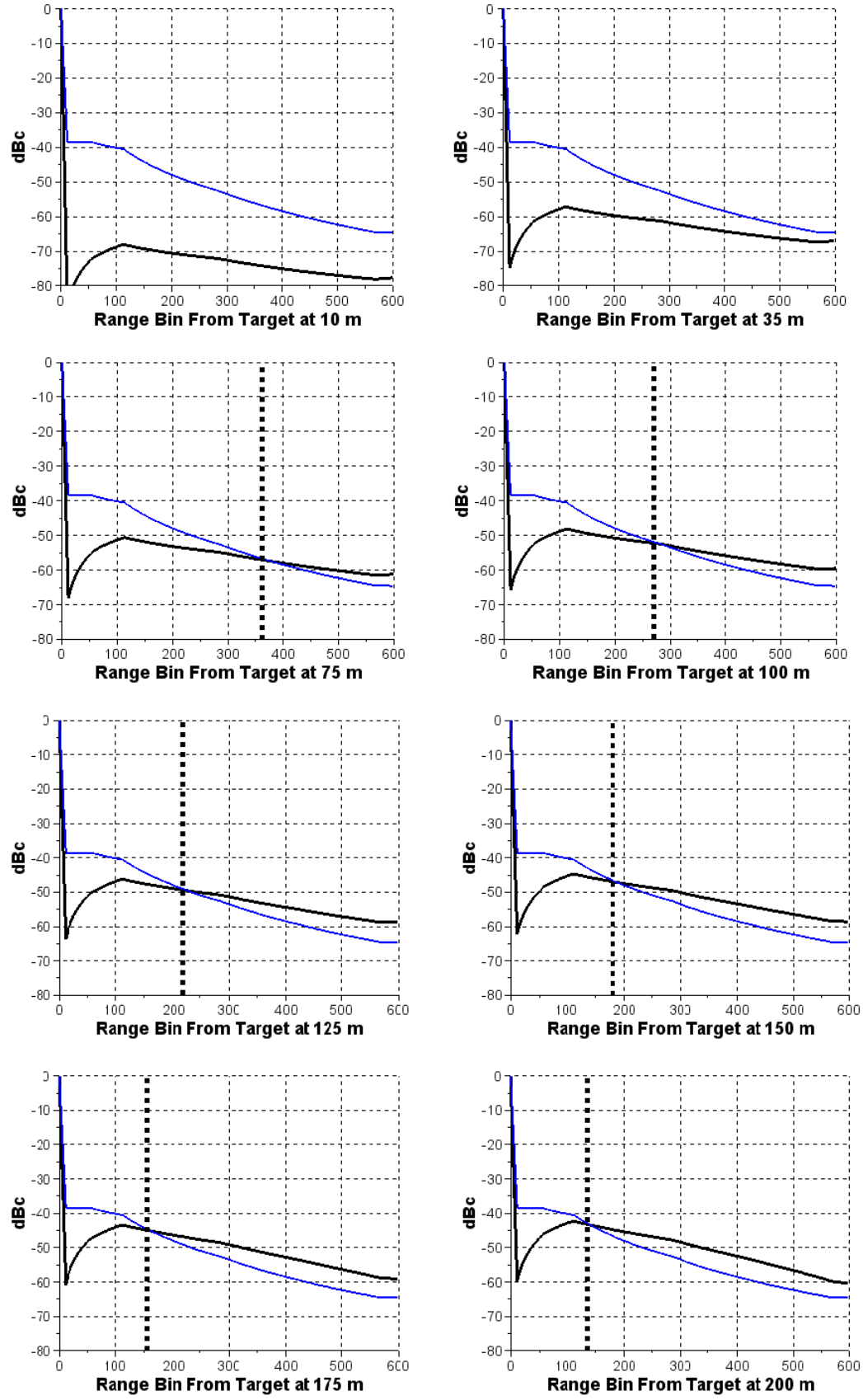

Figure 3.4: Calculated target responses at various ranges. The phase noise decorrelation patterns can be seen. The blue overlay is the expected phase noise without taking decorrelation into account.

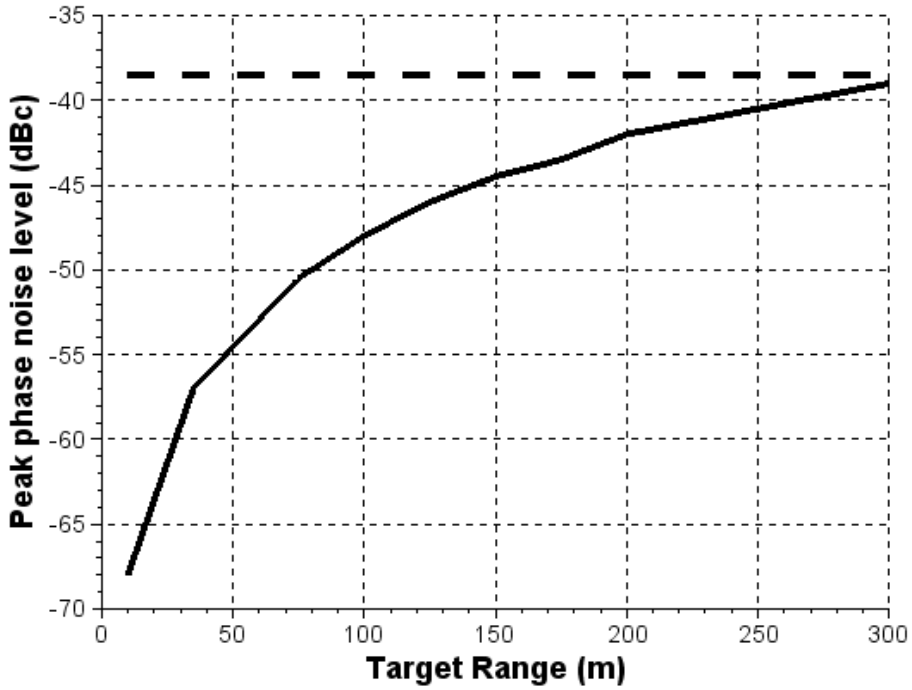

Figure 3.5: Plot of the peak phase noise level versus target range. The horizontal dashed line is the transmitter's peak phase noise level.

Figure 3.6: Triangular corner reflector placed in the scene being measured.

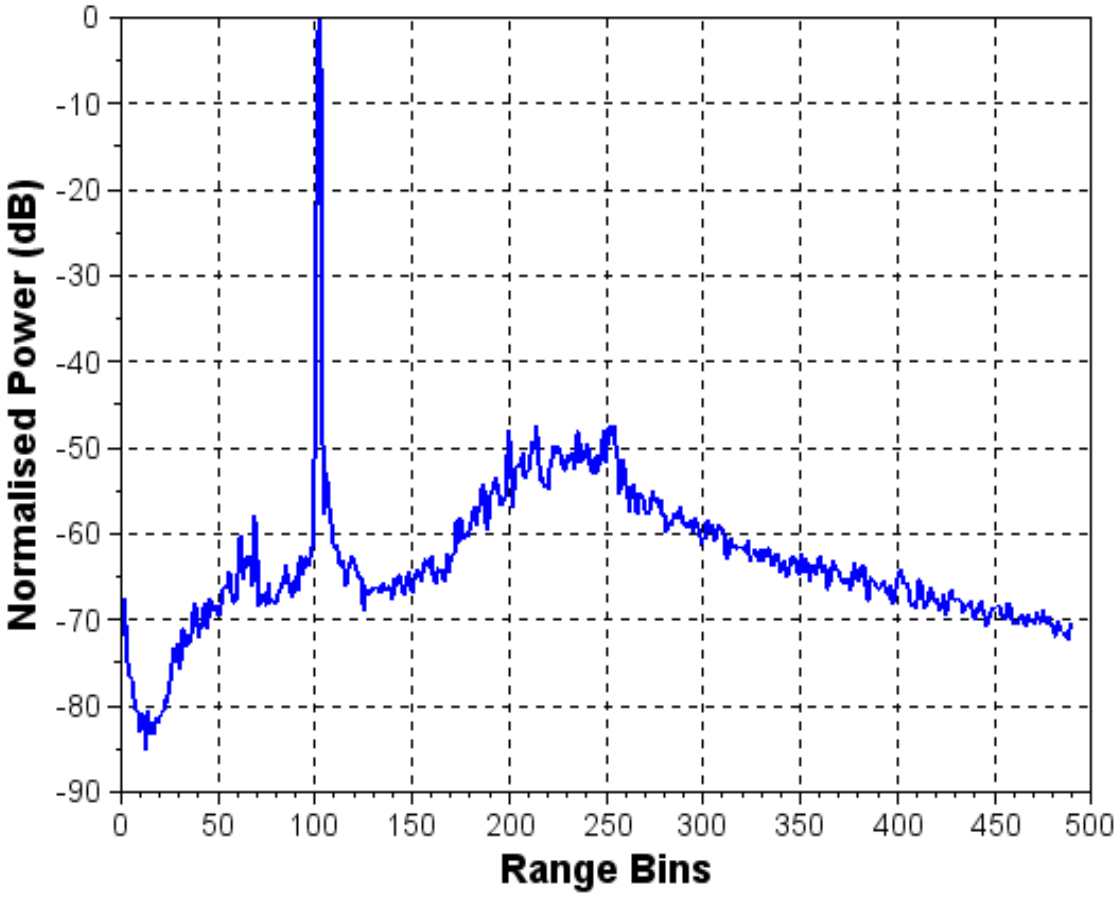

Figure 3.7: Target response of a triangular corner reflector placed at 35 m.

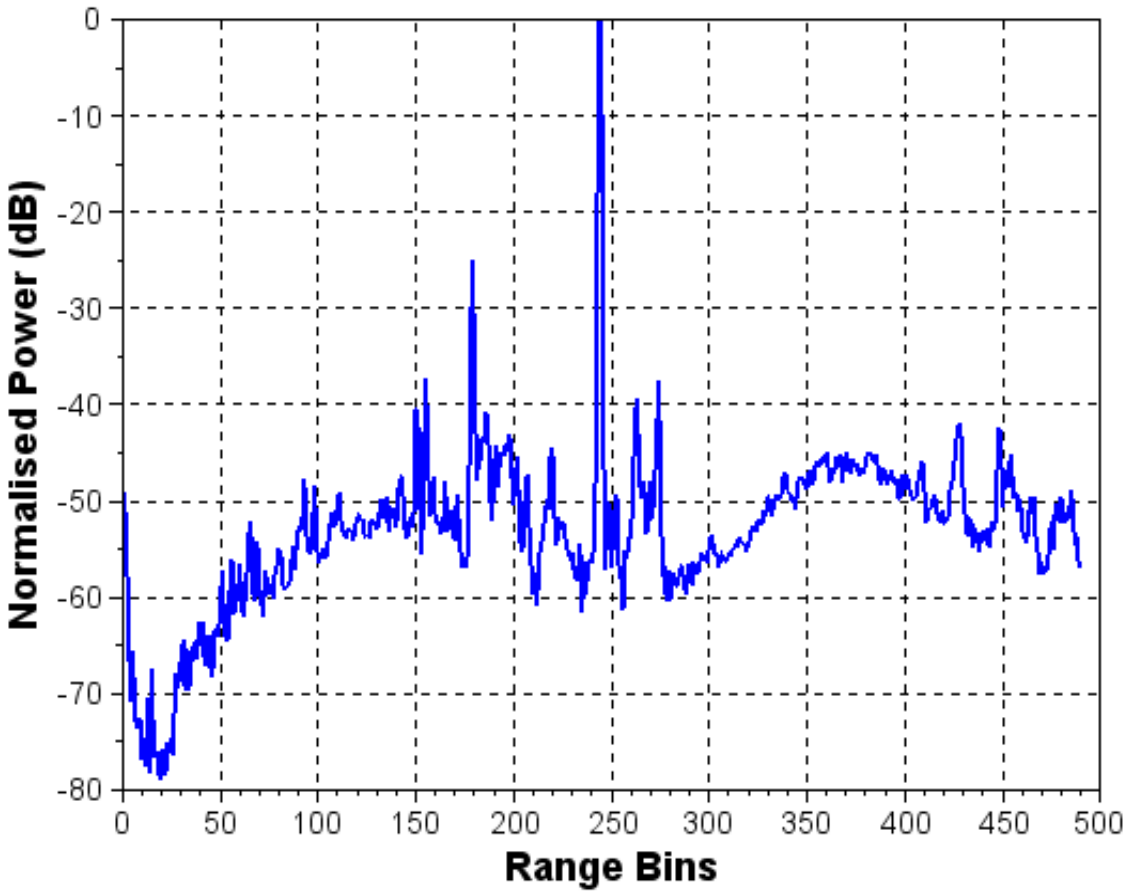

Figure 3.8: Target response of a triangular corner reflector placed at 85 m.

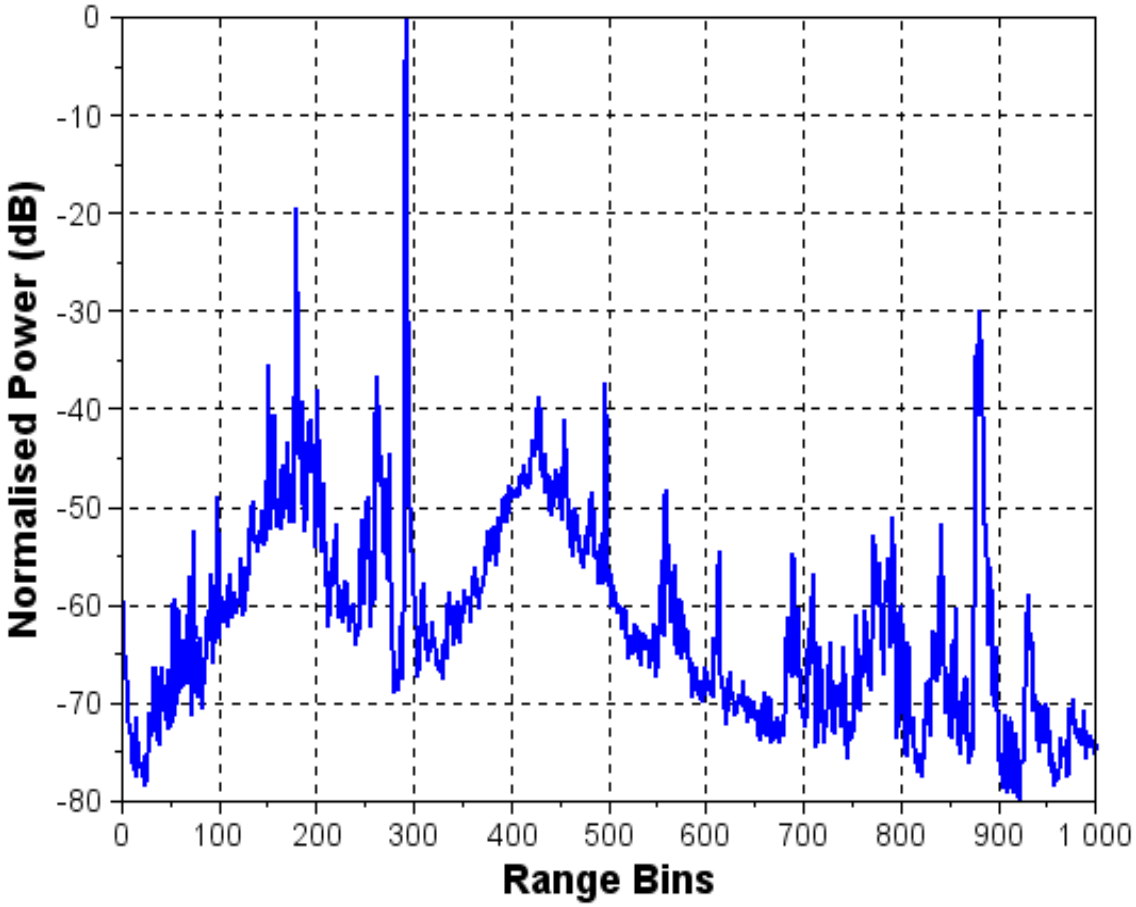

Figure 3.9: Target response of a triangular corner reflector placed at 101 m.

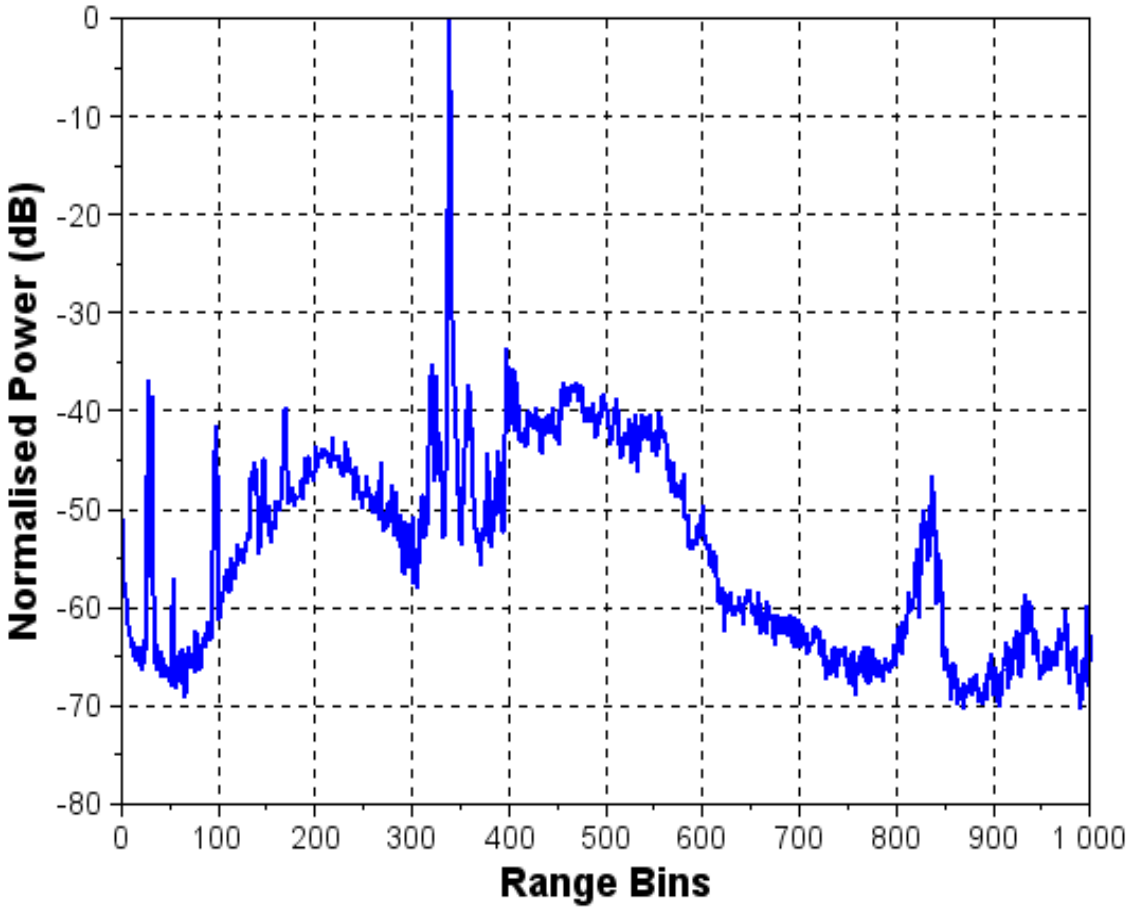

Figure 3.10: Target response of a triangular corner reflector placed at 120 m.

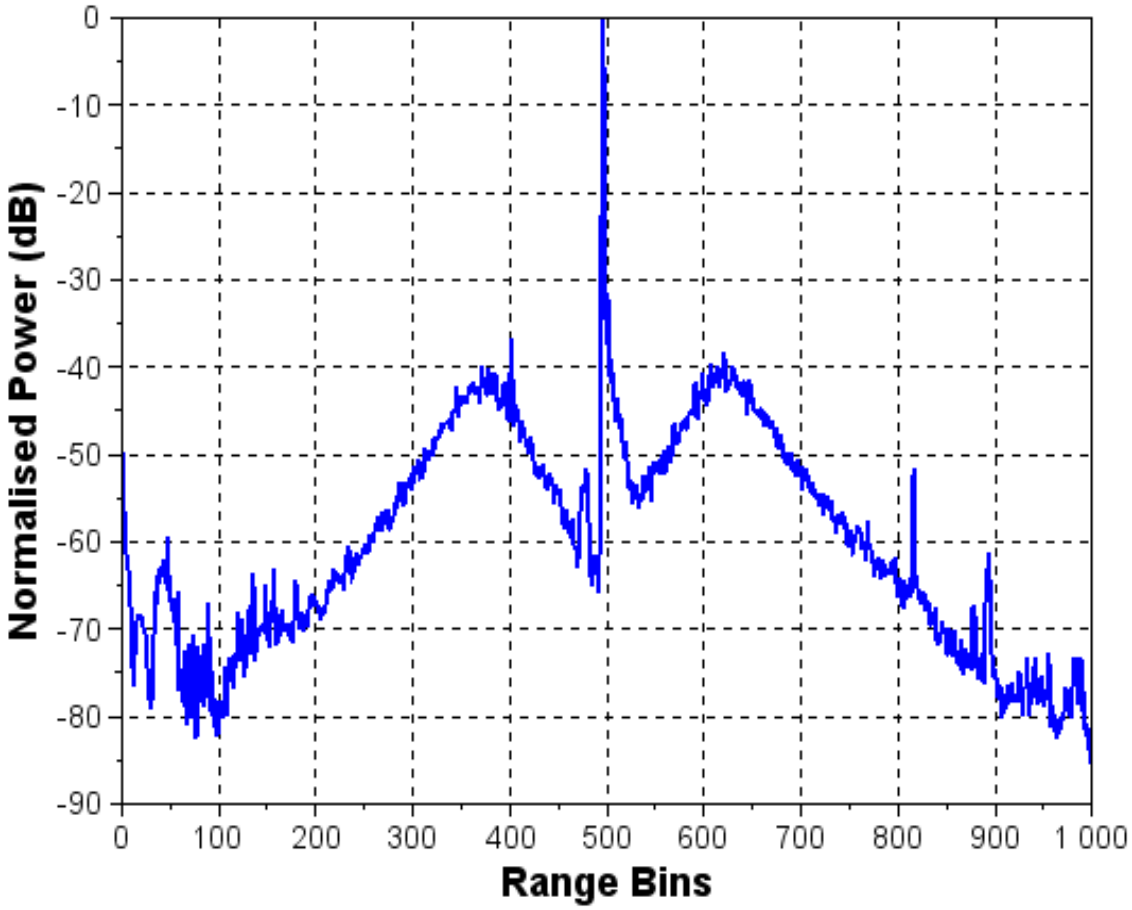

Figure 3.11: Target response of a triangular corner reflector placed at 173 m.

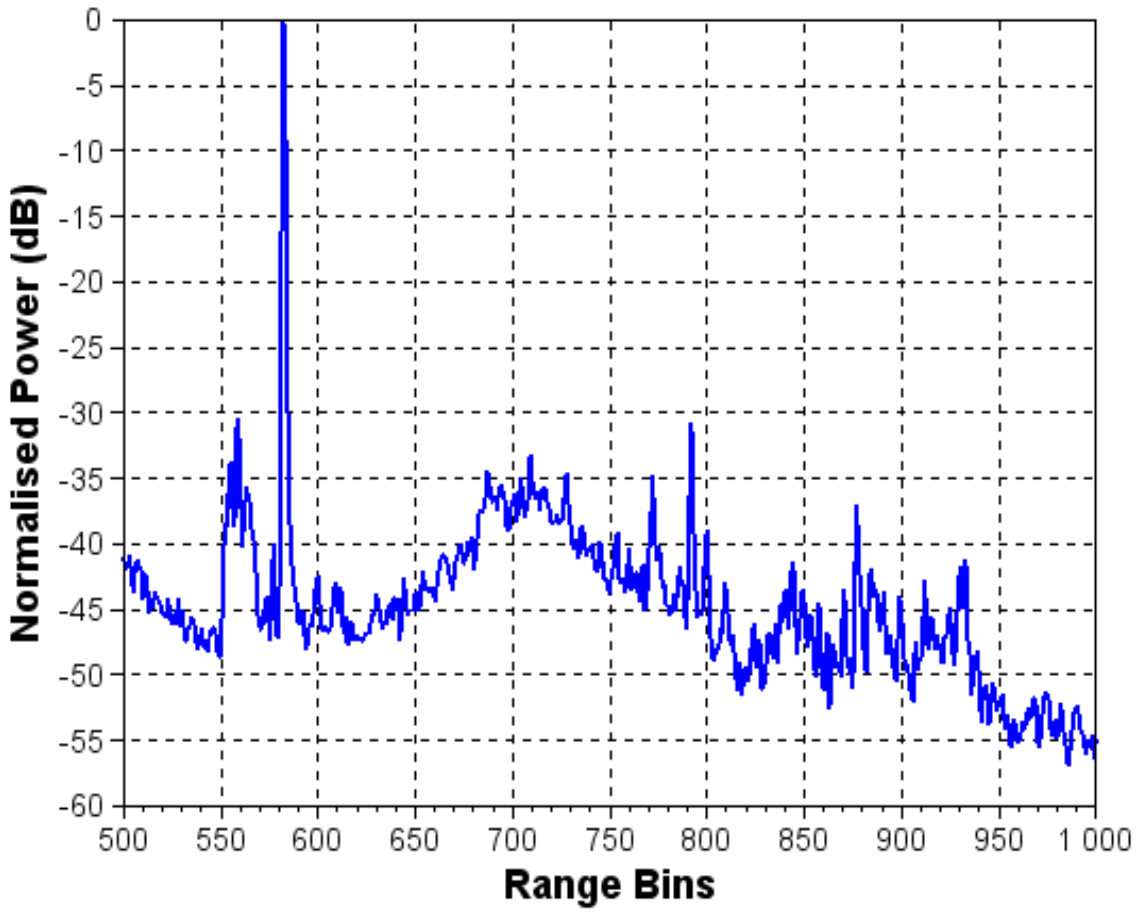

Figure 3.12: Target response of a triangular corner reflector placed at 203 m.

prediction of Fig. 3.5. However, it can be concluded that they are reasonably close considering that some level of clutter is also present.

3.7 Target Response of a Moving Vehicle

Fig. 3.13 illustrates the decrease in phase noise cancellation with increasing range for a moving vehicle. The plots (a)-(e) display measurements done in a tunnel environment. The abscissa shows range in meters, and the ordinate shows the relative power levels as a percentage. Due to the native radar format, 1% $\approx$ 1.28 dB on the ordinate. Clutter-map averaging was used to reduce the variability in the scene to get a better idea of the phase noise levels.

In Fig. 3.13a, the double-arrow marks the phase noise sidebands on a vehicle at 170 m. The size of the sidebands can be estimated as roughly 32 % = -41 dBc. In Fig. 3.13b-e, the vehicle moves from around 240 m to 300 m: it can be noticed that there is very little change in the sideband response. The sidebands are at approximately 26 % = -33 dBc. This implies that the phase noise response of the vehicle at 170 m is around 7 dB lower. This result clearly indicates our hypothesis that phase noise cancellation in coherent radars is ineffective beyond a few hundred meters.

3.8 An Alternative Low Phase Noise Frequency Synthesiser

The system-level noise analysis based on Fig. 3.3 reveals that the source phase-noise in the PLL frequency synthesiser did not meet the phase noise requirement of the LRS system. The phase noise sidebands raise the noise floor in a large region. In Fig. 3.3, the reference clock's phase noise has been reduced to a level where its contribution to the overall phase noise curve is insignificant. Therefore, it is apparent that the frequency synthesiser's architecture has to be changed to achieve the desired level of phase noise improvement. The potential alternatives explored in this work were mentioned in Section 2.4.4.

Fig. 3.14 shows the simulated phase noise plot of the final solution that was actually implemented in the LRS system is described. The measured phase noise of the PLL synthesiser is also included for comparison. It can be seen that a remarkable improvement of more than 30 dB was expected in the critical portion of the phase noise spectrum (10 kHz to 100 kHz) using this technology.

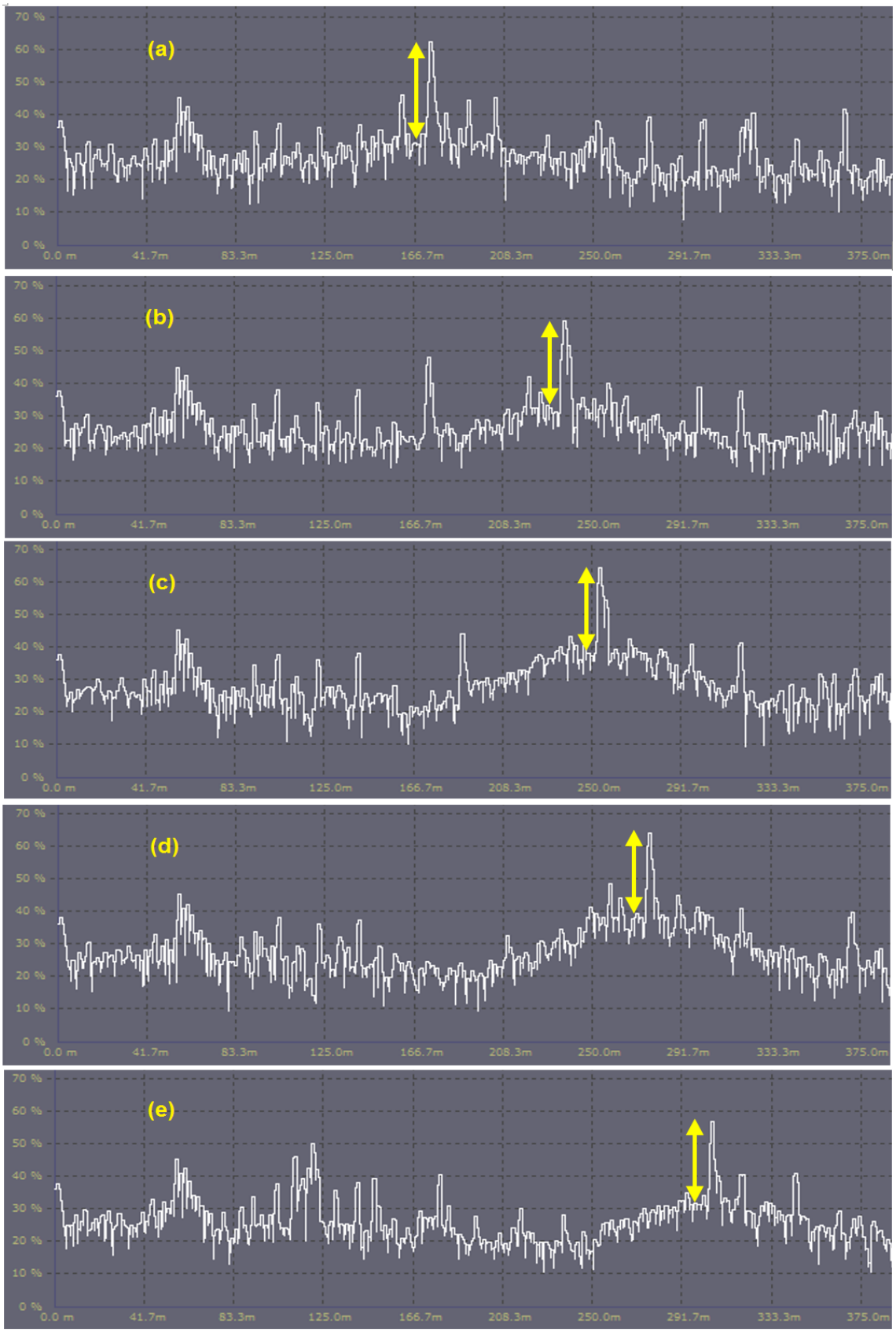

Figure 3.13: Illustration of the phase noise sidebands around a moving target.

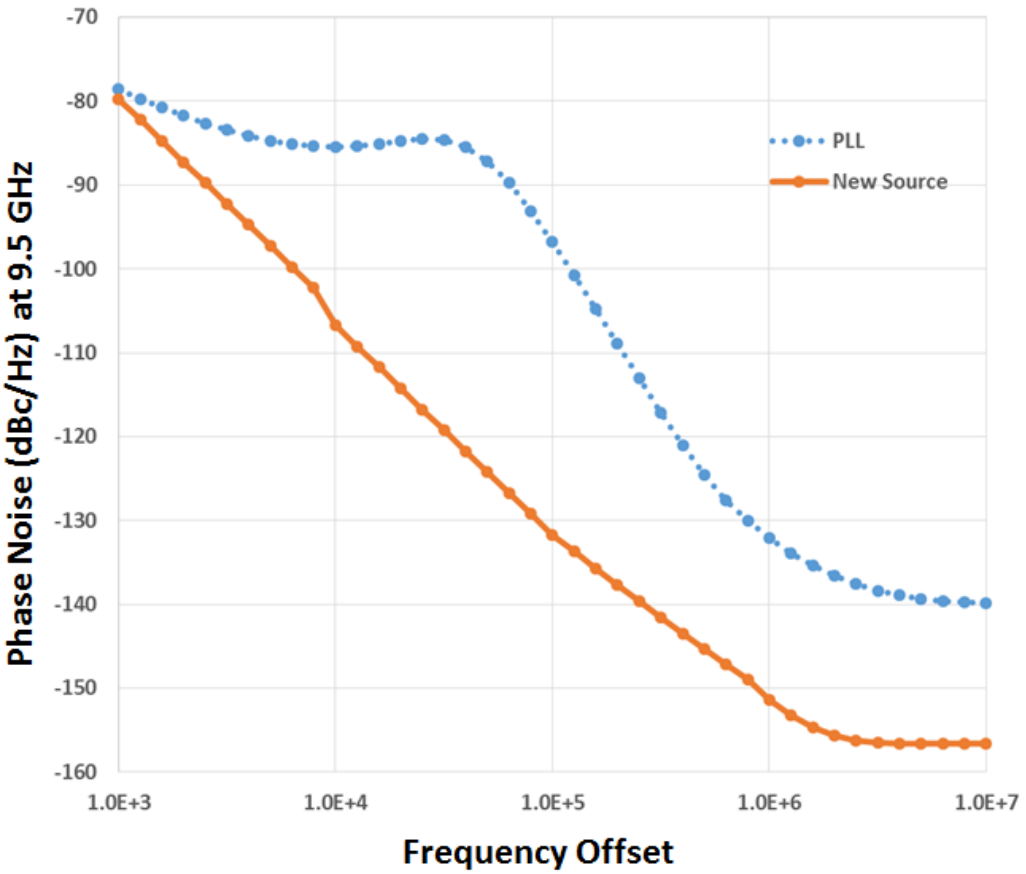

Figure 3.14: Comparison of Phase Noise in the new low phase noise Synthesiser (bottom) with the PLL Synthesiser.

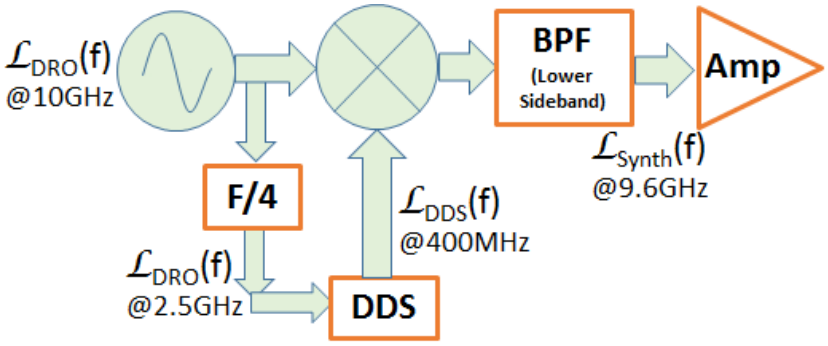

Figure 3.15: Block diagram of the DDS/DRO Frequency Synthesiser

3.8.1 The DDS-Based Frequency Synthesiser

Fig. 3.15 shows a block diagram of the designed frequency synthesiser that uses a 10-GHz DRO acting as the carrier signal. A DDS is used to synthesise the transmit waveform: a swept bandwidth of 120 MHz centred at 440 MHz. The DRO, through a divide-by-4 frequency divider, generates the clock signal for the DDS. The DDS signal is then mixed with the carrier to generate the X-band signal which is filtered and amplified to generate the final waveform. (Although not shown here, the generated waveform was multiplied by 8 to generate the 77 GHz radar signal.)

3.8.2 Phase noise analysis of the DDS solution

Fig. 3.16 shows a phase noise plot showing the phase noise contribution of the major components of the synthesiser. The phase noise contribution of the frequency divider, the mixer, the filter, and the amplifier are not shown as their contribution was much lower than the DDS and DRO themselves. It can be seen that a remarkable improvement of around 35 dB was expected using this technology in the critical portion of the phase noise spectrum (i.e. at the 100 kHz offset). A microwave system simulation was done to finalise the selection of the RF components for this design, followed by the schematic capture and the layout of the microwave PCB. The final microwave PCB has been successfully implemented in the LRS system. The said improvement in the phase noise was then validated through the practical measurements appearing in Chapter 4.

3.9 Conclusion

This chapter presented phase noise modelling for FMCW radar systems. Detailed guidelines for the phase noise modelling of various components and sub-systems were presented followed by techniques to reduce phase noise at each level. The

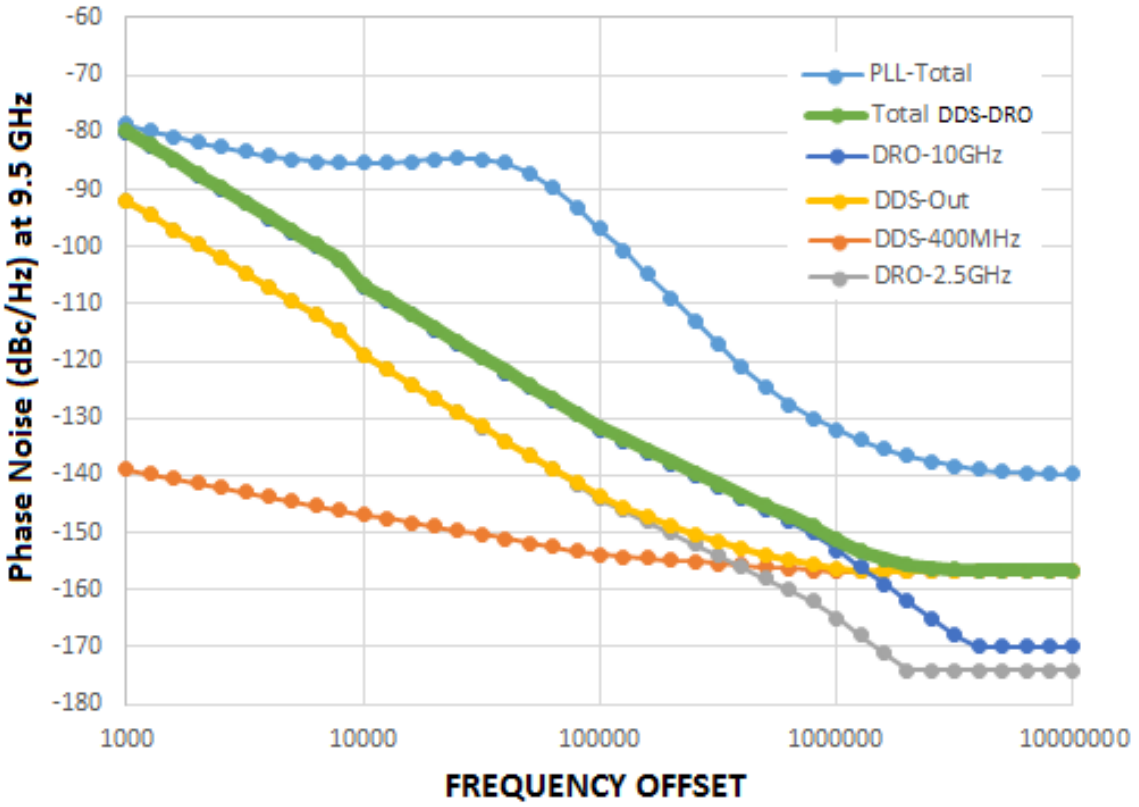

Figure 3.16: Comparison of Phase Noise in the new low phase noise synthesiser with the PLL synthesiser.

modelling was validated using practical measurements from a MMW FMCW radar system. The measurements were done on a triangular corner reflector, and a moving vehicle. Phase noise measurements combined with phase noise modelling help in the system-optimisation process. A relation for the relative sideband levels for targets at different ranges was also derived and validated. The analysis demonstrated that PLL-based frequency synthesisers cannot meet the phase noise requirements of high-dynamic range long-range radar systems. Therefore, the analysis of a low phase noise frequency synthesiser was presented that has the potential to solve the phase noise problem. The measurement results presented were in reasonable conformance with the theoretical calculations. Although the presented method of phase-noise analysis focused on FMCW radars, the developed insight is also useful for other types of radar as well.

Chapter 4

Phase Noise in FMCW Radar Systems[1]

4.1 Summary

Phase noise is one of the fundamental performance parameters in modern radar, communication, spectroscopic, and meteorological systems. In this chapter a phase noise theory has been developed for FMCW radar systems. A new design equation has been derived to specify the maximum bound on the allowable source phase noise level in radar systems. The non-linear phase noise decorrelation function due to coherent mixing has been analysed for propagation delays less than the coherence time of the reference oscillator, and the spectral broadening of target responses has been discussed for delay times greater than the coherence time. The effects of the subsystems in the transceiver chain are presented and a new model of phase noise in ADCs is discussed. Phase noise modelling techniques are presented, followed by a comparison of a PLL frequency synthesiser with a low-noise frequency synthesiser to demonstrate the reduction of phase noise sidebands for improved detection and tracking performance. Practical measurements from two millimetre wave FMCW radar systems utilising the two frequency synthesisers have been presented to validate the developed theory.

4.2 Introduction

A *perfect* monochromatic sinewave is an idealisation available only in textbooks. All natural and man-made oscillators (whether optical, electronic, acoustic, atomic, or any other) exhibit phase and frequency instabilities collectively known as *Phase*

[1]A large part of this chapter has been submitted for publication in [46].

Noise. These instabilities are related to the materials making up the oscillator, the architectural design of the oscillator, and the random noise phenomena in the oscillator. The present chapter deals with the analysis of phase and frequency instabilities in the oscillators used in frequency modulated continuous wave (FMCW) radar systems

It is well-known that the short-term frequency instability in oscillators, described by the phase noise, manifests itself as phase modulation sidebands in oscillator spectra [24,47,48]. Linear phase noise analysis [13,26,43,49] deals with the analysis of the low-noise sidebands only in the RF spectrum of an oscillator [26, 27, 43]. However the phase noise processes also give rise to a nonlinear near-carrier spectrum [11, 50–52], a phase noise *floor*, and broadening of the linewidth of the oscillator signal's RF spectrum [51, 53, 54]. A complete phase noise analysis must include all portions of the RF spectrum.

Excessive phase noise in an oscillator (greater than 1 rad^2) leads to severe distortion in the RF spectrum in the form of a widened central peak and distorted sidebands. A designed coherent radar system should have an integrated phase noise much less than 1 rad^2. An analysis will be presented in this chapter as the phase noise in a signal approaches this limit under frequency multiplication and new results will be presented for the allowable noise-sideband level in the transmitted signal to comply with this limit. The noise sideband response produced by radar systems is a function of the target's range (i.e. time delay) [26] and even if a low-phase noise master oscillator is employed in a radar, the demodulated return signal loses *coherence* with the transmitted signal due to the frequency drift processes present in the oscillator. Therefore, a coherent radar should operate well within the *coherence time* of the oscillator [53, 55] to avoid excessive broadening of the demodulated signal's spectrum.

The problem of phase noise in pulsed radar systems has been addressed extensively in the literature. Detailed phase noise analysis is available for MTI and pulse Doppler radars [56, 57], digital phased array radars [58], distributed synthetic aperture radars (SAR) [59], interferometric SAR [60], efficient simulation of phase noise [61] and AM/FM noise measurement [62]. Phase noise in FMCW radars has not received such a detailed attention. The present chapter attempts to fill in some of this void.

From the systems aspect, phase noise in FMCW radars has been addressed from various aspects in [42,43,63,64]. In [43] the fundamentals of FMCW system design have been presented including some noise aspects. In [42] the impact of coherent integration on phase noise has been addressed. In [63] the impact of oscillator noise parameters like the noise figure and the corner frequency on the phase noise

performance has been analysed. In [43] and [64] the impact of the internal noise leakage through the receiver's mixer has been analysed in detail. An important aspect of the present work is the demonstration of how to accurately relate the source phase noise to the phase noise in the IF signal's spectrum by quantifying the phase noise introduced by the various stage of a typical FMCW radar system, and the demonstration of the reduction in phase noise by utilising a properly designed radar source. Using those guidelines one can work back to determine the source phase noise level required to achieve a given specification of dynamic range.

The contributions of this chapter are as follows:

1. Development of the phase noise models of the subsystems to present a phase noise modelling methodology for FMCW radar systems.

2. Demonstrate the application of the modelling methodology for the accurate modelling of phase noise in a practical radar system..

3. Demonstrate the benefits of using a low-phase noise frequency synthesiser to achieve high dynamic range target discrimination.

4. Present new results on phase jitter cancellation in analog-to-digital converters

5. Derivation of a novel design equation to prevent excessive demodulated phase noise due to the source phase noise and/or frequency multiplication in the transmitter.

4.3 Characterisation of Phase Noise in the RF Spectra

Phase noise in oscillators is most popularly characterised by the *spectral density of phase fluctuations* $S_\phi(f)$ that normally has power law frequency components [8]. On the other hand, practical radio, radar, and spectroscopic systems, to name a few, use the RF spectrum of the oscillator $S_{RF}(f)$ as the *working* spectrum during their operation, and will be the focus in the foregoing discussion. Fig. 4.1a illustrates the RF spectrum $S_{RF}(f)$ of a general oscillator. When the sidebands in $S_{RF}(f)$ are due to phase modulation (PM) noise they are referred to as *Phase noise* sidebands, are denoted by $\mathcal{L}(f) = S_{RF}(f)/P$ (where P is the total power in the measured oscillator signal), and have the units of decibels relative to the carrier per Hertz (dBc/Hz).

As shown in Fig. 4.1a the frequency offset f_α divides the phase noise portion of the spectrum into two part, i.e., the near-carrier phase noise and the far-from-carrier

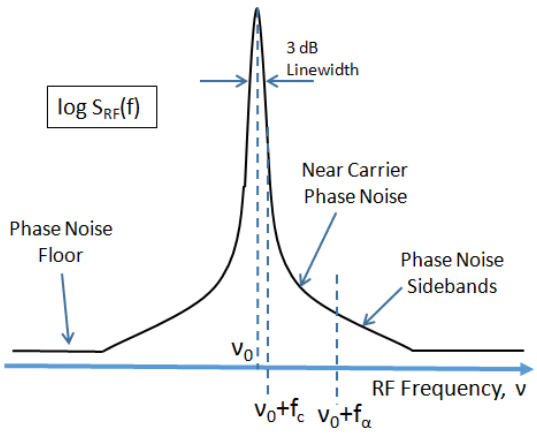

(a) RF spectrum of a general oscillator.

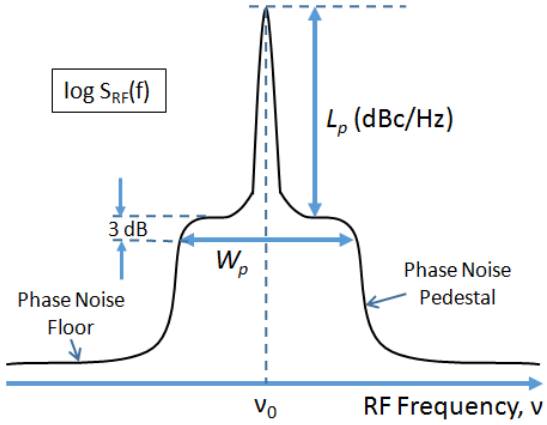

(b) RF spectrum of a synthesised signal source, including the noise pedestal's parameters.

Figure 4.1: Illustration of the RF spectra of radar sources.

phase noise. The IEEE Standard 1139-1999 [8] defines phase noise as,

$$\mathcal{L}(f) = \frac{S_\phi(f)}{2}. \tag{4.1}$$

The $\mathcal{L}(f)$ in this definition is related to $S_{RF}(f)$ only in the far-from-carrier region, i.e., for all $f \geq f_\alpha$ such that,

$$\int_{f_\alpha}^{\infty} S_\phi(f)df = 0.1 \text{ rad}^2. \tag{4.2}$$

Below f_α, $S_{RF}(f)$ is nonlinearly related to $S_\phi(f)$. A nonlinear relationship between $S_\phi(f)$ and the normalised two-sided baseband RF spectrum $S^b_{RF}(f)$ is given in [11, 50, 51] as,

$$S^b_{RF}(f) = e^{-\sigma^2_\phi}\left[\delta(f) + S_\phi(f) + \frac{1}{2!}S_\phi(f) * S_\phi(f) + ...\right], \tag{4.3}$$

where σ^2_ϕ is the variance of the phase noise process $\phi(t)$, or equivalently,

$$\sigma^2_\phi = \int_{-\infty}^{\infty} S_\phi(f)df, \tag{4.4}$$

and is assumed to be finite. Equation (4.3) can be used to model the near-carrier phase noise as well as the far-from-carrier phase noise, although in the latter case (4.1) is easier to use. In (4.3) the carrier has been modelled as a Delta function: in practice $S_{RF}(f)$ has a finite linewidth and a defined lineshape that are a function of the frequency noise processes in the oscillator. These are dealt with in [51, 53].

Fig. 4.1b illustrates a typical target spectrum displayed by a radar system employing a synthesised signal source. The phase noise *pedestal* can originate due to a phase locked loop (PLL) based synthesiser having a finite *loop bandwidth*, or due to the finite bandwidth of the frequency multiplier chain being employed in the system to frequency multiply, say, a crystal reference oscillator to higher frequencies. A detailed analysis of the behaviour of the noise pedestal under frequency multiplication can be found in [51, 65, 66] where measurements of the noise sidebands have been presented.

Equation (4.3) can also be written as,

$$S^b_{RF}(f) = S^c_{RF}(f) + S^p_{RF}(f), \tag{4.5}$$

where $S^c_{RF}(f)$ is the RF spectral density of the central carrier peak and $S^p_{RF}(f)$ is the RF spectral density of the phase noise pedestal. For linear phase noise analysis one has to invoke the low-phase noise condition, $\sigma^2_\phi \ll 1$. Under this condition (4.3) simplifies to:

$$S^b_{RF}(f) \approx e^{-\sigma^2_\phi} \left[\delta(f) + S_\phi(f)\right]. \tag{4.6}$$

The phase noise pedestal shown in Fig. 4.1b can be modelled by a modified Lorentzian function as follows:

$$S^p_{RF}(f) = \frac{L_p}{1 + \left(\frac{|f|}{0.5W_p}\right)^k}, \tag{4.7}$$

where $S^p_{RF}(f)$ is the double-sided RF spectral density of the noise pedestal, L_p is the flat-top level of the pedestal (in dB-rad^2/Hz)^2, W_p is the 3-dB width of the noise pedestal in Hz, and k is the order of the roll-off and is generally between 2 and 4 for microwave frequencies. Under the low-phase noise condition, σ^2_ϕ can also be computed from $S^p_{RF}(f)$ as,

$$\sigma^2_\phi = \int_{-\infty}^{\infty} S^p_{RF}(f) df. \tag{4.8}$$

The assumption of finite σ^2_ϕ in (4.3) is only valid for a finite observation time T_{obs} (or measurement time) for the oscillator signal [49, 67–69], which in fact is equivalent to defining a non-zero low-frequency cutoff at $1/T_{obs}$ for the phase noise spectrum [68]. For excessively large measurement times, the flicker frequency and random-walk frequency components of phase noise cause excessive broadening of the measured RF spectrum [68–71].

Phase noise can be equivalently defined by the *timing jitter* in oscillators. The

[2]These units are numerically equal to Watts/Hz

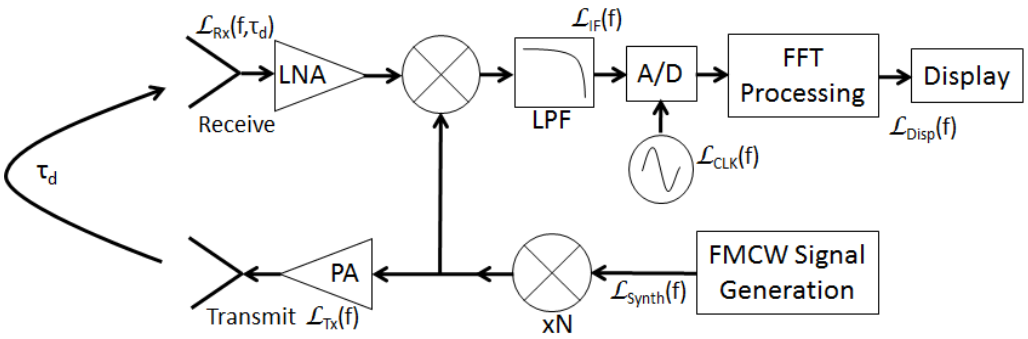

Figure 4.2: Block diagram of a general FMCW radar system. The phase noise $\mathcal{L}(f)$ at various points in the system is marked.

RMS timing jitter σ_t in a signal having a nominal radian frequency of $\omega_0 = 2\pi\nu_0$ is related to σ_ϕ^2 as [38],

$$\sigma_t = \omega_0 \, \sigma_\phi. \tag{4.9}$$

The timing jitter formulation of phase noise is especially helpful when analysing phase noise in ADCs.

4.4 Phase noise in the Electronic Subsystems

Fig. 4.2 shows a block diagram of the system under consideration which is a basic homodyne FMCW radar system. The *FMCW Signal Generation* block synthesises the FMCW waveform which is frequency multiplied up to the transmit frequency band using the $\times N$ frequency multiplier. The received signal is frequency mixed with the transmitted signal using a mixer: the difference frequency between the transmit and the receive is proportional to the target's range [43] and is called the intermediate frequency (IF) signal. The IF signal is digitised using an analog-to-digital converter (ADC or A/D). Complex Fast Fourier Transform (FFT) processing is then used to extract the information about targets like range, phase, signal strength, etc. In the following the phase noise contribution of these electronic subsystems is discussed.

4.4.1 Frequency Synthesisers

Indirect and direct frequency synthesisers [34,36,38] are used to generate the desired transmit waveform in radar systems. Popular examples include Phase Lock Loops (PLL), Direct Digital Synthesisers (DDS), and variants based on these.

In PLL based frequency synthesis it is well-known that inside the loop filter's bandwidth, the reference oscillator's phase noise dominates, while outside the loop bandwidth the voltage controlled oscillator's (VCO) phase noise dominates [38].

Modern phase-frequency detector (PFD) based PLL's are versatile in that they perform automatic phase and frequency locking [38]. However for high dynamic range radar applications the phase noise performance of PFDs may not be acceptable [27] leading to high levels of in-band phase noise. The PLL-synthesised signal has a spectrum of the type shown in Fig. 4.1b which shows a noise pedestal around the carrier frequency.

To reduce the noise pedestal one could play with the loop parameters of the PLL. However, in the Type-2 PLL scheme [38] commonly employed, the synthesised waveform sets a limit on the modulation bandwidth needed from the PLL. In the case of FMCW radars this is the bandwidth required to correctly synthesise the ramping waveform: incorrect loop parameters can cause ringing and cycle slipping in the transient response of PLLs. PLL synthesisers have been discussed in [72–74] in the context of FMCW radar systems.

Offset PLLs [39, 40, 75] have been used successfully to improve the phase noise performance over conventional PLLs. Offset PLLs combine frequency mixing with frequency division in the feedback path to reduce the overall frequency multiplication factor inside the loop. The overall architecture is complicated by the use of DDS sources for frequency sweeping and the spurii generated by the DDS and the mixer have to be filtered. State-of-the-art DDS synthesisers have better phase noise than PLL synthesisers although they are costlier, and they suffer from spurii problems [36]. The DDS output usually needs to be frequency mixed to the desired frequency band, and mixers produce their own spurii.

Parasitic nonlinearities in the linear FMCW waveform due to, for example, non-linear tuning curves of voltage controlled oscillators (VCO), also lead to spectral broadening but are considered systematic noise [75–78] as opposed to phase noise that is random in nature. The influence of sweep linearity on FMCW radar system performance has been addressed in [75, 76]. A combination of VCOs and frequency multipliers is commonly used in FMCW radar systems to reduce the effects of the VCO's non-linear tuning characteristic [79].

4.4.2 Frequency Multipliers

Fig. 4.3a shows the propagation of phase noise through a frequency multiplier [38]. The timing jitter is preserved during the frequency multiplication process while the RMS phase noise increases by N, where N is the frequency multiplication factor. Frequency multipliers are used in conjunction with frequency synthesisers to increase the FM modulation index of the transmitted signal to combat VCO non-linearities [79]. It is well-known that the phase noise sidebands increase as $20 \log_{10} N$ dB under

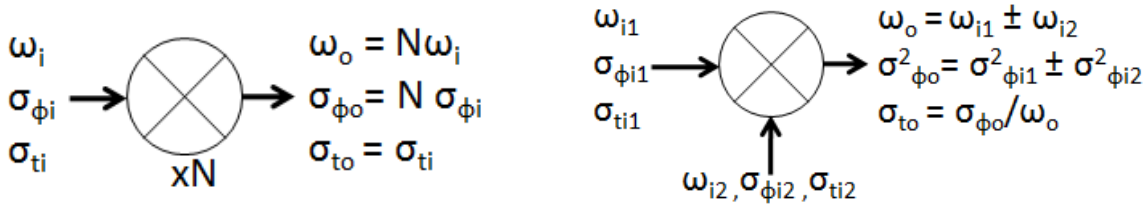

(a) Frequency Multiplier

(b) Mixer

Figure 4.3: Phase noise propagation through electronic subsystems.

frequency multiplication (so that the *phase SNR* degrades by $20\log_{10} N$ dB: however, it is important to note that this increase happens only when the small phase noise approximation is valid, even after frequency multiplication. Special results have been derived for frequency multiplication of the type of spectrum shown in Fig. 4.1b.

In [51, 65, 66] it has been demonstrated using theoretical analysis and practical measurements that if $\sigma_\phi^2 \ll 1$ then under frequency multiplication by N, W_p stays the same while L_p increases as $20\log_{10}(N)$, as expected. However, between $0.1 < \sigma_\phi^2 < 1$, the increase in the phase noise sidebands does not remain linear with N but slows down. Beyond $\sigma_\phi^2 > 1$ the carrier starts broadening[3] and so does the noise pedestal width W_p. For radar systems this phenomenon results in the target response being broader so that it is spread over a larger number of range bins, which is undesirable.

The carrier's 3-dB linewidth also increases under the process of frequency multiplication [53]. In general the linewidth increases N^2-times if the radar signal has white frequency noise, N-times if it has flicker-frequency noise, and $N^{2/3}$-times if it has random-walk frequency noise [51, 53]. However for short time delays, the phase noise processes decorrelate (explained shortly) which leads to a narrower linewidth than predicted [80].

4.4.3 Mixers

Fig. 4.3b shows the propagation of phase noise through a mixer [38]. In a radar context, the inputs are the transmitted and received signals, while the output of the mixer is the IF signal. Mixers add or subtract the phase noise in the input signals: suppression of phase noise happens when the two input signal are *coherent*, i.e. they have a defined phase relationship with each other (or in other words, are derived from the same reference source). It has been shown that in radar systems the mixing of the time-delayed transmitted signal with itself causes phase noise decorrelation

[3]This can be understood by noting that for $\sigma_\phi^2 > 1$, the signal transitions from being phase modulated to frequency modulated. The FM deviation of any signal increases under frequency multiplication, hence the frequency support of the carrier will stretch.

as follows [25, 26, 43, 81]:

$$\mathcal{L}_{IF}(f) = \mathcal{L}_{Tx}(f) \times 4\sin^2(\pi f \tau_d), \tag{4.10}$$

where τ_d is the round-trip time-delay to the target. This relationship will be analysed in detail later in this section. Equation (4.10) implies that the integrated (RMS) phase noise at the IF stage in Fig. 4.2 is:

$$\sigma^2_{\phi_{IF}} = \int_0^\infty 2\mathcal{L}_{Tx}(f) \times 4\sin^2(\pi f \tau_d)\ df. \tag{4.11}$$

In general if τ_d is small, $\sigma^2_{\phi_{IF}}$ will be small and vice versa.

If on the other hand the two inputs to the mixer are uncorrelated, the integrated output phase noise will be the sum of the individual phase noises:

$$\sigma^2_{\phi o} = \sigma^2_{\phi i1} + \sigma^2_{\phi i2} = \omega_1^2\sigma^2_{ti1} + \omega_2^2\sigma^2_{ti2}, \tag{4.12}$$

Even for the difference frequency signal the phase noises will add. If the two signals have *roughly* the same frequency and phase noise we get,

$$\sigma^2_{\phi o} = \omega_o^2\sigma^2_{to} \approx 2\sigma^2_{\phi i} = 2\omega_i^2\sigma^2_{ti}. \tag{4.13}$$

The above result shows that for incoherent inputs the IF signal's phase noise is twice that of the transmitted signal: however the relationship for timing jitter is more interesting. Equation (4.13) can be rearranged as follows:

$$\sigma^2_{to} \approx 2\frac{\omega_i^2}{\omega_o^2}\sigma^2_{ti}, \tag{4.14}$$

or using the radar terminology,

$$\sigma^2_{t_{IF}} \approx 2\frac{\omega_{RF}^2}{\omega_{IF}^2}\sigma^2_{t_{RF}}, \tag{4.15}$$

which implies that the timing jitter in the IF signal is much larger than the timing jitter in the RF signal because generally $\omega_{RF} \gg \omega_{IF}$. This result will be used in the next subsection.

4.4.4 Analog-to-Digital Converter

The subject of phase jitter/noise in ADCs has been dealt with in [28–30, 32, 33, 82]. As shown in Fig. 4.4, from the noise perspective the ADC can be thought of as a time-modulator or a time-mixer. Extending the argument of coherent phase

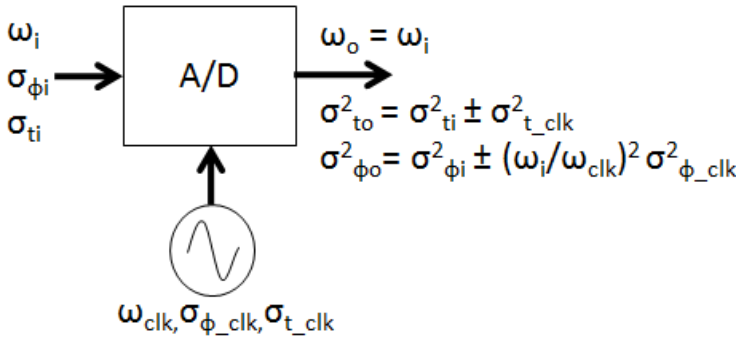

Figure 4.4: Phase noise propagation through an Analog-to-Digital Converter

noise cancellation in mixer, we propose that if the input signal is coherent with the sampling clock, the jitter in the sampled signal is *time-decorrelated* in the same way as the inputs to a mixer are *phase-decorrelated*. The decorrelation will be dependent on the time-delay between the signal being sampled and the clock signal, and most importantly how close the time jitters on the two are.

If the radar's transmitted signal and the sampling clock are derived from the same reference source, then their time jitters can be close to each other. However, as noted in (4.15) the IF signal being sampled has a time jitter greater than the received RF signal by a large factor. So the time jitter cancellation is less effective in this case. Nevertheless, as a guideline the transmitted signal's phase jitter is related to the reference oscillator's phase jitter through the transfer function of the frequency synthesiser being employed. For example, for a PLL synthesiser the *in-band* phase jitter at the output of the PLL is equal to the phase jitter in the reference oscillator, while beyond the loop bandwidth the phase jitter at the input and the output of the PLL are uncorrelated. In this case the ADC's sampling clock can be used to partially cancel the in-band phase jitter (according to the time delay) while there will be no noise cancellation for frequency offsets outside the loop bandwidth.

For the non-coherent case the jitter in the sampling clock adds to the jitter in the input signal. Therefore the integrated phase noise in the sampled signal is,

$$\sigma_{\phi o}^2 = \omega_o^2 \sigma_{to}^2 = \omega_i^2 \left[\sigma_{ti}^2 + \sigma_{t\_clk}^2\right] = \sigma_{\phi i}^2 + \frac{\omega_i^2}{\omega_{clk}^2} \sigma_{\phi\_clk}^2. \tag{4.16}$$

Due to the term $\omega_i^2/\omega_{clk}^2$ a higher frequency input signal experiences a larger phase noise transferred from the sampling clock. A detailed analysis of (4.16) in the context of radars is presented in [82].

4.4.5 FFT Processing

The FFT is the most common method of spectrum estimation. From the phase noise perspective an important parameter is the *FFT Bandwidth* defined as,

$$B_{FFT} = \frac{1}{T_{obs}}, \tag{4.17}$$

where T_{obs} is the time for which the signal was observed. In FMCW radars $T_{obs} \approx T_S$, i.e. the sweep time. The phase noise sideband level (in dBc) at the output of an FFT processor is,

$$\mathcal{L}_{DISP}(f) = \mathcal{L}_{IN}(f) + 10\log_{10}(B_{FFT}). \tag{4.18}$$

It is important to note that the FFT noise integration is not a frequency multiplication operation and does not affect parameters like noise pedestal width or the fundamental carrier linewidth. Nevertheless, the finite observation time does limit the least measurable carrier linewidth to $1/T_{obs}$: if the linewidth is less than the FFT bandwidth it will not be measured. On the other hand, if the linewidth of the demodulated IF signal is larger than $1/T_{obs}$ then it can span many FFT frequency bins.

4.4.6 Phase noise decorrelation

As noted above, $\mathcal{L}_{IF}(f)$ is related to $\mathcal{L}_{Tx}(f)$ by,

$$\mathcal{L}_{IF}(f) = \mathcal{L}_{Tx}(f) \times 4\sin^2(\pi f \tau_d). \tag{4.19}$$

The phase noise decorrelation factor in (4.19) is $4\sin^2(\pi f \tau_d)$ and is plotted for a few values of τ_d in Fig. 4.5. As can be seen in the plot for Range = 150 m, the decorrelation factor has a value of less than 0 dB for small frequency offsets and results in reduction/cancellation of phase noise. The critical value in (4.19) is the frequency offset of $f\tau_d = 1/6$ for which $\mathcal{L}_{IF}(f) = \mathcal{L}_{Tx}(f)$. This works out at $f = 167$ kHz for $\tau_d = 1\ \mu s$ corresponding to R = 150 m. Beyond this frequency offset no further phase noise cancellation happens: in fact $\mathcal{L}_{Tx}(f)$ and $\mathcal{L}_{Rx}(f)$ add *in-phase* so that $\mathcal{L}_{IF}(f)$ starts increasing. The following points can be noted:

- Coherent phase noise cancellation happens for frequency offsets $f \leq 1/6\tau_d$
- At $f\tau_d = 1/4$, $\mathcal{L}_{IF}(f) = 2\mathcal{L}_{Tx}(f)$.
- Finally for $f = 1/(2\tau_d)$, $\mathcal{L}_{IF}(f) = 4\mathcal{L}_{Tx}(f)$.

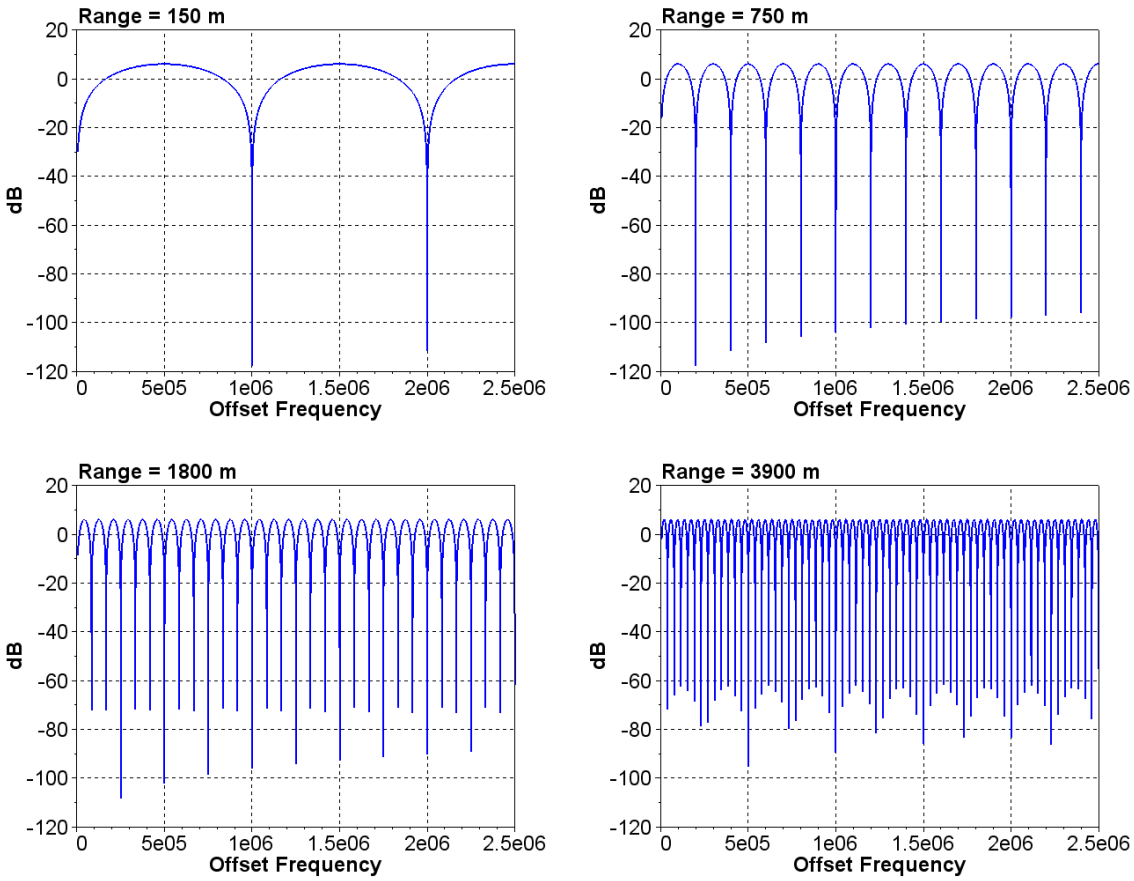

Figure 4.5: Plots of the Delay Function for targets at various ranges

The last point implies that due to coherent mixing the resultant phase noise can be up to 6 dB larger than the transmitter's phase noise as shown in Fig. 4.5. It can be noted in Fig. 4.5 that as the range to the target increases, the phase noise cancellation region shrinks. Depending on B_{FFT} one can estimate the maximum range after which coherent mixing does not result in any improvement.

The above discussion is valid for delay times less that the coherence time of the oscillator [53, 55]. As pointed out earlier, for excessively large measurement times (or measurements at very long ranges in the case of radar systems), the frequency noise processes in the oscillators cause excessive broadening of the measured RF spectrum [68–71]. An analysis of how the power shifts between the carrier portion and the sideband portion of the spectrum as a function of the delay time τ_d is given in [69, 80].

As a final comment, if non-coherent frequency mixing is used in a radar system, no cancellation of phase noise will happen at any range. In fact, the IF phase noise will just be the sum of the transmitter's phase noise and the LO's phase noise. No coherent ripples will be observed. The linewidth of target response will also be broader compared with a coherent radar.

4.5 The maximum bound on the pedestal height L_p

Having discussed the troubles $\sigma_\phi^2 > 1$ can cause it is imperative to analyse this condition further for typical radar sources. Fig. 4.1b shows the phase noise pedestal in the RF spectrum centred at the carrier frequency ν_0 along with the central carrier peak. A double-sided baseband model for the phase noise pedestal is the generalised Lorentzian function described in (4.7) but repeated here for convenience,

$$S_{RF}^{p}(f) = \frac{L_p}{1 + \left[\frac{|f|}{0.5W_p}\right]^k}, \tag{4.20}$$

where L_p (rad^2/Hz)[4] and W_p (Hz) are indicated in Fig. 4.1b, and k is the order of the roll-off of the pedestal.

We will now derive the maximum bound on L_p for a given W_p in order to meet the condition $\sigma_\phi^2 < 1$ for $k \geq 2$. Note that the noise pedestal obviously does not include the central carrier peak and the phase noise floor. If $\sigma_\phi^2 < 1$ then σ_ϕ^2 is approximately equal to the RMS noise power in the pedestal and can be computed

[4] or equivalently Watts/Hz

Table 4.1: Maximum allowable L_p for various values of k.

k	σ_ϕ^2 **(rad^2)**	**Max** L_p **(rad^2/Hz)**	**Max** L_p **for** $W_p =$ **200 kHz**
2	$\frac{\pi}{2} W_p L_p$	$0.64/W_p$	-58 dBc/Hz
2.5	$1.32\ W_p L_p$	$0.76/W_p$	-57.2 dBc/Hz
3	$1.12\ W_p L_p$	$0.89/W_p$	-56.5 dBc/Hz
4	$1.11\ W_p L_p$	$0.9/W_p$	-56.5 dBc/Hz
12	$1.01\ W_p L_p$	$0.99/W_p$	-56.1 dBc/Hz

as:

$$\sigma_\phi^2 = \int_{-\infty}^{\infty} S_{RF}^p(f) df. \tag{4.21}$$

The above integral was solved for various value of k: the results are shown in Table 4.1. The second column shows that the integral converges to $\sigma_\phi^2 = W_p L_p$ in the limit of large k. The third column shows the maximum bound for L_p as a function of W_p for each k.

Also shown in Table 4.1 (fourth column) are computed L_p's for $W_p/2 = 100$ kHz (this value of W_p is used in the plots in the next section). Note that 3-dB is to be subtracted from the value of L_p in dB-rad^2/Hz to compute the single-sideband level of L_p in dBc/Hz: the latter will be the representative value for L_p measured on a spectrum analyser centred at the carrier frequency ν_0.

Table 4.1 shows an interesting result that the maximum bound on L_p does not change significantly with k. The maximum value of the integral is at $k = 2$ and gives the tightest bound on L_p. Therefore, to ensure $\sigma_\phi^2 < 1$ we need,

$$L_p < \frac{2}{\pi W_p}. \tag{4.22}$$

The beauty of (4.22) is that this result does not depend on the actual operating frequency of the radar or the multiplication factor. The radar's transmitter only needs to comply with this limit as a minimum to be an acceptable radar signal source. If L_p and W_p are even lower, the radar source will remain coherent with itself (or *self-coherent*) to a much larger range than a radar source having larger L_p and W_p.

A change in W_p would directly affect the bound on L_p. For example, if a noise bandwidth of 10 kHz was sufficient for the PLL employed in the transmitter then W_p = 20 kHz and the maximum allowable L_p = -48 dBc/Hz to ensure $\sigma_\phi^2 < 1$. Therefore, by reducing W_p the bound on L_p has been relaxed. The model developed here closely conforms to the measurements in [51] which also happen to be at 9.5 GHz: with a single-sided bandwidth of 60 kHz (i.e. W_p = 120 kHz), the reported $L_{p(max)}$ is close to -52 dBc/Hz.

Finally we emphasise that the bound on L_p has been stated in the units of dBc/Hz (i.e. normalised to the integration bandwidth) and should be used as such, or with the proper scaling factors if other units are to be used.

4.6 An Optimistic Estimate for the Coherence Time of Radars

In this section we highlight another aspect of phase noise, that a source with larger phase noise will lose coherence faster with delay time compared with a source having low phase noise. In our work [82], an important relationship has been derived for the integrated phase noise in signal sources. Assuming the Lorentzian model for the phase noise pedestal, it was shown in [82] that,

$$\sigma_\phi^2 = R_\phi(0) = K\left[1 - e^{-\pi W_p \tau_d}\right], \tag{4.23}$$

where $K = 2\pi N^2 L_p W_p$ and τ_d is the delay time to the target. Setting $\sigma_\phi^2 = 1$ and inverting the equation one can find the coherence time for a given source as,

$$\tau_c = \frac{1}{\pi W_p} \ln\left(\frac{K}{K-1}\right). \tag{4.24}$$

There are two caveats in using (4.24). First, (4.24) is an optimistic estimate of τ_c because the low phase noise condition has been assumed in its derivation. It is therefore expected that τ_c will be smaller/shorter than predicted by (4.24). Secondly, the exact Lorentzian spectrum (power of 2) is assumed in deriving (4.24), instead of k as in (4.20), due to analytical convenience. However, the error introduced will be small (a maximum of 1.5 dB for $k = 4$) if the roll-off is > 2, as evidenced in the previous section. As a final comment, we believe that (4.24) is applicable to any coherent radar system.

Table 4.2: Parameters of the FMCW radar being studied.

Parameters	**MMW Radar**
Carrier Frequency, ν	76.5 GHz
Swept Bandwidth, B_S	660 MHz
Sweep Time, T_S	1.25 ms
FFT Bandwidth, $1/T_S$	800 Hz
Freq. Multiplication Factor, N	8
PLL Loop Bandwidth, B_L	100 kHz
PLL In-band noise level, L_1	-88 dBc/Hz

4.7 Application of Phase Noise Modelling to a MMW FMCW Radar System

The phase noise modelling methodology was applied to a MMW FMCW radar system having subsystems as in Fig. 4.2. The parameters of the radar system are shown in Table 4.2. First, a PLL-based radar source will be used to measure the target response of trihedral corner reflectors. The phase noise sidebands will be visible in this measurement. Next a low phase noise source will be used for the same measurement to demonstrate the performance improvement.

4.7.1 Phase noise modelling of a PLL based system

The radar used for measurements initially employed a PLL/VCO scheme to generate the X-band signal that was frequency multiplied to 76.5 GHz. Fig. 4.6 show a spectrum analyser display of centred at the carrier frequency. The phase noise sidebands are visible: for example, at 100 kHz the phase noise is around -88 dBc/Hz. In Fig. 4.7 (lower plot) one phase noise sideband from the spectrum in Fig. 4.6 has been modelled and the expected phase noise level at 77.6 GHz has been displayed using a frequency multiplication factor of $N = 8$. Also shown for reference (top dashed plot) is the expected IF phase noise due to the noise integration done by the FFT ($B_{FFT} = 800$ Hz) without taking into account the effects of phase noise decorrelation, due to which the actual peak sideband level will be 6 dB higher.

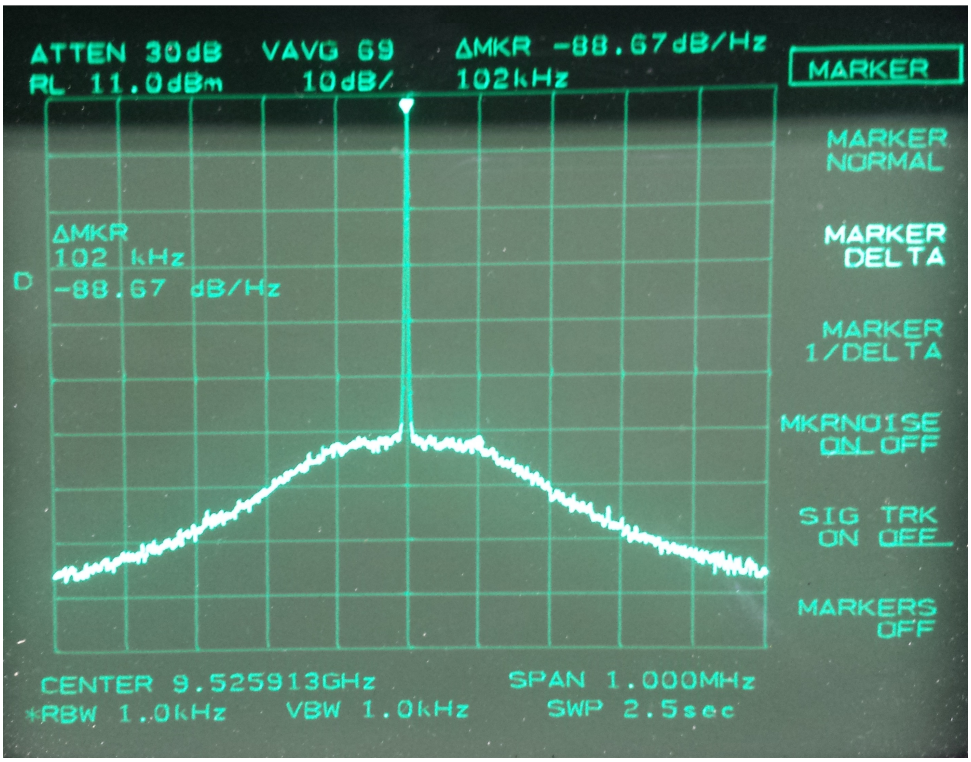

Figure 4.6: Measured RF Spectrum of an X-band PLL synthesised oscillator.

A spectrum measurement of the transmitted signal at 76.5 GHz was performed (but not included here) which confirmed that there was no change in the width of the noise pedestal, and the pedestal height did go up by $20 \log N = 18$ dB. This conforms to the theory presented in the last section: the noise pedestal height $L_p = -88$ dBc/Hz is much less than the maximum bound suggested by Table 4.1.

Fig. 4.8 shows the final simulated single sideband target response at various target ranges taking into account the effects of phase noise decorrelation using (4.19). This type of simulation model is extremely useful in predicting the expected target response to analyse the phase noise performance of radar systems. The simulated target response is 6 dB higher at the peak of the coherent ripples as expected. The critical frequency offset $f_{crit} = 1/6\tau_d$ (converted to range bin values) is plotted as a vertical dotted line: it can be seen that beyond this point the phase noise sideband increases up to 6 dB beyond the transmitter's integrated phase noise level, and there is no further phase noise cancellation other than the troughs of the ripples.

The simulated target response at 150 m has a peak phase noise level of -45 dBc, while the simulated target response at 750 m has a peak phase noise level of -33 dBc. These values are to be compared with the measurement results of the next subsection. Due to the large difference between the operating RF frequency (76.5 GHz) and the IF frequency (up to 7 MHz) the computed effect of the ADC jitter

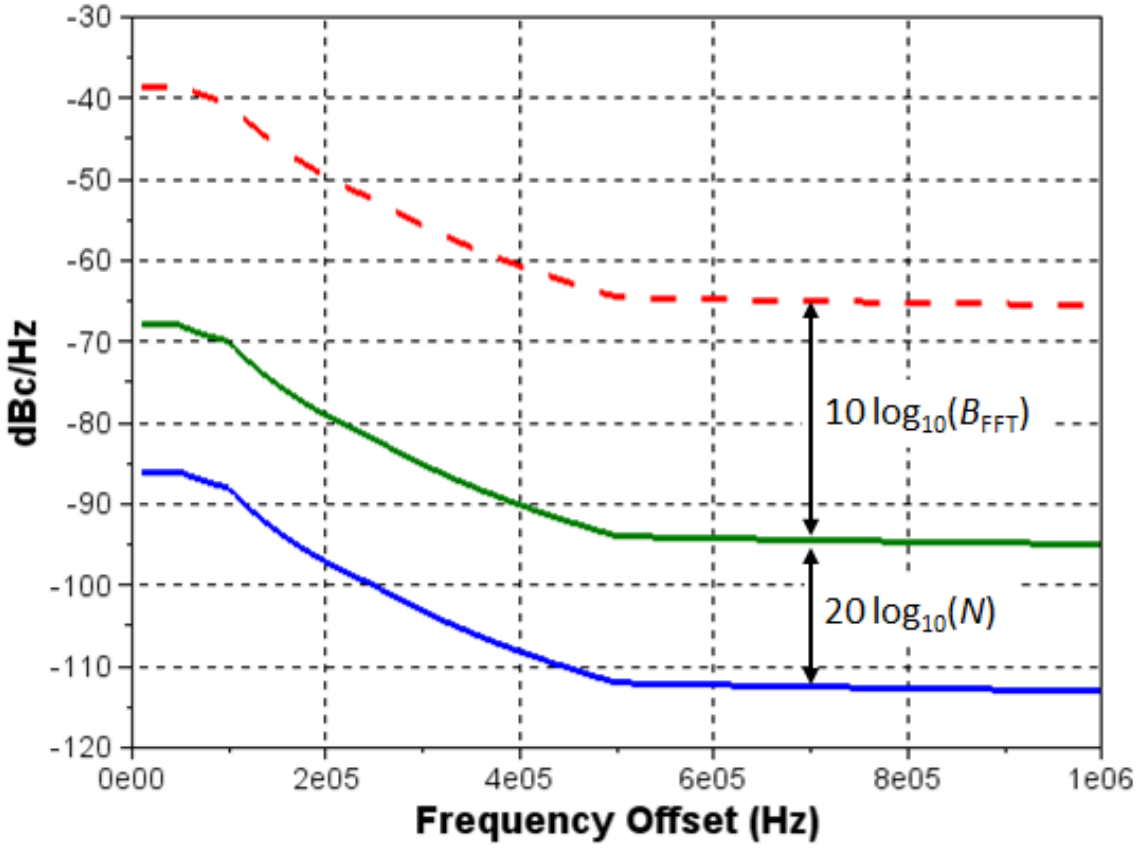

Figure 4.7: Single-sideband phase noise plots (bottom to top) at the X-band synthesiser (measured), at the 76.5 GHz transmitter with N=8 (calculated), and at the FFT output (B_{FFT} = 800 Hz) (calculated).

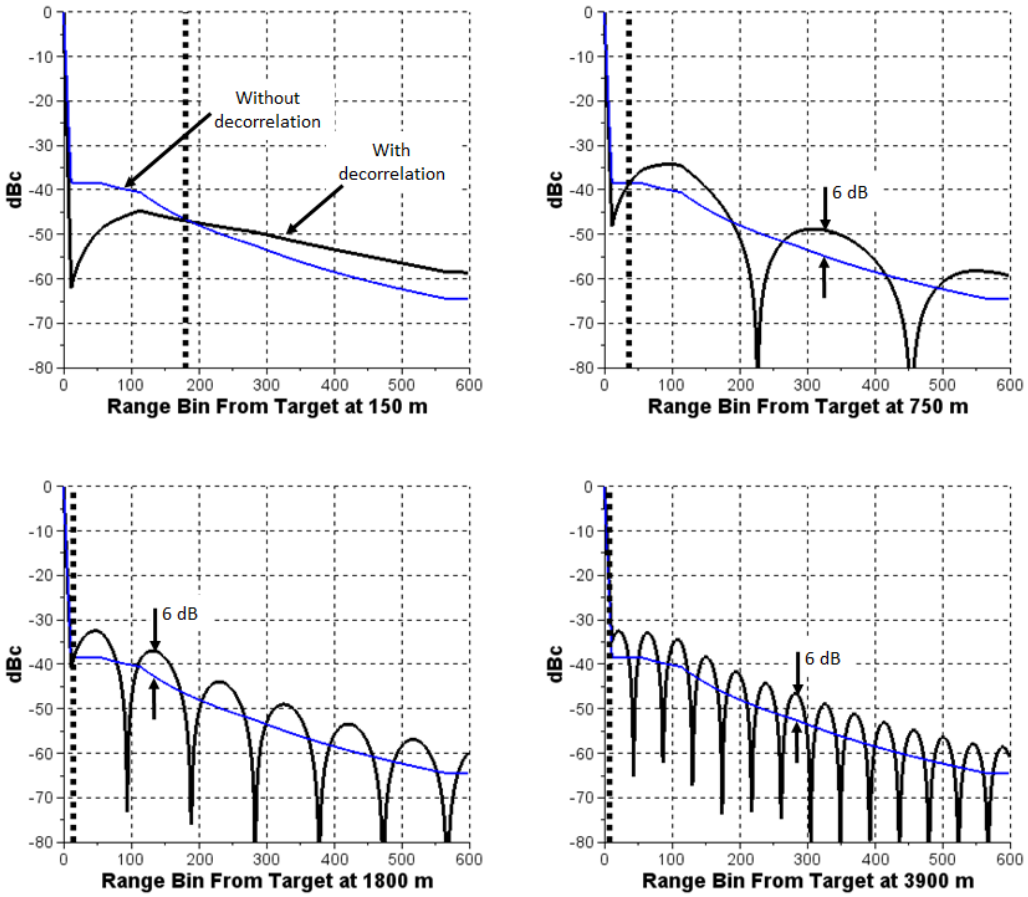

Figure 4.8: Plots of the simulated target response (single-sideband) at various ranges. Coherent phase noise cancellation gives an improvement (reduction) in phase noise in the region to the left of the vertical dotted line. The blue overlay is the top plot in Fig. 4.7.

was minimal and had minimal effect on the measurements.

4.7.2 Measurement results from the PLL based radar

Fig. 4.9 displays the radar measurement of two corner reflector targets placed at 173 m and 770 m respectively. This is the same scene reported in Chapter 3, but the data has been subjected to new analysis. The measurements were done using a CTS radar system developed by Navtech Radar Ltd. having the parameters displayed in Table 4.2. It can be seen that thermal noise is superimposed on the phase noise sidebands, so the average noise level should be taken as the representative value of phase noise. The phase noise sideband levels have been marked with double-arrows, and the lower arrow is placed at the expected average noise level. Comparing with Fig. 4.8 it can be seen that these measurements are compatible with the theoretical modelling: the measured target response at 173 m has an average phase noise level

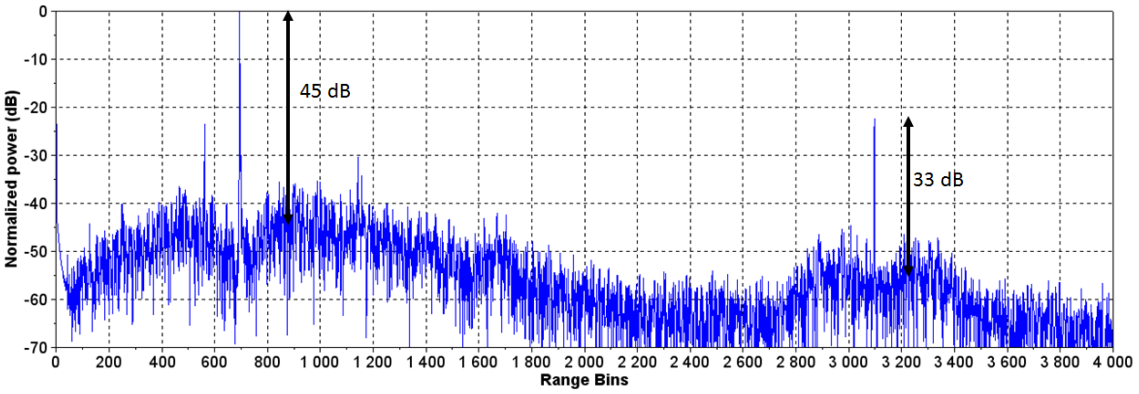

Figure 4.9: Targets at 173m and 770m. Range bins are 25 cm each.

close to -45 dBc, while the measured target response at 770 m has an average phase noise level close to -33 dBc.

4.7.3 Discussion on the measurements from the PLL based radar

The modulation loop bandwidth of 100 kHz causes the PLL to have a large noise bandwidth (or noise pedestal width) of 200 kHz. The upshot is that both targets in Fig. 4.9 have large shoulder-like sidebands superimposed on them. This phenomenon causing severe difficulties in the detection and tracking of the objects in the region having a raised noise floor: the detection of all targets is degraded and small target can disappear in this noise floor.

To gain a better understanding of the artefacts of phase noise, we used a higher power radar with 17.5 cm range bins. Fig. 4.10 displays the measured target response of the 770 m corner reflector. Averaging was turned on to reduce the thermal noise in the display. The coherent sideband structure is much more visible in this plot along with other small targets (grass at shorter-ranges and trees at longer ranges). The coherent ripples can be compared with the top-right inset in Fig. 4.8. It can be noticed that the measured sideband level is now at -30 dBc instead of -33 dBc because this particular radar uses a tighter loop bandwidth, causing an increase in the in-band phase noise. However this does not affect the width of the coherent ripples.

It is worth noting that the coherent ripples in Fig. 4.10 were only visible after the *systematic noise* was mitigated in the frequency synthesiser [34]. The presence of systematic noises can smear the sideband structure and also cause a raised noise floor. We will not dwell further on systematic noise.

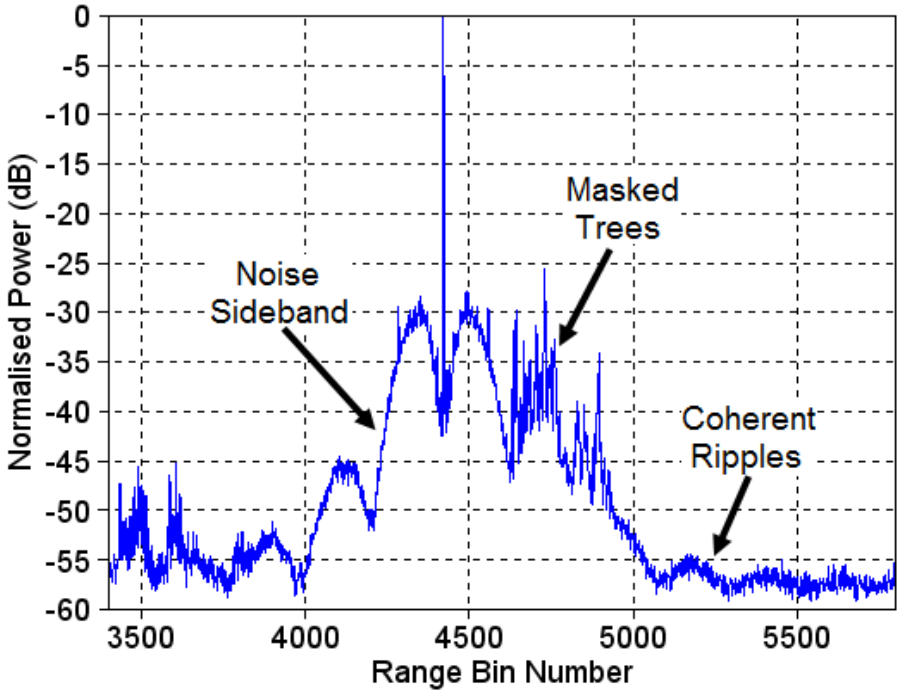

Figure 4.10: The 770 m target's response produced by a higher power radar employing a PLL-based source. The coherent ripples in the phase noise sidebands can be seen.

4.7.4 Improved phase noise design

To lower the phase noise sidebands we designed a low-phase noise frequency synthesiser detailed in Chapter 3. A spectrum analyser display of the synthesiser's output is shown is Fig. 4.11. A comparison with Fig. 4.6 shows that the new synthesiser is indeed a very low phase noise source. At the 100 kHz offset the measured phase noise is -111.8 dBc/Hz which is at least 23 dB better than the PLL-based source (as this measurement is close to the spectrum analyser's noise floor the improvement is even greater, as detailed below). The effects of decorrelation in the new low-noise synthesiser can be worked out using plots similar to Fig. 4.5.

Fig. 4.12 shows the same scene as in Fig. 4.10, viewed with the higher-power radar system employing the new low-noise frequency synthesiser. A remarkable improvement in the phase noise sidebands of around 30 dB can be seen, significantly improving the definition in the scene. The grassy patch before the target and the trees after the target are clearly visible now. In addition, a hedge right behind the corner reflector has now been revealed that was completely hidden in Fig. 4.10. Therefore, any small targets near this large target can now be detected with precision. Potential applications of this type of improvement are in perimeter security systems where an intruder is walking right next to a large building: a conventional

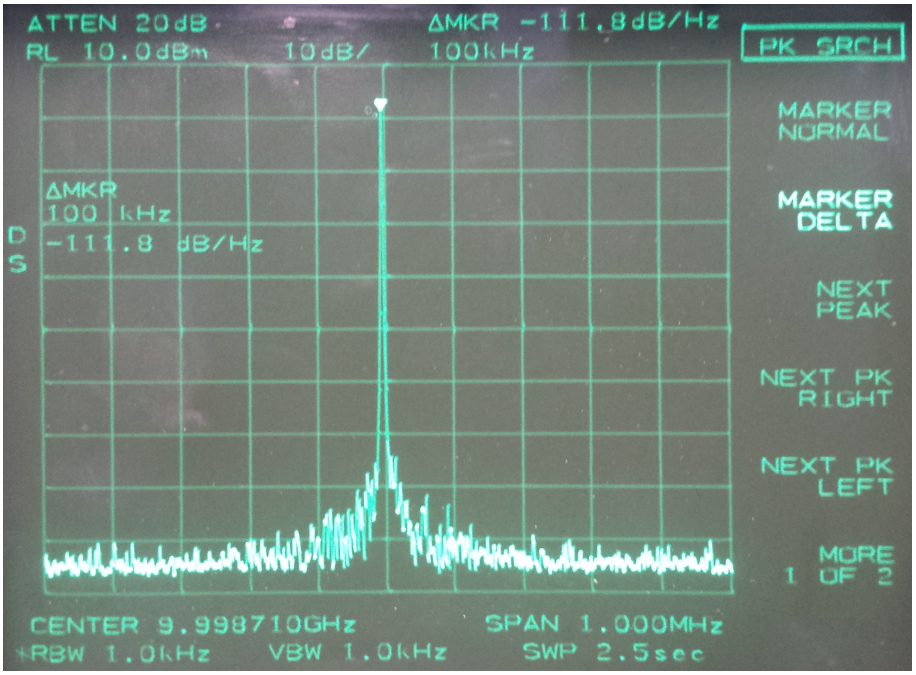

Figure 4.11: Measured RF Spectrum of the low phase noise source.

radar sensor will fail to pick up the intruder due to the spread of the phase noise sidebands around the building's large radar response. However an improved radar system based on low-phase noise technology will indeed be able to detect the intruder and raise an alarm.

4.8 Conclusion

There are many causes of spectral broadening of the target responses in FMCW radar systems including internal factors like phase noise, unfocused lenses, and parasitic nonlinearities due to VCO tuning curves, and external factors like cross-demodulated radar interference signals [2], environmental precipitation, and distributed targets. This chapter exclusively focused on the spectral broadening of radar targets due to phase noise. A complete phase noise analysis methodology was described to model the phase noise at various stages of a complete radar system. New models of phase noise in ADCs and of phase noise pedestals were presented and applied to modelling phase noise in radar systems. Factors effecting the linewidth of the demodulated signal were discussed. Measurements were presented that are in very good agreement with the developed theory. Finally, the use of a low-phase noise frequency synthesiser was described to reduce the phase noise sidebands by 30 dB, significantly improving the detection and tracking performance of the radar.

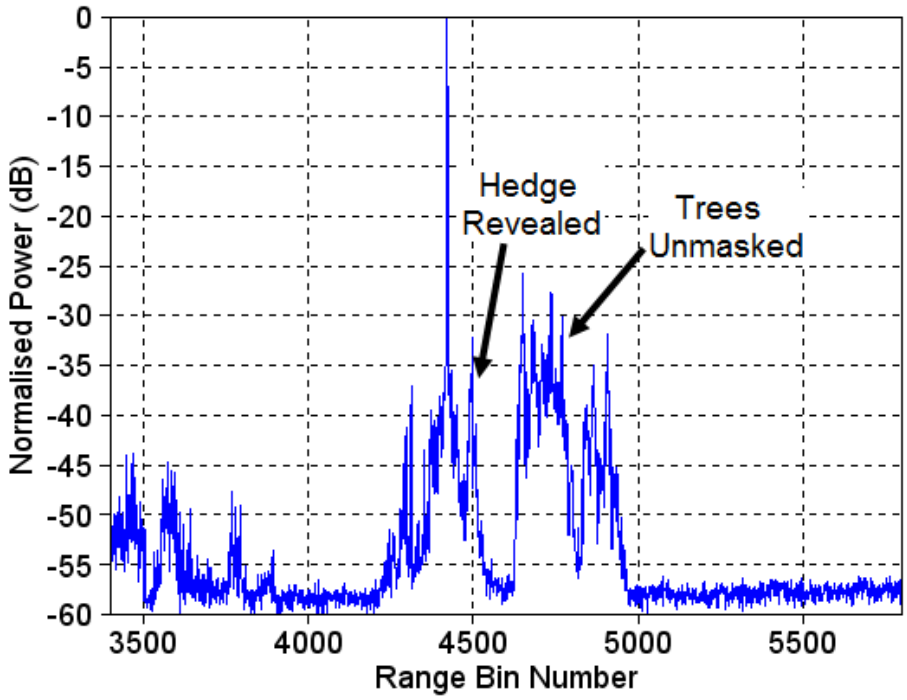

Figure 4.12: The 770 m target displayed by a higher power radar with the low phase noise source. The phase noise sidebands have been largely eliminated.

Chapter 5

Analysis of Sampling Clock Phase Noise in Homodyne FMCW Radar Systems[1]

5.1 Summary

In many contemporary electronic systems, phase noise sets the bound on the achievable performance. Radar systems are no exception, with the actual radar signals carrying significant amounts of phase noise due to the high transmit frequencies. In coherent radars, some of the phase noise sidebands on the received signal are cancelled due to mixing in the receiver. The sampling clock used to sample the intermediate frequency (IF) signals also introduces phase noise/jitter. This chapter focuses on the contribution of the sampling clock's phase noise to the overall phase noise in the sampled signal in coherent homodyne FMCW radar systems. A model will be developed to relate the phase noise in the sampled signal to the phase noise in the radar signals and the jitter in the sampling clock. The developed analysis is applied to example FMCW radar systems. The derived model can be used to work out the phase noise requirement on the sampling clock for a given phase noise level in radar signals.

[1]The contents of this chapter have been published in [82].

5.2 Introduction

Phase noise in the frequency domain, written as $\mathcal{L}(f)$, is defined as one half of the spectral density of phase fluctuations $\mathcal{S}_\theta(f)$ having units of rad^2/Hz [8]. The conventional definition of phase noise around a carrier signal is the ratio of the power in the noise sidebands per Hz relative to the power in the carrier, and is specified in dBc/Hz on a plot of the power spectrum. The latter definition is only valid for signals having *small* phase noise and negligible AM noise [10].

Phase noise appears as phase-modulation sidebands around a carrier's spectrum. For radar systems having a high dynamic range this causes the clutter-floor to increase around large targets, making the detection and tracking of small targets impossible in the region of raised clutter-floor [13]. Decreasing the overall phase-noise, therefore, is a prime challenge in high-performance radars. In FMCW radars the phase noise appears as noise-sidebands in range around each target [43]. An additional effect in coherent radars is the cancellation of phase noise at shorter ranges due to coherence.

The effect of phase jitter in sampling clocks has been addressed before as contributing to the overall system noise floor [28–30], and as the clock's noise spectrum being transferred to a noise-less signal under the sampling process [29,31]. However, the case of sampling a signal corrupted with phase noise using a clock having its own phase jitter, and their relative contribution to the total phase noise in the sampled signal has been mentioned rarely. In [32] the total phase noise in the sampled signal is accurately estimated using an iterative optimization-based approach. However this approach does not give insight into the phase jitter requirements of the ADC clock or how the clock jitter compares with the received signal's phase noise. In [33] the problem of the transfer of the sampling clock's noise to a generic input signal has been addressed. However, the relative contributions of the input's phase noise and the clock's phase noise has not been addressed. Ultra-low phase noise oscillators and sampling clocks are expensive, so an estimation of the phase noise requirement is imperative to select the oscillator meeting the requirement with the lowest cost.

In this chapter an analysis of the effect of the phase jitter in the analog-to-digital converter's (ADC) sampling clock on the sampled radar signals having their own phase noise is presented. Building on our previous work [27] the total phase noise in the demodulated radar signal will be computed taking into account the effect of coherent phase noise cancellation in the radar receiver. Afterwards a model for the total phase noise in the sampled radar signal as a function of the phase noise in the demodulated radar signal and the phase noise in the sampling clock will be

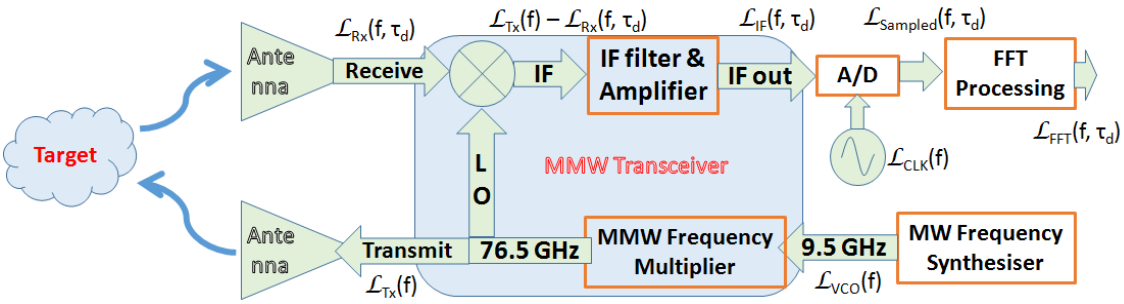

Figure 5.1: Block diagram showing phase noise propagation in a FMCW radar system.

developed. A generalised analysis will be presented first followed by application to two FMCW radar systems.

5.3 System description

Fig. 5.1 shows a block diagram of the 77 GHz radar system being studied. The *Frequency Synthesiser* block generates a signal synthesised using a phase-frequency detector (PFD)-based phase lock loop (PLL). The synthesised signal is frequency-multiplied to the transmit frequency by the *Transceiver* block. The backscatter from the target is received by the receive-antenna and passed on to the transceiver which demodulates the signal to an intermediate-frequency (IF). The IF signal is digitised after filtering and amplification. Fig. 5.1 shows the phase noise at various points in the system using the symbol $\mathcal{L}_{sub}(f)$, where *sub* is the subscript showing the phase noise measurement point in the system.

The phase noise in the sampling clock $\mathcal{L}_{CLK}(f)$ and the IF signal $\mathcal{L}_{IF}(f)$ are shown. Next a relationship will be derived for the total phase noise in the sampled signal as a function of $\mathcal{L}_{CLK}(f)$ and $\mathcal{L}_{IF}(f)$.

5.4 Noise analysis

As discussed earlier, the IF signal corrupted with phase noise is sampled using a clock signal having its own phase noise. Let $x(t)$ be the IF signal and $y(mT)$ be the sampled signal, m being the sample number and T being the inverse of the sampling rate. Using a Taylor Series approximation, it was shown in [33] that the autocorrelation function of $y(mT)$ can be written as,

$$r_y(mT) = r_x(mT) - r_x''(mT) \cdot r_{tj}(mT), \tag{5.1}$$

where r_{tj} is the autocorrelation of the *time jitter* process on the ADC sampling clock and r_x is the autocorrelation of $x(t)$. The essential conditions for (5.1) to hold are that $x(t)$ be smooth enough for the existence of a local derivative and the RMS time jitter in the sampling clock, σ_{tj}, be much less than the reciprocal of the maximum signal frequency in $x(t)$, or,

$$\sigma_{tj} \ll \frac{1}{F_{Sig_{max}}}. \tag{5.2}$$

We propose that under the same condition, (5.1) can be extended to the case where $x(t)$ is corrupted by phase noise. This is especially true for sinewaves. Phase jitter essentially causes randomness in the zero-crossings of the waveform [14]. So on the time-scale of phase jitter, the signal's level and its derivatives do not change significantly for a sufficiently smooth function. The same argument holds for a sum of sinewaves, as in the IF signal of a real FMCW radar - if (5.2) could be satisfied, (5.1) would still hold.

With this in mind, (5.1) can be used for a signal $x(t)$ having phase noise that is sampled with a sampling clock having its own phase noise/jitter. The total signal plus noise power in the sampled signal is given by,

$$r_y(0) = r_x(0) - r_x^{''}(0) \cdot r_{tj}(0). \tag{5.3}$$

Note that $r_{tj}(0)$ can either be measured using a suitable instrument, or representative values can be read directly off oscillator datasheets where the RMS jitter $\sigma_{tj} = \sqrt{r_{tj}(0)}$ is specified. So in this analysis the sampling clock's frequency spectrum is not needed to work out the total RMS jitter. In the following expressions for $r_x(0)$ and $r_x^{''}(0)$ are derived.

5.4.1 Phase noise in the IF signal

The Frequency Synthesiser block in Fig. 5.1 generates a 9.5 GHz signal using a PFD-based PLL. Fig. 5.2 shows a generic phase noise plot of this type of frequency synthesisers. It can be seen that the noise below the loop bandwidth B_L is dominated by the PFD (and not the reference oscillator [31], [27]) at a level L_1 dBc/Hz, whereas outside B_L it is dominated by the VCO. Assuming a 20 dB/decade roll-off on the VCO phase noise, a simplified expression for this phase noise plot is [31],

$$\mathcal{L}_{Synth}(f) = \frac{10^{L_1/10}}{1 + \left(\frac{f}{B_L}\right)^2}. \tag{5.4}$$

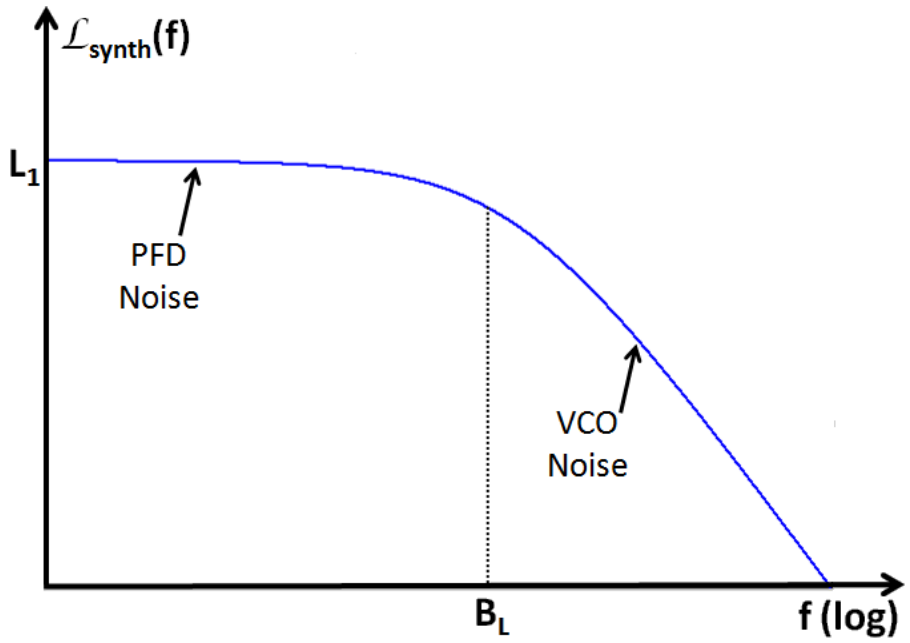

Figure 5.2: Phase Noise at the output of a generic PLL synthesiser.

Due to frequency multiplication by N, the transmitter phase noise can be written as,

$$\mathcal{L}_{Tx}(f) = N^2 \times \mathcal{L}_{Synth}(f). \tag{5.5}$$

The signal scattered by the target at range R is received at the radar after a delay $\tau_d = 2R/c$, c being the speed of light. The phase noise at the output of the homodyne mixer is given by [26],

$$\mathcal{L}_{IF}(f) = \mathcal{L}_{Tx}(f) \times 4\sin^2(\pi f \tau_d). \tag{5.6}$$

For small τ_d some of the phase noise is cancelled due to coherence. Using (5.4) and (5.5) we can write,

$$\mathcal{L}_{IF}(f) = \frac{4N^2 10^{L_1/10} \times \sin^2(\pi f \tau_d)}{1 + \left(\frac{f}{B_L}\right)^2}. \tag{5.7}$$

5.4.2 Signal model for the noisy IF signal

The IF radar signal $x(t)$ is a sinewave having the phase noise in (5.7) and can be written as,

$$x(t) = A_0 \sin(\omega_0 t + \theta(t)), \tag{5.8}$$

where $\theta(t)$ is the zero-mean phase noise process. Assuming $\theta(t) \ll 1$, (5.8) can be written as,

$$x(t) \approx A_0 \sin(\omega_0 t) + A_0 \theta(t) \cos(\omega_0 t). \tag{5.9}$$

The autocorrelation function of $x(t)$ is,

$$r_x(\tau) = E\left[x(t)x(t+\tau)\right]. \tag{5.10}$$

Inserting (5.9) we get,

$$\begin{aligned} r_x(\tau) = E[(A_0 \sin(\omega_0 t) + A_0 \theta(t) \cos(\omega_0 t)) \times \\ (A_0 \sin(\omega_0 (t+\tau)) + A_0 \theta(t+\tau) \cos(\omega_0 (t+\tau)))]. \end{aligned} \tag{5.11}$$

The expected value of the cross terms are zero, as can be verified. Expanding and computing the expectation we get,

$$r_x(\tau) = \frac{A_0^2}{2} \cos(\omega_0 \tau)(1 + R_\theta(\tau)), \tag{5.12}$$

where $R_\theta(\tau) = E[\theta(t)\theta(t+\tau)]$ is the autocorrelation of the phase noise process $\theta(t)$. It follows that,

$$r_x(0) = \frac{A_0^2}{2}(1 + R_\theta(0)). \tag{5.13}$$

The phase noise in the IF signal, $\mathcal{L}_{IF}(f)$, is given by (5.7). So the spectral density of $\theta(t)$ is $S_{\theta_{IF}}(f) = 2\mathcal{L}_{IF}(f)$. Computing the inverse Fourier Transform of $S_{\theta_{IF}}(f)$ we get,

$$R_\theta(\tau) = K\left[e^{-2\pi B_L|\tau|} - \frac{1}{2}\left(e^{-2\pi B_L|\tau-\tau_d|} + e^{-2\pi B_L|\tau+\tau_d|}\right)\right], \tag{5.14}$$

where $K = 4\pi N^2 10^{L_1/10} B_L$. Therefore,

$$R_\theta(0) = K\left[1 - e^{-2\pi B_L \tau_d|}\right]. \tag{5.15}$$

Using (5.12) one may verify that,

$$r_x''(0) = \frac{A_0^2}{2}\left[-\omega_0^2 - \omega_0^2 R_\theta(0) + R_\theta''(0)\right]. \tag{5.16}$$

That is, to compute (5.16) one needs to compute $R_\theta''(0)$. From (5.14) one can verify that,

$$R_\theta''(0) = (2\pi B_L)^2 R_\theta(0). \tag{5.17}$$

Therefore,

$$r_x''(0) = \frac{A_0^2}{2}\left[-\omega_0^2 - \omega_0^2 R_\theta(0) + (2\pi B_L)^2 R_\theta(0)\right]. \tag{5.18}$$

The second term in (5.18) is negligible compared with the first assuming $R_\theta(0) \ll 1$. So we can write,

$$r_x''(0) \approx \frac{A_0^2}{2}\left[-\omega_0^2 + (2\pi B_L)^2 R_\theta(0)\right]. \tag{5.19}$$

Finally, note that the IF signal's frequency $\omega_0 = 2\pi f_0$ is related to the propagation delay time τ_d as,

$$f_0 = \tau_d \frac{B_S}{T_S}, \tag{5.20}$$

where B_S and T_S are the swept bandwidth and the sweep time respectively in an FMCW radar. For B_S in the range of 100's of MHz and T_S in the range of milliseconds, f_0 can range from fractions of a kHz to 10's of MHz.

5.4.3 Total noise in the sampled signal

Inserting (5.13) and (5.19) in (5.3) we get,

$$r_y(0) = \frac{A_0^2}{2}(1 + R_\theta(0)) - \frac{A_0^2}{2}\left(-\omega_0^2 + (2\pi B_L)^2 R_\theta(0)\right) r_{tj}(0)$$

$$\Rightarrow r_y(0) \approx \frac{A_0^2}{2} + \frac{A_0^2}{2} R_\theta(0) + \frac{A_0^2}{2}\omega_0^2 r_{tj}(0). \tag{5.21}$$

The first term in (5.21) is the signal power. The second term is the noise power due to phase noise in the IF radar signal, which is termed $P_{\theta_{IF}}$. The third term is the noise power due to the sampling clock, and conforms to a well-known result [30,31,83]. As can be noticed, the fourth term has been ignored because σ_{tj} for clocks is specified in pico- or femto-seconds. Computing $r_{tj}(0) = \sigma_{tj}^2$ will make this term minuscule compared with the second term in (5.21). Equation (5.21) is an important and powerful result appealing to intuition - the total phase noise is the sum of the phase noise in the IF signal and the phase jitter in the sampling clock scaled by ω_0^2. It can be concluded from (5.21) that in order to see the effect of sampling clock jitter on the total phase noise, the two noise terms need to be compared. Fig. 5.3 illustrates the signal and the phase noise transfer under analog-to-digital conversion.

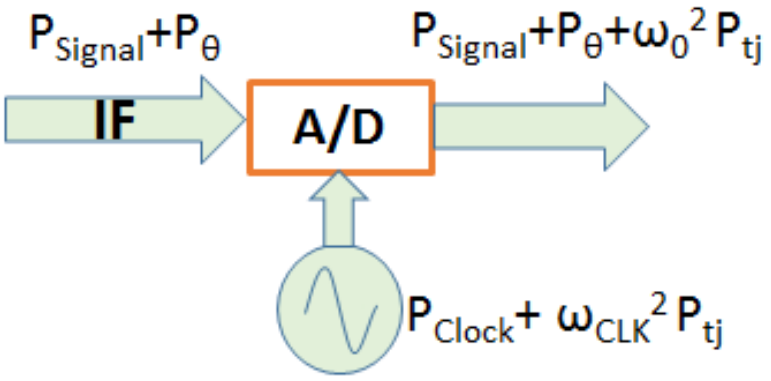

Figure 5.3: Illustration of how the clock jitter adds to the IF signal's phase noise.

Table 5.1: Parameters of the FMCW radars being studied

Parameters	**MMW Radar**	**MW Radar**
Swept Bandwidth, B_S	600 MHz	500 MHz
Sweep Time, T_S	1 ms	0.5 ms
Loop Bandwidth, B_L	100 kHz	50 kHz
Freq. Multiplication Factor, N	8	1
In-band noise level, L_1	-90 dBc/Hz	-120 dBc/Hz

5.5 Application to FMCW Radar Systems

In this section the total phase noise in the sampled signal in two example FMCW radar systems working at 77 GHz and 5 GHz respectively will be analysed. Due to the difficulty in synthesising a low-noise source at 77 GHz the noise in the IF signal is much higher than in the 5 GHz Microwave (MW) radar. The goal here is to ascertain which of the noise terms in (5.21) dominates the overall noise in the sampled signal. The noise terms vary with τ_d, i.e., the target range, so it is appropriate to compute them as a function of τ_d (and parametrized by $R_{tj}(0)$).

The system parameters of the two radar systems are shown in Table 5.1. Using those parameters the noise terms for the two radars can be computed as follows:

The 77 GHz Radar

$$R_\theta(0) = 0.0804\left(1 - e^{-2\pi 10^5 \tau_d}\right), \tag{5.22}$$

Table 5.2: Variation of the noise terms versus target range

	Range (m)	15	150	300	750	1500
	τ_d (μs)	0.1	1	2	5	10
77 GHz Radar	$R_\theta(0)$	0.005	0.0375	0.0575	0.077	0.08
	$\omega_0^2 r_{tj1}(0)$	1.42×10^{-13}	0.142×10^{-10}	$+0.568 \times 10^{-10}$	3.55×10^{-10}	14.2×10^{-10}
	$\omega_0^2 r_{tj2}(0)$	1.42×10^{-11}	0.142×10^{-8}	0.568×10^{-8}	3.55×10^{-8}	14.2×10^{-8}
	$\omega_0^2 r_{tj3}(0)$	1.42×10^{-9}	0.142×10^{-6}	0.568×10^{-6}	3.55×10^{-6}	14.2×10^{-6}
5 GHz Radar	$R_\theta(0)$	3.83×10^{-8}	2.93×10^{-7}	4.5×10^{-7}	6.01×10^{-7}	6.27×10^{-7}
	$\omega_0^2 r_{tj1}(0)$	3.95×10^{-13}	3.95×10^{-11}	1.58×10^{-10}	9.87×10^{-10}	3.95×10^{-9}
	$\omega_0^2 r_{tj2}(0)$	3.95×10^{-11}	3.95×10^{-9}	1.58×10^{-8}	9.87×10^{-8}	3.95×10^{-7}
	$\omega_0^2 r_{tj2}(0)$	3.95×10^{-9}	3.95×10^{-7}	1.58×10^{-6}	9.87×10^{-6}	3.95×10^{-5}

$$\omega_0^2 r_{tj}(0) = 1.42 \times 10^{25} \tau_d^2 \times r_{tj}(0). \tag{5.23}$$

The 5 GHz Radar

$$R_\theta(0) = 6.28 \times 10^{-7} \left(1 - e^{-2\pi 10^4 \tau_d}\right), \tag{5.24}$$

$$\omega_0^2 r_{tj}(0) = 3.95 \times 10^{25} \tau_d^2 \times r_{tj}(0). \tag{5.25}$$

Note that (5.22) and (5.24) imply that $R_\theta(0) \ll 1$ for all τ_d as assumed in the previous section to ignore the second term in (5.18). Table 5.2 summarizes the noise terms versus target range. We have considered three sampling clocks as follows:

1. $\sigma_{tj1} = \sqrt{r_{tj1}(0)} = 1$ ps (representing a low-phase noise clock source)
2. $\sigma_{tj2} = \sqrt{r_{tj2}(0)} = 10$ ps
3. $\sigma_{tj3} = \sqrt{r_{tj3}(0)} = 100$ ps (representing the equivalent of a modern FPGA-based clock source).

In the case of the 77 GHz radar it can be seen that all sampling clocks have a negligible noise contribution compared with the IF signal's inherent phase noise. This result makes the selection of the sampling clock much easy (and cheap). For the 5 GHz radar, however, it can be seen that Clock 1 has lower noise contribution than the IF signal, Clock 2 is comparable, and Clock 3 has a higher noise contribution than the IF signal. It should be noted that for a given radar the noise terms depend directly on the noise parameters in Table 5.1, and not directly on the actual operating frequency of a radar.

From (5.21) it can be concluded that, as a figure-of-merit, one noise term dominates the other if it is at least 10 times larger. So the sampling clock's noise contribution must be 10 times less than the radar signal's phase noise to have a minimal effect.

5.6 Conclusion

In this chapter we analysed the effect of jitter in the sampling clock on radar signals having their own phase noise. An intuitive and powerful equation for the total phase noise in the sampled radar signal was derived. In summary, to select a sampling clock for a given radar system one needs to compare the intrinsic phase noise in the IF radar signal with the phase noise transferred from the sampling clock to the IF signal. A detailed analysis of a higher-noise MMW radar and a lower-noise Microwave radar showed that a lower-cost sampling clock may be adequate for a

MMW radar having a noisy IF signal, while a more expensive clock will be needed for a radar with a relatively low-noise IF signal. The analysis can be extended easily to radars operating in other frequency bands.

Chapter 6

On Phase Measurement in FMCW Radar Systems [1]

6.1 Summary

Unlike AM and PM systems, FM systems do not necessarily require the use of a dual I/Q receiver for unambiguous phase measurement. In this chapter this phenomenon is described in detail and work out the conditions when single-channel phase measurements can be used for the reliable measurement of the phase and the Doppler frequency of targets in FMCW radars systems. The developed theory is applied to surveillance and automotive radar systems to determine the velocity bounds for the unambiguous measurement of phase. The influence of phase noise in the same context is discussed. Results of coherent averaging on the data acquired using a single-channel radar system are presented to validate the theory.

6.2 Introduction

Accurate measurements of frequency and phase is central to the working of modern radar systems and are directly related to the accurate measurement of parameters like range, bearing, and velocity that are fundamental to the successful detection, tracking, and imaging, etc. of the targets of interest. This chapter focuses on the fundamental systems engineering problem of analysing simple system architectures for the reliable measurement of the phase in target returns using homodyne FMCW radar systems.

[1] The contents of this chapter have been submitted for publication in [84]

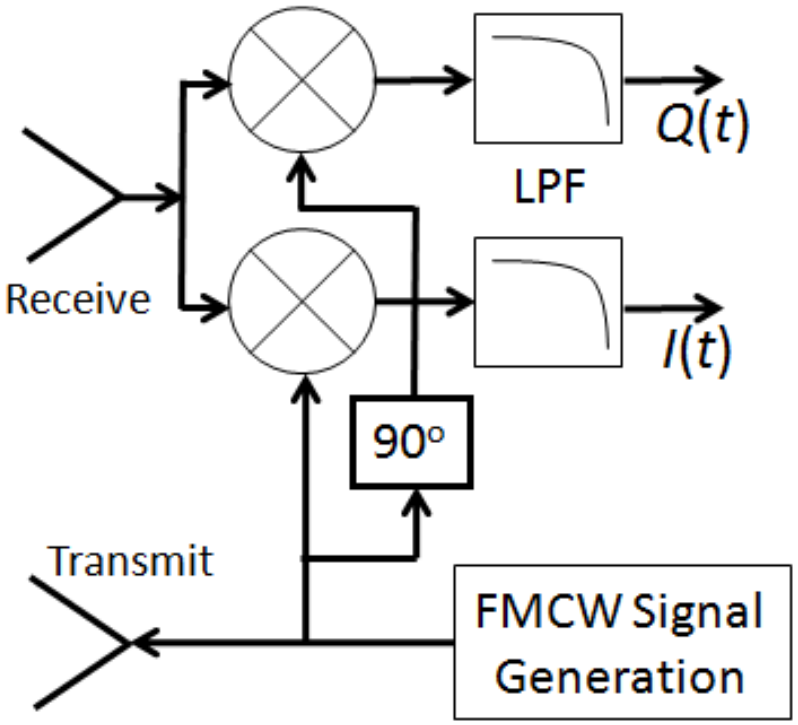

Figure 6.1: Block diagram for time-domain phase measurement using an FMCW radar

Fig. 6.1 shows a homodyne FMCW architecture employing in-phase (I) and quadrature (Q) mixers to demodulate the received radar signal. The instantaneous time-domain amplitude and phase can be extracted by employing this scheme. Fig. 6.2 shows a simpler architecture utilising a single mixer to demodulate the received signal which is then digitised and operated on by complex Fast Fourier Transform (FFT) processing. Although this method cannot be used to obtain the instantaneous phase of the received signal, we note that this is not required for many radar applications. Post-FFT phase measurement can prove sufficient for the desired targets, and it is the purpose of this chapter to analyse the conditions under which no ambiguity will occur in the phase measurement when using the system in Fig. 6.2. An application of this type of system in coherent averaging will also be demonstrated.

When the system in Fig. 6.2 is used, it results in a significant saving in costly hardware and engineering effort especially at microwave and millimetre wave frequencies. However this system cannot measure the negative frequency portion of the spectrum. Therefore, the system shown in Fig. 6.2 will measure the phase unambiguously only if the demodulated frequency spectrum is confined to one sideband. After down-conversion, the spectra of AM (amplitude-modulated) and PM (phase-modulated) signals are zero-centred which means that half of the modulation

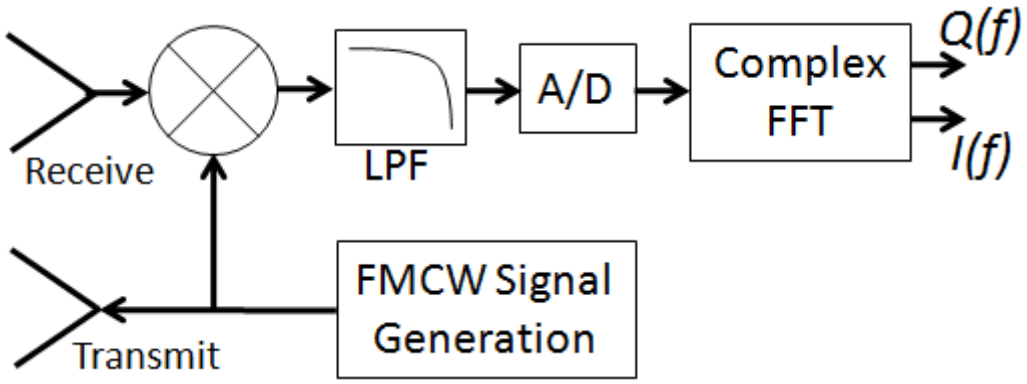

Figure 6.2: Block diagram for frequency-domain phase measurement using an FMCW radar

spectrum lies in the negative frequency region. Therefore, the I/Q demodulation scheme of Fig. 6.1 becomes necessary to extract the full (amplitude and phase) spectrum. In contrast FM (frequency-modulated) spectra are centred at an offset f_m from the carrier. Therefore after demodulation the baseband spectrum having bandwidth B is centred around the baseband modulation frequency f_m. If $|f_m| - B/2 > 0$ then all the modulation power lies in only one side of the origin and the system in Fig. 6.2 can be used to extract the phase information in the signal unambiguously. The only cost is that the thermal noise from the image sideband will always be present, so the noise floor will be 3 dB higher than could be achieved using I/Q mixers. In the following this phenomenon is analysed for FMCW radars.

6.3 General analysis of modulated signals

In this section a mathematical analysis of AM, PM and FM signals is presented. Our analysis is motivated by [85]. Let the AM, PM and FM carrier signals be defined as below:

$$S_{AM}(t) = A_1 [1 + m_a(t)] \cos(\omega_0 t + \theta_0) \quad (6.1)$$

$$S_{PM}(t) = A_2 \cos(\omega_0 t + m_\theta(t) + \theta_0) ; |m_\theta| < 1 \quad (6.2)$$

$$S_{FM}(t) = A_3 \cos([\omega_0 - \omega_m] t + \theta_0), \quad (6.3)$$

where θ_0 represents an unknown phase shift relative to the local oscillator (LO) signal. In (6.3) we have considered frequency modulation resulting in a frequency translation by ω_m. Now consider the demodulation of these signals with a LO at the carrier frequency ω_0 as illustrated in Fig. 6.3. The signal components in the

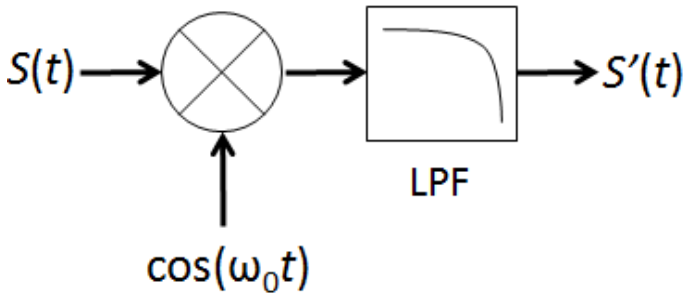

Figure 6.3: Illustration of the demodulation scheme for all three types of modulation.

baseband will be as follows:

$$S'_{AM}(t) = A'_1 m_a(t) \cos(\theta_0) \tag{6.4}$$

$$S'_{PM}(t) \approx A'_2 m_\theta(t) \sin(\theta_0) \tag{6.5}$$

$$S'_{FM}(t) = A'_3 \cos(\omega_m t - \theta_0). \tag{6.6}$$

Note that $S'_{AM}(t)$ is scaled by $\cos(\theta_0)$ that scales the amplitude from maximum (for $\theta_0 = 0$) to zero (for $\theta_0 = \pi/2$). We also notice that in $S'_{PM}(t)$ the $\sin(\theta_0)$ term scales the message signal from maximum (for $\theta_0 = \pi/2$) to zero (for $\theta_0 = 0$). In practice θ_0 varies randomly [86]. Hence, for the faithful reproduction of the AM and PM signals the quadrature channel needs to employed.

In contrast, it can be noted that $S'_{FM}(t)$ is immune to any amplitude or phase ambiguities even in the case of employing a single channel detector. The reason is that instead of residing around the carrier (as in the case of AM and PM signals), the FM signal resides at an offset from the carrier. In other words, while the spectrum of the demodulated AM and PM signals are centred at zero frequency, the spectrum of FM signals is centred at the offset frequency ω_m. Therefore, the full phase information can be extracted from FM signals using various signal post processing techniques, most notably the complex FFT.

In practice instead of a signal tone (ω_m in (6.3)) the demodulated FM signal may contain a band of frequencies, due to signal components (like multiple targets) or due to noise components (like phase noise around a single target). For unambiguous phase measurement using a single-channel receiver, therefore, all signal and noise components must remain at a frequency offset from the carrier.

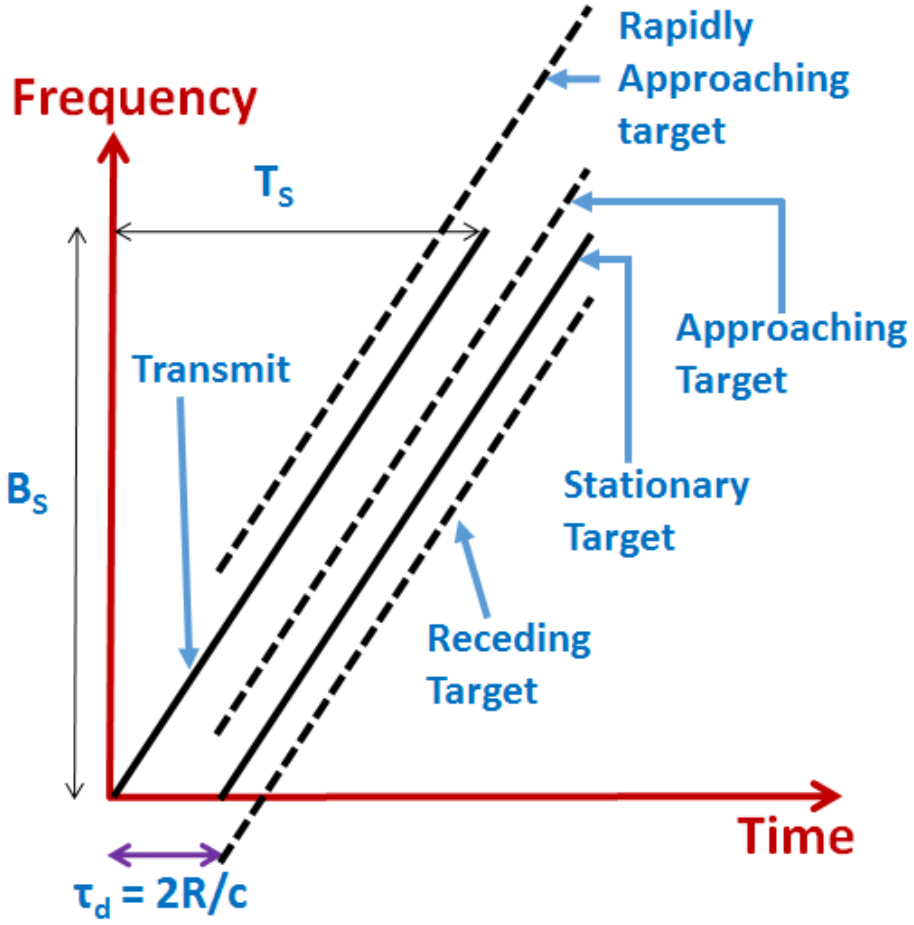

Figure 6.4: Illustration of the swept frequency vs time for a stationary, an approaching, and a receding target. The beat frequency is positive in all cases.

6.4 Analysis of FMCW radar signals

FMCW radars use various types of waveforms and corresponding signal processing schemes to extract the range and Doppler information of the targets of interest [87]. In this section the linear up-ramp signal will be used bearing in mind that the result can be extended to other linear ramp waveforms.

Fig. 6.4 shows the transmit ramp as well as the receive ramps for a stationary, an approaching, and a receding target. B_S and T_S are the swept-bandwidth and sweep-time respectively. τ_d is the round trip time delay due to a target at range R. The beat signal due to the stationary target can be written as,

$$S_{IF}(t) = A_0 \cos\left(2\pi f_{b0} t - \theta_0\right), \tag{6.7}$$

where,

$$|f_{b0}| = \frac{B_S}{T_S}\tau_d. \tag{6.8}$$

Note the similarity between (6.6) and (6.7). The Doppler shift due to an approaching target at R causes the instantaneous received frequency to be larger than that for a stationary target. The beat frequency decreases correspondingly. For a fast enough target, the Doppler shift could be large enough so that the received signal's instantaneous frequency is larger than the instantaneous transmit frequency as shown in the top plot in Fig. 6.4. The beat frequency will be positive in this case. One can easily extend the same arguments for a down-ramp: in that case the beat frequencies will normally be positive except for a rapidly receding target.

6.4.1 Phase measurement in the absence of Doppler

The rapid-approaching situation in Fig. 6.4 cannot happen for stationary targets. Therefore it is reasonable to conclude that for stationary target detection applications, like foreign object debris (FOD) detection, the full phase spectrum can be measured unambiguously using the system in Fig. 6.2.

6.4.2 Phase measurement for moving targets

Let the beat (IF) frequency produced by the stationary target at range R be $-f_{b0}$. The beat frequency for an approaching target at the same range will be $-f_{b0} + f_D$. It follows from Fig. 6.4 that the beat frequency will always remain negative if $f_D < |f_{b0}|$ (assuming an up-chirp). Therefore, for a given set of radar parameters, a relationship can be derived for the maximum allowable target velocity ν that does not change the sign of the beat frequency as follows:

$$f_D = \frac{2\nu}{\lambda} < \frac{B_S}{T_S}\tau_d \Rightarrow \nu < \frac{\lambda B_S R}{cT_S}, \tag{6.9}$$

where λ is the carrier's wavelength and c is the speed of light. For down-ramps, (6.9) also sets the bound on the maximum velocity receding targets could have without changing the sign of the beat frequency. Thus for triangular sweeps (6.9) sets the dynamic range of allowable velocities that would result in unambiguous phase measurement.

From (6.9) it is apparent that the velocity dynamic range can be increased by reducing the Doppler frequency relative to the beat frequency of a given target. This can be done by increasing λ and/or increasing the sweep rate B_S/T_S.

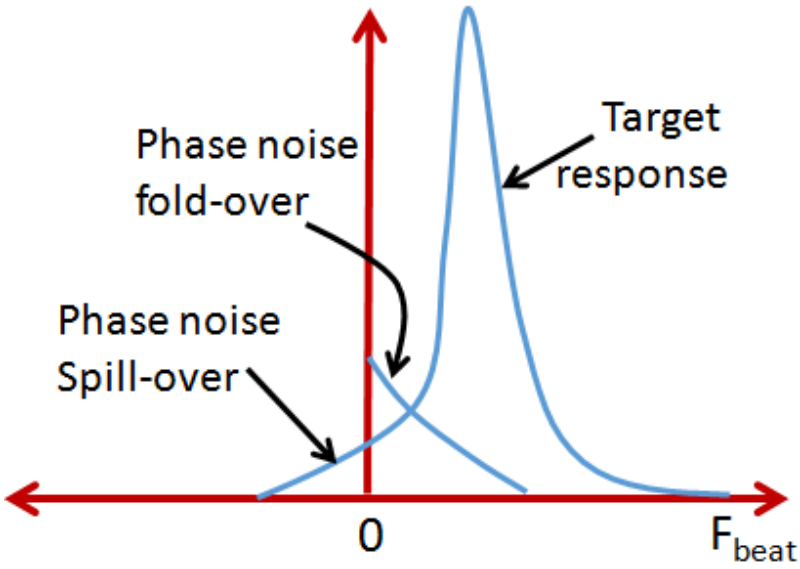

Figure 6.5: Phase noise leakage in the negative frequency region.

6.4.3 The effect of phase noise

Phase noise appears as noise sidebands on the target response. When the target is very close in range some of the noise sidebands can spread into the negative frequency region. When using the single-channel receiver of Fig. 6.2 the negative frequency portion of the target spectrum would wrap around and appear as increased noise in the positive frequency region. This is illustrated in Fig. 6.5.

However it is known that for close ranges the phase noise decorrelates heavily so that the noise sidebands are minimised [27]. For short ranges, the phase noise is decorrelated as 20 dB/decade [27], so if the target's spectrum is steeper than -20 dB/decade there will be residual phase noise that can spill-over and then fold-over. This can happen when a large target is close to the radar.

This effect can be even more pronounced when the target is at a farther range but the target peak appears at a lower frequency due to Doppler shift. The phase noise decorrelation (i.e. the difference in the transmitted and received phase noise processes) will essentially be according to the target's actual range. Detailed calculations of the effect must be carried out using the detailed phase noise spectra. This problem can also be alleviated if λ and/or the sweep rate is increased as explained above.

Table 6.1: Parameters of example radars

Parameters	Surveillance	Automotive
Carrier Frequency	76.5 GHz	24 GHz
Carrier Wavelength	3.9216 mm	12.5 mm
Sweep Time T_S	2 ms	1 ms
Coherent Processing Interval (CPI)	2 ms	64 ms
Doppler Resolution, $1/CPI$	500 Hz	15.625 Hz
Velocity Resolution, $\lambda/(2CPI)$	0.98 m/s	0.0977 m/s
Swept Bandwidth B_S	600 MHz	150 MHz
Doppler Shift at 1 m/s	510 Hz	160 Hz

6.5 Application to FMCW radar systems

6.5.1 Maximum velocity calculations

The application of (6.9) to radar systems is straightforward. Table 6.1 shows the parameters of a surveillance radar and an automotive radar. Table 6.2 shows the maximum permitted velocities calculated using (6.9) for targets at various ranges. It is apparent that in most practical situations the target velocities are under these limits. This is a strong result that suggests that a single-channel demodulator followed by complex FFT processing can be used for coherent processing and phase measurement in a wide variety of situations. For lower carrier frequencies the requirement for the maximum velocities is even more relaxed as evidenced by this example.

6.5.2 Effect on Range-Doppler algorithms

FMCW radars employ various waveforms to extract the true range and Doppler information from radar signals. These include triangular sweeps, the chirp sequence waveform, the multiple FSK waveform, and the intertwined chirp sequence waveform [87]. In general the triangular sweep will have the Doppler limit of (6.9) on both the

Table 6.2: Maximum velocity for unambiguous phase measurement

Range	**Surveillance**		**Automotive**	
	m/s	**mph**	**m/s**	**mph**
1 m	3.92	8.77	6.25	14
10 m	39.2	87.7	62.5	140
100 m	392	877	625	1400

up-sweep and the down-sweep (i.e. approaching as well as receding targets). Other waveforms employing only the up-ramp or the down-ramp respectively will have the Doppler limit for approaching or receding targets only.

6.6 Measurement results from a practical FMCW radar system

This section presents the results of coherent averaging performed on signals measured using the 76.5 GHz surveillance radar system of Table 6.1 based on Fig. 6.2. If the phase is measured faithfully using the system in Fig. 6.2 then coherent averaging should result in M-times improvement in the SNR, where M is the number of signal records being averaged [88].

A raw display of the scene being analysed is shown in Fig. 6.6. Three target peaks can be seen along with the raised noise floor due to phase noise around them. The bins displayed in the abscissa are 25 cm each. The ordinate is normalised to the highest signal in the scene. The dB units are arbitrary in that they are not relative to any common reference (this is a common way of displaying range-profiles in radar systems).

50 sweeps of complex radar data from this scene were recorded and the coherent average was computed. First the phase noise bins shown in Fig. 6.6 were analysed. The dotted line in Fig. 6.7 shows the decrease in noise power versus an increasing number of averages by varying M from 1 to 50. The result has been normalised to the noise power when $M = 1$. The solid line is a plot of the function $1/M$ on the semi-log scale. The result shows an agreement with the theoretical prediction of the improvement in SNR.

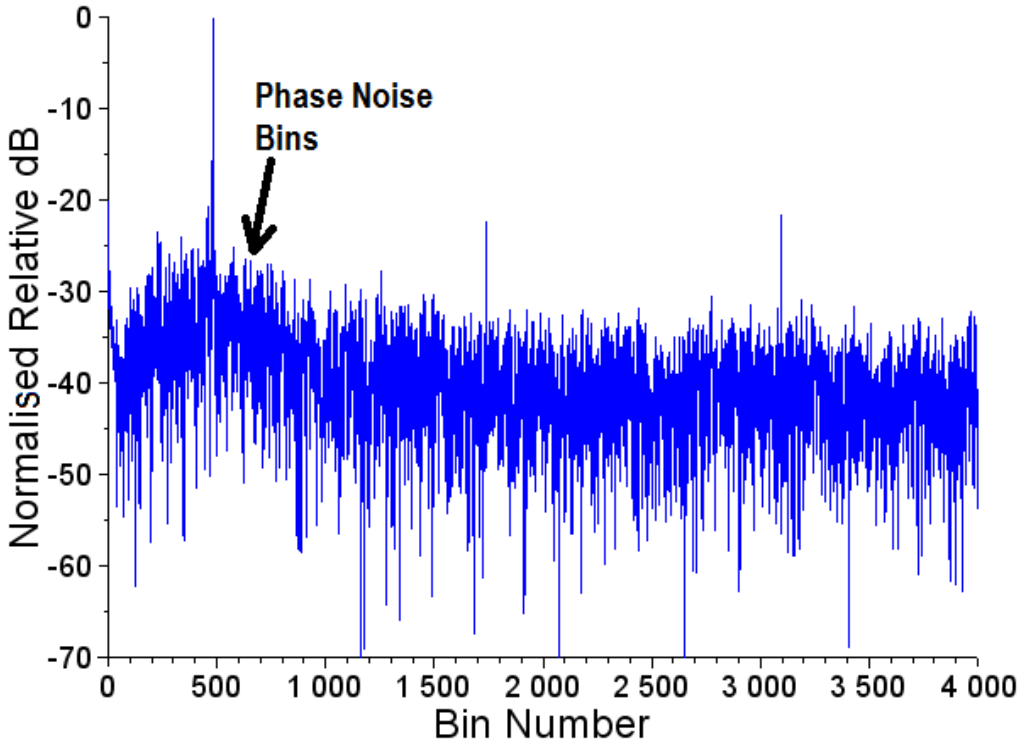

Figure 6.6: Radar scene display from a single FMCW sweep. Three target peaks are visible. The bin size is 25 cm.

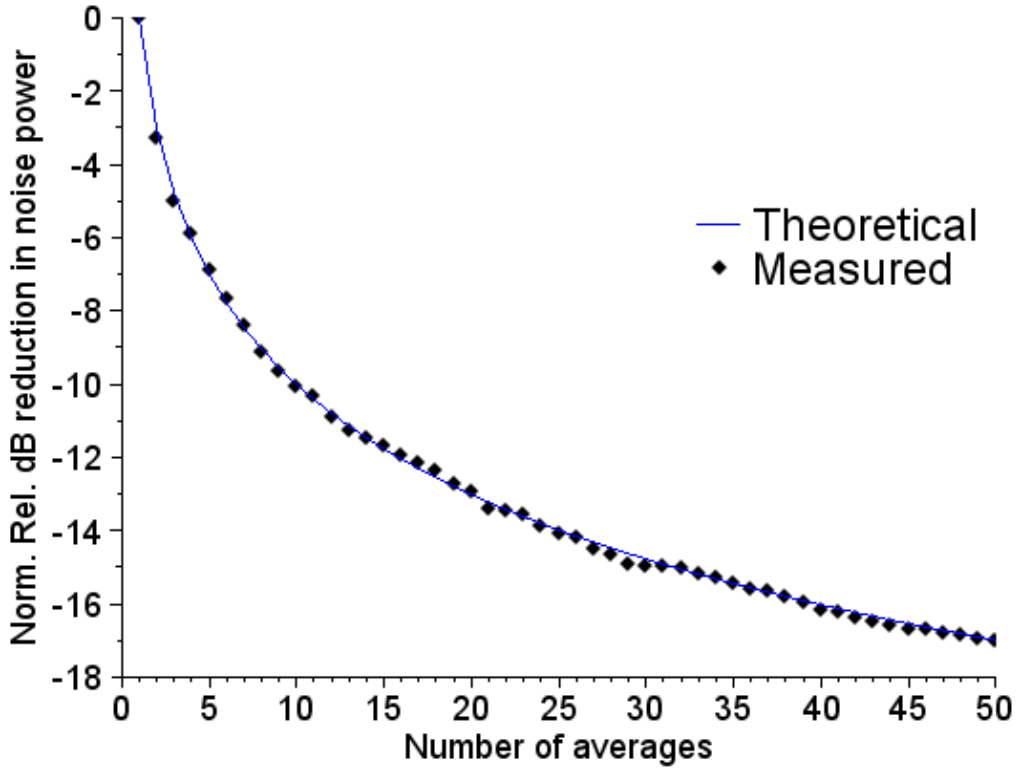

Figure 6.7: Variation of noise power with averaging

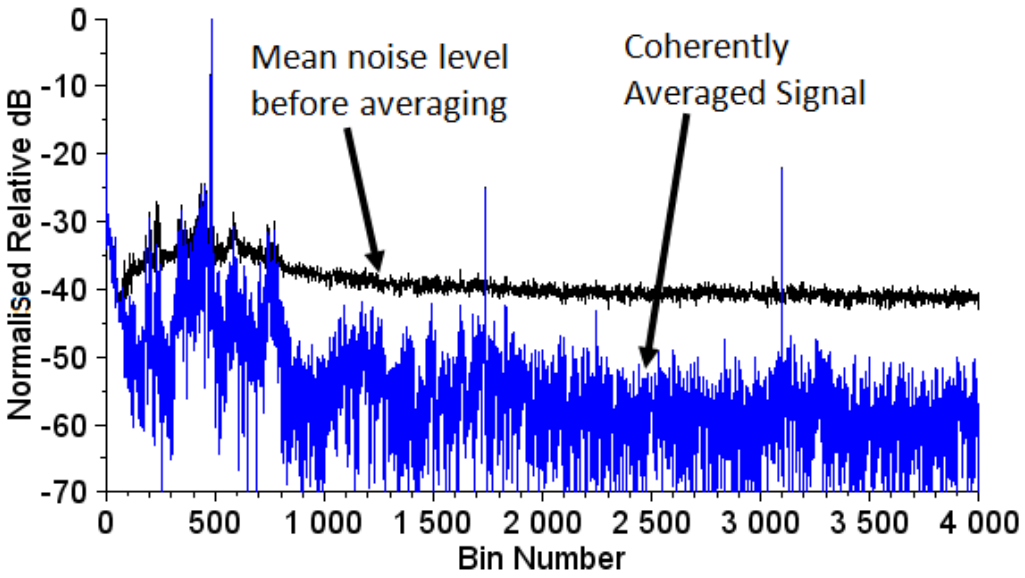

Figure 6.8: Improvement in SNR due to coherently averaging 50 sweeps. The mean noise level before averaging is also displayed for comparison.

In Fig. 6.8 the coherently averaged data using 50 sweeps has been plotted, along with the mean noise level from Fig. 6.6 (i.e. the incoherent average). The improvement in SNR as well as the phase noise sidebands of around 17 dB is apparent, which is compatible with Fig. 6.7. This leads to better definition in the scene.

6.7 Conclusion

In this work the effectiveness of the FMCW radar architecture employing only a single channel detector followed by complex FFT processing to extract the phase information was analysed. A mathematical analysis of various modulation schemes was presented to give the idea a strong theoretical foundation. It was found that the said radar architecture successfully measures the phase information for static targets. For moving targets a maximum velocity condition was derived for unambiguous phase measurement. Practical examples demonstrated that this condition is easily met in a wide variety of applications. Coherent averaging performed on measurements from a surveillance FMCW radar system shows an improvement in SNR according to the theoretical prediction, signifying reliable phase measurement.

Chapter 7

A Generalised Brownian Motion Model of RF Spectral Dispersion due to Phase Noise[1]

7.1 Summary

In this chapter a unified Brownian motion-based model for the dispersion in the RF spectrum of oscillators due to the phase and frequency noise processes will be presented. A novel analysis of the spectral dispersion due to random-walk frequency noise will be presented that shows the possibility of the existence of satellite peaks around the mainlobe of the RF spectrum along with time-varying spectral broadening. Fourier Transform based models will be used for the even-order phase noise process while fractional calculus based models will be used for the odd-order flicker phase and frequency processes. The generalised Gaussian function (GGF) is shown to be an appropriate model for the RF autocorrelation function in all cases.

7.2 Introduction

Phase noise is a physical process that causes the RF spectra of sinewaves to broaden. This results in various problems including reduced resolution in radar and spectroscopic systems and adjacent channel power leakage in communication systems. A large body of literature exists for the characterisation and measurement of phase noise. However a relatively small literature exists that relates exactly the spectral dispersion in the RF spectrum of a sinusoidal signal impaired with the phase

[1]The contents of this chapter have been submitted for publication in [89].

and frequency noise processes. Our interest in this work is in terms of predicting the ultimate target resolution capability of FMCW radar systems, where the range resolution is defined by the phase noise in the transmitted RF signal [27, 43].

Previous attempts at relating the phase spectrum to the RF spectrum of a signal include [70, 90–92]. In this chapter a clear association of each constituent phase noise process with a Brownian motion process will be introduced. The power-law spectral coefficients of the phase spectral density will be related to the variances of the individual Brownian motion processes. Based on existing results the RF spectral dispersion due to the white and flicker phase and frequency processes will be analysed. A novel RF spectrum of a signal impaired with random-walk frequency noise will be presented that suggests the possibility of the existence of *satellite peaks* in the RF spectrum. The application of the generalised Gaussian function (GGF) to model the autocorrelation function of an RF signal impaired with the phase and frequency noise processes will also be presented.

7.3 Theoretical Background

Consider the unity amplitude RF signal,

$$x(t) = \sin\left(2\pi f_0 t + \phi(t)\right), \tag{7.1}$$

where $\phi(t)$ represents the phase noise processes, and f_0 is the carrier (or 'steady-state') frequency that is really defined under the small phase noise condition $\sigma_\phi^2 \ll 1$ which is valid only for short measurement times. The amplitude noise is assumed to be negligible.

7.3.1 Spectral density of phase fluctuations

$\phi(t)$ can be written in terms of its constituent phase noise processes as,

$$\phi(t) = \sum_{\beta=0}^{4} \phi_\beta(t), \tag{7.2}$$

where each of the $\phi_\beta(t)$ are independent zero-mean Gaussian random processes with different covariances, and can be identified by their *colour* [91]. Each of the $\phi_\beta(t)$ can be described by a type of Brownian motion as summarised in Table 7.1. This association implies that all the phase noise processes can be treated using the mathematical tools developed for Brownian motion processes. We note that the white

Table 7.1: The Phase Noise Processes Identified with the Corresponding Brownian Motion of Phase

$\phi_0(t)$	White Phase Noise	differential Brownian motion
$\phi_1(t)$	Flicker Phase Noise	fractional Gaussian noise
$\phi_2(t)$	White Frequency Noise	ordinary Brownian motion
$\phi_3(t)$	Flicker Frequency Noise	fractional Brownian motion
$\phi_4(t)$	Random-walk Frequency Noise	integral Brownian motion

and the flicker phase processes are stationary random processes: however, the three frequency noise processes are non-stationary.

The spectral density of $\phi(t)$ is defined as follows [8],

$$S_\phi(f) = \sum_{\beta=0}^{4} S_{\phi_\beta}(f) = \sum_{\beta=0}^{4} \frac{h_\beta}{f^\beta}. \tag{7.3}$$

$S_\phi(f)$ is the Spectral Density of Phase Fluctuations or the one-sided phase PSD.

7.3.2 The autocorrelation of the RF signal

We use the analytic form of (7.1) as follows:

$$\widehat{x}(t) = e^{j[2\pi f_0 t + \phi(t)]}. \tag{7.4}$$

As noted above, the frequency noise processes in general are non-stationary. Therefore the covariance of $\widehat{x}(t)$ is given as

$$\begin{aligned} R_{\hat{x}}(t_1, t_2) &= E\left[\widehat{x}^*(t_1)\widehat{x}(t_2)\right] \\ &= E\left[e^{j[\phi(t_2)-\phi(t_1)]}\right]. \end{aligned} \tag{7.5}$$

Therefore, for the autocorrelation $R_{\hat{x}}(\tau) = R_{\hat{x}}(t_2 - t_1)$ to exist, the phase noise processes don't need to be stationary but do need to be *first-difference stationary.*

It has been shown that for Gaussian phase noise processes (stationary or other-

wise) the above expectation can be evaluated as [92]:

$$R_{\hat{x}}(t_1, t_2) = \exp\left(-\frac{1}{2}\left[R_\phi(t_1, t_1) + R_\phi(t_2, t_2) - 2R_\phi(t_1, t_2)\right]\right), \tag{7.6}$$

where $R_\phi(t_i, t_j) = E[\phi(t_i)\phi(t_j)]$. Therefore, in order to compute the covariance of the RF signal the covariance of $\phi(t)$ is required.

7.3.3 The covariance and spectrum of $\phi(t)$

Assuming all $\phi_\beta(t)$ being independent of each other one can write using (7.2),

$$\begin{aligned} R_\phi(t_1, t_2) &= E\left[\sum_{\beta=0}^{4}\phi_\beta(t_1)\sum_{l=0}^{4}\phi_l(t_2)\right] \\ &= \sum_{\beta=0}^{4}\sum_{l=0}^{4}E\left[\phi_\beta(t_1)\phi_l(t_2)\right] \end{aligned}$$

$$R_\phi(t_1, t_2) = \sum_{\beta=0}^{4}E[\phi_\beta(t_1)\phi_\beta(t_2)] = \sum_{\beta=0}^{4}C_\beta R_{\phi_\beta}(t_1, t_2). \tag{7.7}$$

That is, the covariance R_ϕ is a linear superposition of the covariance of the individual phase noise processes. The C_β are constant multipliers of the normalised autocorrelation functions $R_{\phi_\beta}(t_1, t_2)$. We note that $R_\phi(t_1, t_2) = R_\phi(\tau)$ for $\beta = 0$ and 2, where $\tau = t_2 - t_1$. The Fourier Transform of $R_\phi(\tau)$ is $S_\phi(2\pi f)$, i.e.,

$$S_\phi(2\pi f) = \mathcal{F}[R_\phi(\tau)]. \tag{7.8}$$

Inserting (7.7) we get,

$$\sum_{\beta=0}^{4}\frac{(2\pi)^\beta h_\beta}{(2\pi f)^\beta} = \mathcal{F}\left[\sum_{\beta=0}^{4}C_\beta \times R_{\phi_\beta}(\tau)\right]$$

$$\Rightarrow C_\beta \times \mathcal{F}[R_{\phi_\beta}(\tau)] = \frac{(2\pi)^\beta h_\beta}{\omega^\beta}. \tag{7.9}$$

For $\beta = 0$ and 2, (7.9) can be solved as shown in Table 7.2. For odd β the $\phi_\beta(t)$ are fractional noise processes and as such direct Fourier Transformation is not the correct tool for analysing them. The covariance of fractional Brownian motion

Table 7.2: The autocorrelation of even-order Phase Noise Processes

$\beta = 0$	$R_{\phi_0}(\tau) = \delta(\tau)$	$C_0 = h_0$
$\beta = 2$	$R_{\phi_2}(\tau) = \lvert\tau\rvert$	$C_2 = -\frac{1}{2}(2\pi)^2 h_2$

(fBm) noise can be derived using fractional calculus, and is given by [93]:

$$R_{fBm}(t_1, t_2) = \frac{\sigma^2_{2H+1}}{2}\left[|t_1|^{2H} + |t_2|^{2H} - |t_1 - t_2|^{2H}\right], \tag{7.10}$$

where $0 < H \leq 1$ is the Hurst exponent and σ^2_{2H+1} is the coefficient of *drift variance* (the subscript $2H + 1$ has been chosen to comply with the notation used in this chapter). The variance of a fBm process can be computed by setting $t_1 = t_2 = t$:

$$\sigma^2_{fBm} = \sigma^2_{2H+1}|t|^{2H}, \tag{7.11}$$

which shows that the variance grows with time. $H = 1$ corresponds to true flicker frequency noise.

As shown in Table 7.1 the flicker phase noise can be modelled as a fractional Gaussian noise. The derivative of fractional Brownian motion would be fractional Gaussian noise (fGn) by analogy with the derivative of ordinary Brownian motion being white Gaussian noise. Unfortunately the derivative of fBm does not exist [92, 94]. However the difference does exist and fGn has been analysed successfully as a discrete stationary random process [92, 93]. The covariance between samples 0 and m of the fGn sequence is given by [93]:

$$R_{fGn}(m) = \frac{\sigma^2_{fGn}}{2}\left[|m + 1|^{2H} - 2|m|^{2H} + |m - 1|^{2H}\right], \tag{7.12}$$

where $0 < H \leq 1$ is again the Hurst exponent. Interestingly σ^2_{fGn} is not a function of H. $H = 1/2$ corresponds to the white noise case and $H = 1$ corresponds to the flicker phase noise case. The approximate spectrum of fGn is given by,

$$S_{fGn}(f) \approx \sigma^2_{fGn} C^2(H)|f|^{1-2H}. \tag{7.13}$$

It is evident that the spectrum approaches h_1/f as $H \to 1$ and one can identify $h_1 = \sigma^2_{fGn} C^2(H)$. An expression for $C^2(H)$ can be found in [93].

7.3.4 The Generalised Gaussian Function

The generalised Gaussian function (GGF) in its normalised form is defined as follows [95]:

$$g_{norm}(x) = \frac{\zeta}{2\alpha\Gamma(1/\zeta)} e^{-(|x|/\alpha)^{\zeta}}. \tag{7.14}$$

For reasons to be apparent soon, the following non-normalised version of the generalised Gaussian function (GGF) will be considered:

$$g(t) = e^{-\alpha|t|^{\zeta}}. \tag{7.15}$$

Using this definition, $\zeta = 1$ results in the Laplacian function and its Fourier Transform is the Lorentzian spectrum:

$$e^{-\alpha|t|} \longleftrightarrow \frac{2\alpha}{\alpha^2 + f^2} = \frac{2/\alpha}{1 + \frac{f^2}{\alpha^2}}. \tag{7.16}$$

At $t = 1/\alpha$ the Laplacian function decreases to $1/e$ of its peak value.

$\zeta = 2$ results in the usual Gaussian function and being an eigen-function of the Fourier transform, the spectrum is also Gaussian:

$$e^{-\alpha|t|^2} \longleftrightarrow \sqrt{\frac{\pi}{\alpha}} e^{-\omega^2/4\alpha}. \tag{7.17}$$

The variance of the Gaussian spectrum is 2α.

The case of $\zeta = 3$ is also important for the present work and will be discussed in Section 7.4.3.

7.4 The RF Spectrum of a signal with phase noise

In this section the phase and frequency noise processes will be related to the RF spectrum of the RF signal that consists of a central peak and the noise sidebands.

7.4.1 White and Flicker Phase Noise

Both white and flicker phase noise contribute to the RF noise sideband power with slope zero and $1/f$ respectively. White noise do not contribute to the central peak of the RF spectrum. The variance of the white noise process is given by $\sigma_0^2 = h_0$. A detailed analysis of the RF spectrum due to flicker phase noise is given in [91] using Correlation Theory and in [92] by treating it as fractional Gaussian noise.

The analysis in [92] suggests that the translation of $1/f$ phase noise to $1/f$ RF sideband spectrum is valid even for large phase noise conditions with σ_ϕ^2 only just under 1. Based on this analysis it appears that $1/f$ noise does not contribute much to the central peak. Both [91] and [92] conclude that at very close offsets (only visible at very long measurement times), the RF spectrum deviates from $1/f$ and levels off.

We note that a measurement of this type of levelling off is not possible in practice due to the frequency noise processes that contribute largely to the central peak of the RF spectrum.

7.4.2 White and Flicker Frequency Noise

Oscillators perform phase-to-frequency conversion due to the fact that they lock onto the frequency point for which the total phase shift around the oscillator loop is zero [96]. Therefore the white and flicker phase noise processes give rise to the white and flicker frequency processes with phase spectrum slopes of $1/f^2$ and $1/f^3$ respectively. These also contribute to the overall lineshape of the central peak of the RF spectrum.

It is well-known that the white frequency noise gives rise to a random-walk phase noise that that can be modelled as ordinary Brownian motion (Bm) with non-stationary variance $\sigma_2^2|t|$. The coefficient of variance can be identified as $\sigma_2^2 = 4\pi^2 h_2$. Analysis of an RF signal impaired with white frequency noise leads to an exponential autocorrelation and Lorentzian spectrum as follows:

$$\begin{aligned} R_{\hat{x}_2}(\tau) = e^{-4\pi^2 h_2|\tau|/2} \quad &\longleftrightarrow \quad \frac{4\pi^2 h_2}{(2\pi^2 h_2)^2 + \omega^2} \\ &= \quad \frac{1/\pi^2 h_2}{1 + (\frac{\omega}{2\pi^2 h_2})^2}. \end{aligned} \tag{7.18}$$

It can be seen that the slope of the RF sideband spectrum approaches $1/f^2$. The autocorrelation is clearly a GGF with $\beta = 1$.

For flicker frequency noise, using (7.10) and (7.6) it has been shown in [92] that the covariance of an RF signal with fractional Brownian phase noise is:

$$R_{\hat{x}_3}(t_1, t_2) = \exp\left(-\sigma_{2H+1}^2 |t_2 - t_1|^{2H}/2\right), \tag{7.19}$$

which shows that the RF signal impaired with fBm phase noise is stationary in the autocorrelation even though the fBm noise is non-stationary itself. Therefore for

exact flicker frequency one can write,

$$\lim_{H\to 1} R_{\hat{x}_3}(\tau) = e^{-Kh_3|\tau|^2/2} \longleftrightarrow \sqrt{\frac{2\pi}{Kh_3}} e^{-\omega^2/2Kh_3}. \tag{7.20}$$

Thus, flicker frequency noise gives rise to a time-invariant Gaussian RF spectrum. The autocorrelation is clearly a GGF with $\beta = 2$.

7.4.3 Random-Walk Frequency Noise

Noting that random-walk frequency noise causes integral Brownian motion (iBm) of phase, it is shown in Appendix A that the covariance of $\phi_4(t)$ is given by,

$$R_{\phi_4}(t_1, t_2) = \sigma_4^2 t_1^2 \left(\frac{t_2}{2} - \frac{t_1}{6}\right), \tag{7.21}$$

for $t_2 \geq t_1$. The variance of a random-walk frequency noise process is given by $\sigma_4^2|t|^3/3$: σ_4^2 is the coefficient of *drift variance* and can be identified as $16\pi^4 h_4$. Inserting (A.1), (A.3) and (A.4) into (7.6) and simplifying the terms we get,

$$\begin{aligned} R_{\hat{x}_4}(t, \tau) &= \exp\left(-\frac{\sigma_4^2}{2}\left[\frac{|\tau|^3}{3} + t\tau^2\right]\right); \quad t \geq 0 \\ \Rightarrow R_{\hat{x}_4}(t, \tau) &= \exp\left(-\frac{\sigma_4^2|\tau|^3}{6}\right) \exp\left(-\frac{\sigma_4^2 t}{2}\tau^2\right). \end{aligned} \tag{7.22}$$

Equation (7.22) shows that the covariance, and hence the RF spectrum, of a signal impaired with iBm noise is non-stationary and has a non-Gaussian spectral shape. The first term in (7.22) is time-invariant while the second term is a time-dispersing Gaussian function. Both of these terms can be identified as Generalised Gaussian Functions with $\beta = 3$ and $\beta = 2$ respectively.

Further analysis of the second (Gaussian) term shows that as time t increases, the spread (or variance) of this term decreases. Due to its multiplicative effect, the covariance also decreases. This shows that as the spectral spread in the RF spectrum increases with time without a bound. Such dispersion has been report in the measurements shown in [70]. For short observation times, however, the Gaussian term will be very large so that its spectrum will be closer to $\delta(f)$ and the spectrum of the first term will dominate the overall spectrum.

A closed-form Fourier Transform of the first term i.e., $\mathcal{F}\left(\exp\left[-\frac{\sigma_4^2|\tau|^3}{6}\right]\right)$ does not appear to be available in the literature. In the absence of that one can first compute the Fourier Transform of $\mathcal{F}\left(\exp\left[-\frac{|\tau|^3}{6}\right]\right)$ numerically, as shown in Fig. 7.1 which reveals that in addition to the central peak, two sets of *satellite peaks* can

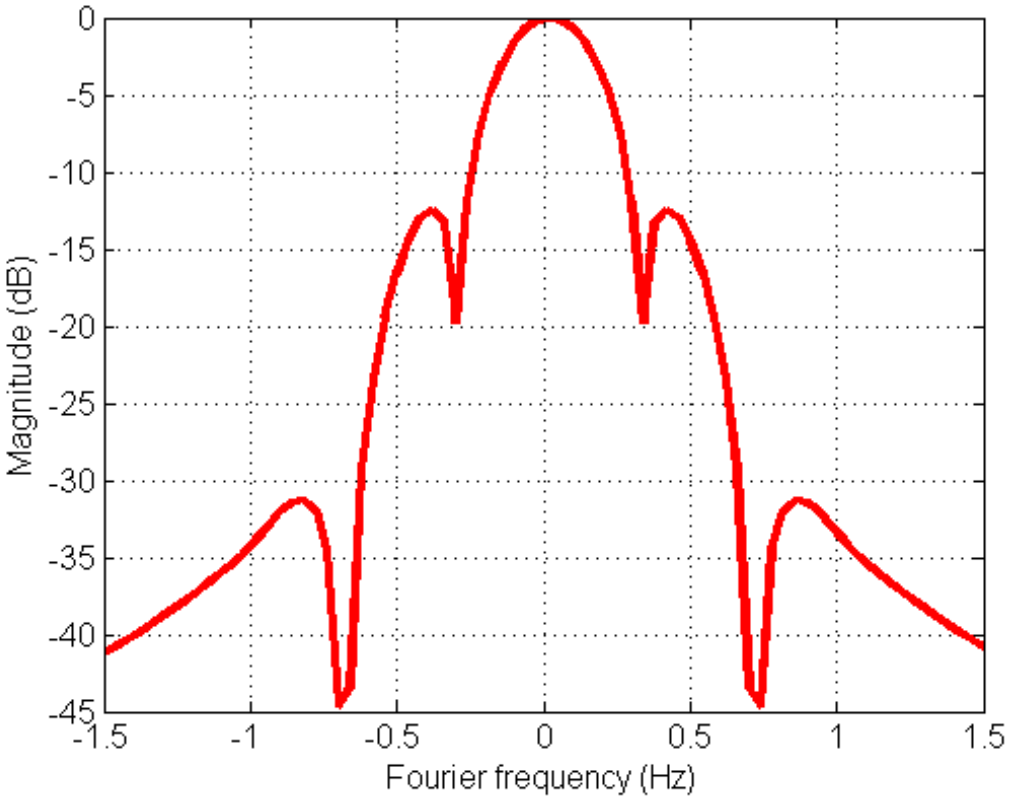

Figure 7.1: Non-Gaussian part of the spectrum of an oscillator having random-walk frequency noise.

be observed. Using the Scaling Property of Fourier Transforms it is apparent that the spectrum $\mathcal{F}\left(\exp\left[-\frac{\sigma_4^2|\tau|^3}{6}\right]\right)$ will be a stretched version of that in Fig 7.1.

The existence of satellite peaks has been reported in the measurements conducted in [97–99]. Our analysis provides a rigorous framework for analysing such phenomena.

7.5 Conclusion

In this chapter the RF spectral dispersion of signals due to phase noise processes modelled using the Brownian motion processes was analysed. The variances of the individual Brownian motion processes were found to be related to the power-law spectral coefficients of the phase spectrum. The RF signal spectrum under white and flicker phase and frequency noises was analysed. A novel RF spectrum of a signal impaired with random-walk frequency noise was presented that highlighted the possibility of the existence of satellite peaks in the RF spectrum. The autocorrelation of the RF signal in each case was successfully modelled using the generalised Gaussian function (GGF). The model developed here can be used to predict the expected lineshape and sideband power of practical oscillators.

Chapter 8

The Linewidth of Oscillators with Power-Law Phase Noise[1]

8.1 Summary

Oscillator linewidth is an important parameter that defines the resolution capability of radar and spectroscopic systems. In this chapter the existing models for the linewidth of the RF spectra of oscillators having power-law phase noise will be reviewed and a new model for the linewidth due to random-walk frequency instability will be developed. The dependence on measurement time of the linewidth due to the flicker frequency process has also been addressed. It will be shown that the RF spectrum of an oscillator having random-walk frequency noise can have a much more complicated shape than the Gaussian shape reported in other works. The effect of frequency multiplication on the linewidth for each type of phase noise will be discussed. Correction factors have been worked out for each frequency noise process to correct for the artefacts introduced by the linewidth measurement system. The chapter ends with a discussion on how the oscillator linewidth defines range resolution in FMCW radar systems.

8.2 Introduction

The characterisation of an oscillator's phase and frequency stability and drift phenomena is done using the spectral density of phase fluctuations $S_\phi(f)$, which is a composite of various phase noise processes [9]. Practical radio systems like radars,

[1] A research paper based on some of the contents of this chapter has been submitted for publication in [100] and is currently under review.

communication systems, and meteorological systems measure and process the RF spectrum $S_{RF}(f)$ of the received signals. Due to the importance of these two quantities, they have received much attention in the literature where the characteristics of each and their inter-relationship has been explored [11, 49, 101]. It is well-known that, within a scaling factor, the two quantities are equal when the phase noise is small, which is essentially at the frequency offsets far from the carrier, and models the short-term frequency instability of the oscillator. Further it is also known that the low-frequency phase noise processes in $S_\phi(f)$ model the medium-term and long-term frequency instability. In addition the low-frequency noise processes have a relationship with the line-shape of $S_{RF}(f)$ and the *linewidth* which is a very important quantity for high-resolution radio systems.

Halford [53], over 40 years ago, presented a heuristic model to compute the linewidth of oscillators having power-law phase noise based on a *generalised Lorentzian spectrum* which has been widely used to estimate oscillator linewidths. Since that time, researchers have investigated the relationship between $S_{RF}(f)$ and $S_\phi(f)$ for low frequency offsets [11, 49, 53, 90, 91, 102]. However an improved model of oscillator linewidth for power-law noise processes has not been presented. Our interest in oscillator linewidths is due to the fact that they define the range resolution in coherent as well as non-coherent FMCW radar systems.

This chapter addresses the problem of computing the linewidth of the RF spectra $S_{RF}(f)$ as a function of the low-frequency phase noise processes in oscillators specified by $S_\phi(f)$. An attempt will be made to consolidate the existing models for $S_{RF}(f)$ proposed over the recent years and analyse their effectiveness in predicting oscillator linewidths by discussing their pros and cons. The derived results will be compared with Halford's heuristic model for oscillator linewidth [53] and in doing so the need for better linewidth models for flicker frequency noise and random-walk frequency noise will become apparent. In theory, the RF spectrum of an oscillator having pure flicker frequency noise does not exist because the noise process is non-stationary. After analysing a few models that diverge for pure flicker frequency noise, alternative models will be discussed that include the effect of finite measurement time and measurement bandwidth, resulting in expressions for finite measured oscillator linewidths. The latter models are more useful in practice. Afterwards a new model for the $S_{RF}(f)$ for the random-walk frequency case will be discussed and the oscillator linewidth will be worked out from that model. The effect of frequency multiplication on the linewidth for each noise type will also be discussed.

The organisation of this chapter is as follows. Section III introduces the precise relationship between various regions of $S_{RF}(f)$ and $S_\phi(f)$. Section IV introduces

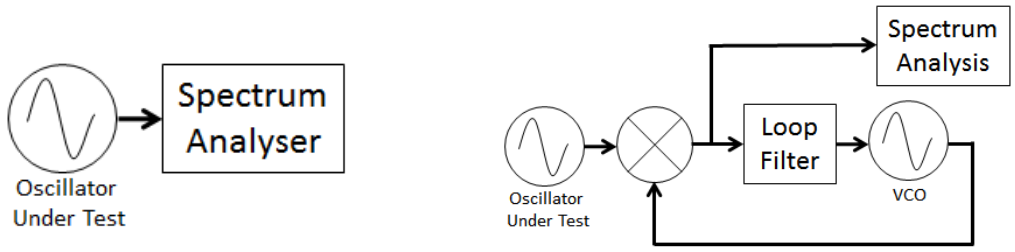

(a) Measurement of $S_{RF}(f)$ (b) Measurement setup for $S_\phi(f)$

Figure 8.1: Measurement setups for (a) the RF Spectrum and (b) the spectral density of phase fluctuations of an Oscillator.

two popular linewidth measurement systems. In Section V an analysis of oscillator linewidths for each type of phase noise is presented separately along with the effects of frequency multiplication in each case. In addition to a critical analysis of existing models, a new model for linewidth due to the random-walk frequency noise will be presented. The section will conclude with a discussion on computing the overall linewidth. Section VI discusses the relationship of oscillator linewidth with radar range resolution for sub-coherence time delays (i.e. short ranges) as well as longer ranges. Section VII contains the conclusion.

8.3 The RF Spectrum and the Spectral Density of Phase Fluctuations

The RF Spectrum $S_{RF}(f)$ of an oscillator and the Spectral Density of Phase Fluctuations $S_\phi(f)$ of an oscillator are distinct quantities that are related to each other in a rather complicated way. Fig. 8.1a shows the setup to measure $S_{RF}(f)$: this is also called direct spectrum measurement. A spectrum analyser can be used to measure $S_{RF}(f)$ at microwave and millimetre wave frequencies. A scanning Fabry-Pérot interferometer can be used at optical frequencies to measure the RF spectrum [68]. Fig. 8.2 shows an illustration of a typical plot displayed using this setup for an oscillator having a nominal frequency ν_0. The labelling highlights some common terms used in the literature in connection with phase noise.

Fig. 8.1b shows the set up to measure $S_\phi(f)$. This scheme is commonly used in *signal source analysers* where the actual implementation in some modern signal source analysers use a digital PLL followed by FFT and correlation processing. Fig. 8.3 shows an illustration of a typical plot displayed using this set up. The labelling highlights the common phase noise processes in oscillators [8].

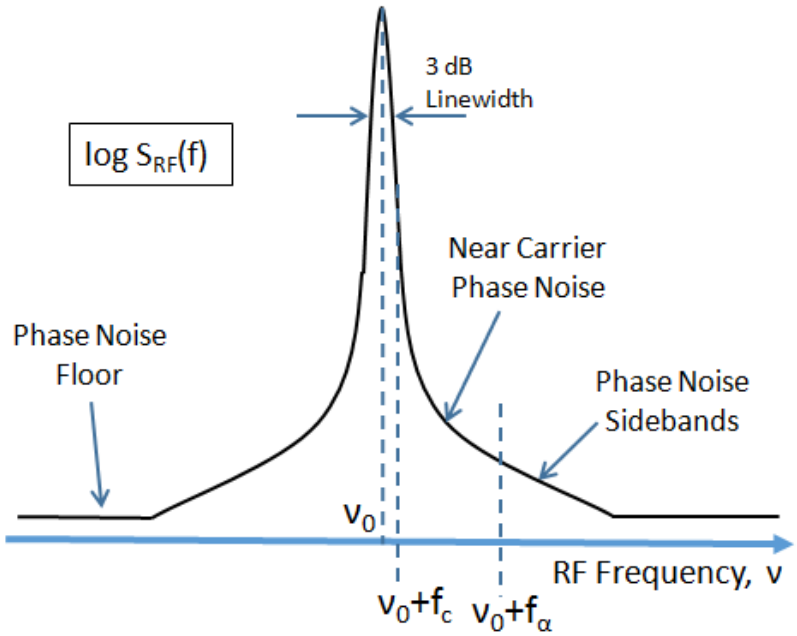

Figure 8.2: Illustration of the RF Spectrum of an oscillator

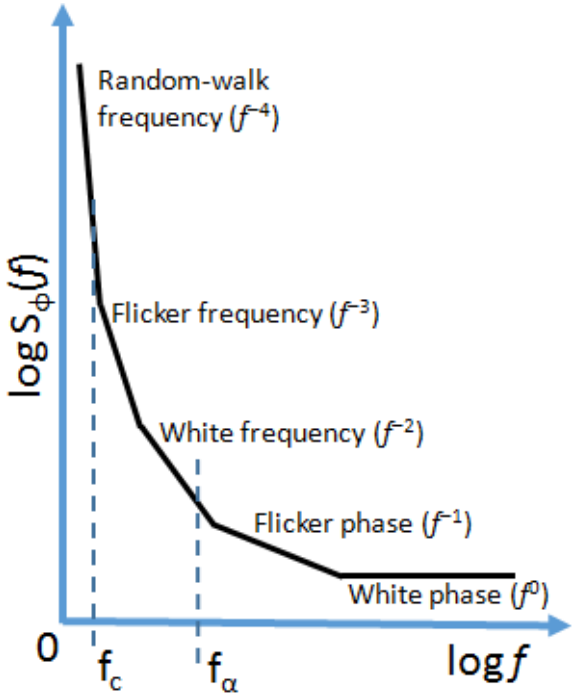

Figure 8.3: A generic plot of the Spectral Density of Phase Fluctuations [8].

The IEEE Standard 1139-1999 [8] defines the relationship between $S_{RF}(f)$ and $S_\phi(f)$ at large frequency offsets as follows. The phase noise $\mathcal{L}(f)$ measured from $S_{RF}(f)$ in dBc/Hz is equal to one-half of $S_\phi(f)$ for all frequencies greater than f_α defined as [9], [8]:

$$\int_{f_\alpha}^{\infty} S_\phi(f)df = 0.1 \ \mathtt{rad}^2. \tag{8.1}$$

Below f_α there exists another frequency f_c, called the *coherence frequency* of the oscillator, defined as:

$$\int_{f_c}^{\infty} S_\phi(f)df = 1 \ \mathtt{rad}^2. \tag{8.2}$$

f_c defines the 3-dB linewidth of $S_{RF}(f)$ [53], [55] which is the main focus of this chapter. f_c and f_α are notionally shown in Fig. 8.3. In addition to defining the 3-dB linewidth f_c also defines the *coherence time* $\tau_c = 1/2\pi f_c$, which is the time lag after which an oscillator signal becomes 1 rad^2 RMS out of phase with itself (due to phase noise). Below f_c the RF line shape of an oscillator is a function of the low-frequency portion of $S_\phi(f)$ [53, 91, 102]. Note that the white-phase (f^0) portion of $S_\phi(f)$ is not used in computing f_c and f_α because the integrals would diverge. The portion of $S_{RF}(f)$ between f_c and f_α defines the *near-carrier phase noise*. In this region, $S_{RF}(f)$ is nonlinearly related to $S_\phi(f)$ [101], [102], [51]. Some authors also use interpolation as an approximation of the RF spectrum between f_c and f_α instead of using the non-linear relationship.

From the preceding discussion it is clear that $S_{RF}(f)$ and $S_\phi(f)$ are related to each other in a complicated but distinctive way. For low to moderate phase noise sidebands, the phase noise measured using $S_{RF}(f)$ is always less than 0 dBc . On the other hand, for a low-enough frequency offset, $S_\phi(f)$ can indeed be greater than 0 dB-rad^2/Hz for typical oscillators: even when the phase noise sidebands are very low. In fact measurements have not shown any upper limit for $S_\phi(f)$ [103]. As a final note, an attempt must *not* be made to compute f_c and f_α using $S_{RF}(f)$. The reason is that the $\int_{-\infty}^{\infty} S_{RF}(f)df$ is equal to the power P in the RF signal: so f_c and f_α computed using $S_{RF}(f)$ will be a function of P which does not make sense. One could argue that one could estimate f_c and f_α using $S_{RF}(f)/P$, i.e., the normalised RF spectrum. However, note that $\int_{-\infty}^{\infty} [S_{RF}(f)/P]\, df = 1$ so that $f_c = -\infty$, which doesn't make sense again. Also f_α computed using $S_{RF}(f)$ would be incorrect if AM noise is present in addition to phase noise . We conclude that f_c and f_α must be computed from $S_\phi(f)$. Once computed, they can be used to identify the three regions of $S_{RF}(f)$.

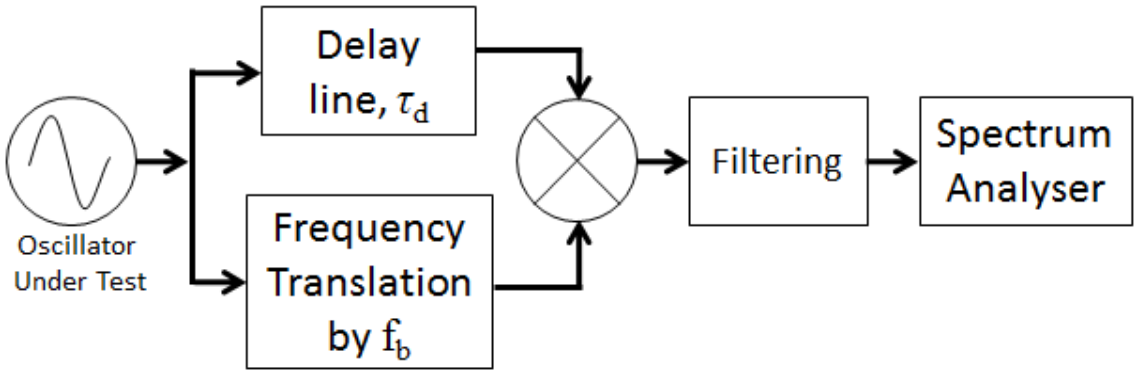

Figure 8.4: Delayed self-heterodyne setup for linewidth measurement

8.4 Measurement of the linewidth

Direct spectrum measurement has been used for the measurement of the linewidth of highly stable lasers at low resolutions [68]. While using direct linewidth measurement the measurement time τ_m sets the lower frequency limit in the measurement: frequency variations slower than $1/\tau_m$ will have no contribution in the measured $S_{RF}(f)$.

However, in general, fine resolution measurement of the linewidth of noisy oscillators on a spectrum analyser may not be possible due to the frequency noise processes causing the spectrum to drift over the analyser's display. The drifting RF spectrum makes it impossible to use averaging over multiple measurements to reduce the display noise. Also, an attempt to lower the resolution bandwidth (RBW) of the spectrum analyser (to measure the linewidth accurately) would require longer sweep times. Therefore, the power in a single measurement may not remain confined in a single frequency point due to the frequency drift. This will give rise to distorted measured spectra.

Reference [104] reviews several measurement setups that have been devised to measure the linewidth of oscillators with high resolution. Of those, a commonly used setup is the delayed self-heterodyne system [105] shown in Fig. 8.4. In the top branch the oscillator signal is passed through a delay-line having a length such that the time-delay τ_d is greater than the coherence time τ_c of the oscillator so that the two inputs to the mixer are effectively uncorrelated. In the lower branch the oscillator signal is frequency translated by f_b which is usually much smaller than the oscillator's nominal RF frequency ν_0 but needs to be larger than the spectral spread being measured. The mixer produces a signal at the beat frequency f_b and a spectrum analyser is used to measure the linewidth.

The phase noise in the beat signal produced by the mixer is $\phi(t) - \phi(t - \tau_d)$.

This implies that the low-frequency FM noise processes cancel out for all $f < 1/\tau_d$. Therefore τ_d in this setup has the same effect as τ_m in direct spectrum measurement [71]. The measurement system of Fig. 8.4 modifies the actual linewidth of the oscillator: the measured linewidth needs to be corrected by a factor depending on the type of power-law phase noise in order to compute the correct linewidth. For the delayed self-heterodyne system it has been shown that the measured Lorentzian linewidth (for the white-frequency case) is twice the original linewidth and the measured Gaussian linewidth (for the flicker frequency case) is $\sqrt{2}$ times the original [69]. We will discuss the increase in the linewidth for the Random-Walk Frequency process in Section 8.5.5.

It should be noted that the above-mentioned increase in the measured linewidth is only valid when $\tau_d > \tau_c$. When $\tau_d < \tau_c$, the difference phase term $\phi(t) - \phi(t - \tau_d)$ causes the noise processes to decorrelate, which results in measured linewidths narrower that those stated above [69, 80].

It has been shown that the measured linewidth is also a slow function of the measurement time, and increases indefinitely in the limit of increasing measurement time [68, 69, 71]. The excess increase in the measured linewidth is attributed to the flicker frequency noise process.

As a final note, the effects of the dispersion in the delay-line being used in the measurement setup must be characterised to estimate any linewidth broadening due to the dispersive effects [106].

8.5 Theoretical analysis of oscillator linewidth

In this section models of the oscillator linewidth are presented based on the models of $S_{RF}(f)$ for each phase noise process separately. Expressions for the increase in the linewidth under frequency multiplication for each case will also be derived.

$S_\phi(f)$ has the following well-known form [8]

$$S_\phi(f) = h_0 + \frac{h_1}{f} + \frac{h_2}{f^2} + \frac{h_3}{f^3} + \frac{h_4}{f^4}, \tag{8.3}$$

so that the general form is $S_\phi(f) = \sum h_\beta / f^\beta$. Under frequency multiplication by N, it is well-known that all the coefficients h_β are multiplied by N^2. Therefore, the multiplied up phase spectrum is,

$$\widehat{S}_\phi(f) = N^2 h_0 + \frac{N^2 h_1}{f} + \frac{N^2 h_2}{f^2} + \frac{N^2 h_3}{f^3} + \frac{N^2 h_4}{f^4}. \tag{8.4}$$

In the following the notation $S_\beta(f)$ will be used for the oscillator's RF spectrum due to the β-th phase noise process, W_β for the respective linewidth, and $\widehat{W}_\beta$ for the multiplied up linewidth.

8.5.1 White Phase Noise

White phase noise has a flat frequency spectrum. Theoretically an oscillator signal in white phase noise will have a linewidth of zero. Practically the linewidth will be defined by the measurement time, τ_m, as follows:

$$W_0 = 1/\tau_m. \tag{8.5}$$

It is interesting to note that the residual FM deviation in this case is zero, so a frequency multiplier will not have any effect on the linewidth. Therefore, the linewidth after frequency multiplication will be,

$$\widehat{W}_0 = W_0. \tag{8.6}$$

In other words the coefficient k_0 defines the level of white phase noise in the oscillator's sideband spectrum.

8.5.2 Flicker PM Noise

Flicker PM noise arises due to parametric fluctuations in the oscillator (such as changes in the gain and noise figure of the amplifier, and the resonator Q-factor in the oscillator's loop [24]) and are fundamentally non-stationary. One runs into severe mathematical difficulties while analysing flicker noise. For example, the Fourier Transforms do not converge when applied to flicker noise [11], [107].

Chorti [91] derived the exact RF spectrum of oscillators having phase noise of the form $1/f^{1+\delta}$. The model diverges for flicker PM noise (i.e. when $\delta = 0$) as expected due to the noise being non-stationary. Demir [108] derived an expression for the RF spectrum of oscillators with flicker PM noise by assuming a low-frequency cut-off for the RF spectrum,

$$S_1(f) = \frac{1}{|f|} - \frac{4}{2\pi f}\tan^{-1}\left(\frac{\gamma_c}{2\pi f}\right), \tag{8.7}$$

where γ_c is related to the corner frequency. One may be tempted to define the 3-dB linewidth by normalising (8.7) by $S(0) = 4/\gamma_c$ and equating that to 1/2. It can be

shown that,

$$f_{3dB} \stackrel{?}{=} 0.527\gamma_c. \tag{8.8}$$

However, we believe that this is an incorrect result because the the total power in (8.7) is,

$$P = \int_{-\infty}^{\infty} S(f)df = \infty, \tag{8.9}$$

which is not possible physically. To define phase noise the RF spectrum needs to be normalised by the total power. This problem has also been pointed out in [103]. The reason for the infinite result in this model (or any other O($1/f$) model) is that the power spectrum does not decrease fast enough with frequency for the integral to converge. In this case the oscillator linewidth cannot be defined.

Inspired by the Lorentzian spectrum, consider the simplified general model for the RF spectrum of an oscillator with flicker phase noise as follows,

$$S_1(f) = \frac{A_0}{1 + \left(\frac{|f|}{\frac{1}{2}W_1}\right)^k}. \tag{8.10}$$

It can be shown that the total power in (8.10) is finite only if $k > 1$ while it is infinite for $0 \leq k \leq 1$.

Thus it can be concluded that the flicker noise processes having power greater than 1 have some contribution to the oscillator linewidth. The model proposed by Chorti [91] can be used to estimate the effect on the linewidth in this case. Restricting to integer powers it is apparent that pure flicker-phase noise does not contribute to the linewidth, as also noted by Halford [53].

8.5.3 White Frequency Noise

The RF spectrum of the oscillator having white frequency noise has a well-known Lorentzian shape [53],

$$S_2(f) = \frac{A_0}{1 + \left[\frac{f}{W_2/2}\right]^2}, \tag{8.11}$$

where $A_0 = 2P/(\pi W_2)$, W_2 is the linewidth, and P is the total RF power $P = \int_{-\infty}^{\infty} S_2(f)df$. At large offset frequencies this spectrum should be equal to the power-law phase noise spectrum as,

$$S_2(f)|_{f \gg W_2} = A_0 \left(\frac{W_2}{2}\right)^2 f^{-2} = P\frac{1}{2}h_2 f^{-2}, \tag{8.12}$$

which implies that,

$$W_2 = \pi h_2. \tag{8.13}$$

The linewidth after frequency multiplication by N will be,

$$\widehat{W_2} = \pi N^2 h_2 = N^2 W_2. \tag{8.14}$$

The oscillator linewidth due to white frequency noise does not depend on the measurement time τ_m because the frequency drift due to the white frequency noise process is always confined around the nominal frequency ν_0.

8.5.4 Flicker Frequency Noise

According to Halford's model, the linewidth due to flicker frequency noise is [53],

$$W_3 = 2.2\sqrt{h_3}, \tag{8.15}$$

and the multiplied up linewidth due to frequency multiplication by N is,

$$\widehat{W_3} = 2.2\sqrt{N^2 h_3} = 2.2N\sqrt{h_3} = NW_3. \tag{8.16}$$

Therefore, the oscillator linewidth increases $N-$times (instead of N^2 as for the white frequency case). In [90, 102] Klimovitch has derived the exact RF spectrum of oscillators having phase noise of the form $1/f^{\delta+2}$ where $\delta = 1$ corresponds to the case of flicker frequency noise. The model shows that close to the carrier, the RF spectrum has a Gaussian shape,

$$S_3(\omega) \approx \frac{\sqrt{2\pi}}{\sigma} \exp\left[-\frac{\omega^2}{2\sigma^2}\right]. \tag{8.17}$$

For $\delta \approx 1$ Klimovitch has shown that,

$$\sigma = \left[\frac{2h_3}{1-\delta}\right]^{\frac{1}{1+\delta}}. \tag{8.18}$$

The linewidth of the oscillator can be defined using the formula for the full width at half maximum (FWHM) for a Gaussian function,

$$W_3 = 2\sqrt{2\ln 2}\frac{\sigma}{2\pi} = \frac{2.355}{2\pi}\left[\frac{2h_3}{1-\delta}\right]^{\frac{1}{1+\delta}}. \tag{8.19}$$

As $\delta \to 1$ the predicted linewidth becomes excessively large and diverges at $\delta = 1$. While correct for a true non-stationary flicker frequency noise process, this gives us limited information about the RF spectrum of an oscillator having a finite bandwidth measured over a finite observation time. However, the increase in the linewidth under frequency multiplication by N can be derived as follows:

$$\widehat{\sigma} = \left[\frac{2N^2 h_3}{1-\delta}\right]^{\frac{1}{1+\delta}} = N^{\frac{2}{1+\delta}}\sigma, \tag{8.20}$$

so that,

$$\widehat{W_3} = N^{\frac{2}{1+\delta}} W_3. \tag{8.21}$$

For exact flicker frequency noise $\delta = 1$, which implies that $\widehat{W_3} = NW_3$. This result is in agreement with (8.16).

The Gaussian spectrum for the flicker frequency noise process has also been derived by Herzel [109] by modelling the noise process as an Ornstein–Uhlenbeck process. The approximate autocorrelation function is,

$$R_3(\tau) = \exp\left[-\sigma^2\tau^2\right], \tag{8.22}$$

where σ is the variance of the VCO controlling voltage. While the Gaussian shape is confirmed by this model, unfortunately it is not possible to link σ to h_3 to derive an expression for the linewidth.

A useful relationship of the $S_3(f)$ was developed by O'Mahony et al. [68]. Using the scanning Fabry-Pérot interferometer as the measuring instrument it was noted that the finite measurement bandwidth sets an upper limit F_u and the finite measurement time τ_m sets a lower limit $F_l = 1/\tau_m$ on the measured spectrum. In the notation used in this chapter, the derived RF spectrum is [68],

$$S_3(f) = C_0 \exp\left[-\frac{f^2}{4h_3 \ln\left(F_u/F_l\right)}\right], \tag{8.23}$$

where C_0 is a constant. Therefore, the 3-dB linewidth is,

$$W_3 = 2.355 \times \sqrt{2h_3 \ln\left(\tau_m F_u\right)}, \tag{8.24}$$

which verifies the dependence of W_3 on $\sqrt{h_3}$ as predicted by (8.15). The linewidth is seen to be nonlinearly related to the measurement time and has been verified using measurements [68]. For infinite measurement time or infinite measurement bandwidth (8.24) predicts an infinite linewidth as expected because the oscillator

RF spectrum due to the flicker frequency noise is non-stationary (as the noise process itself).

Another useful model has been worked out by Mercer [69]. The reported relationship for the linewidth is,

$$W_3 = 2.355 \times \frac{1}{2\pi}\sqrt{\frac{h_3}{\pi}\left[1 + \ln\left(\tau_m\sqrt{\frac{h_3}{2\pi^3}}\right)\right]}. \tag{8.25}$$

The $\sqrt{h_3}$ dependence can be seen, as well as the dependence on τ_m. Mercer also used the delayed self-heterodyne measurement system to measure the linewidth. The Gaussian line-shape has been confirmed in [69] having a linewidth of,

$$W_{3(meas)} = 2.355 \times \frac{1}{2\pi}\sqrt{\frac{h_3}{\pi}\left(4.3 + \ln\frac{4.3h_3\tau_d^{2.1}}{\pi}\right)}, \tag{8.26}$$

for $h_3\tau_d^2/\pi \gg 1$. For a fixed delay time τ_d, the linewidth is still roughly proportional to $\sqrt{h_3}$ (along with an additional weak logarithm dependence). The linewidth is related in a more complicated way to τ_d due to the operation of the delayed self-heterodyne system and due to the fact that the flicker frequency noise is never entirely uncorrelated even for very long delay times due to its low-frequency nature [69].

From the preceding discussion it is clear that the line-shape of the $S_3(f)$ is Gaussian near the carrier when the flicker frequency noise is dominant. Away from the carrier the RF spectrum approaches one half of h_3/f^3: however in many cases the RF spectrum in that region is dominated by the $1/f^2$ portion of the white-frequency noise spectrum due to its relatively gradual slope [69]. Finally note that Halford's heuristic formula (8.15) gives no information about the dependence of W_3 on measurement time or measurement bandwidth.

8.5.5 Random Walk Frequency Noise

According to Halford's model, the linewidth due to random walk frequency noise is [53],

$$W_4 = 2.08\sqrt[3]{h_4}, \tag{8.27}$$

and the multiplied up linewidth is,

$$\widehat{W_4} = 2.08\sqrt[3]{N^2h_4} = 2.08N^{2/3}\sqrt[3]{h_4} = N^{2/3}W_4. \tag{8.28}$$

Chorti [91] has proposed a model of the oscillator spectrum having random walk frequency noise by assuming a low-frequency cutoff for the frequency noise spectrum $S_{\nu_4}(\omega)$ as follows:

$$S_{\nu_4}(\omega) = \frac{16\pi^4 h_4}{\rho^2 + \omega^2}, \tag{8.29}$$

where ρ is the corner frequency. Using the above model, the near-carrier RF spectrum turns out to be [91],

$$S_4(\omega) = \frac{\sqrt{\rho}}{2\pi\sqrt{\pi h_4}} \exp\left[-\frac{\rho\omega^2}{16\pi^4 h_4}\right]. \tag{8.30}$$

The 'variance' of the Gaussian spectrum can be identified as $\sigma_\omega^2 = 8\pi^4 h_4/\rho$. Therefore, one can attempt to define the linewidth using the FWHM relation as follows,

$$\begin{aligned} W_4 &= 2.355 \times \sigma_\omega/2\pi \quad \texttt{Hz} \\ &\stackrel{?}{=} 2.355 \times \sqrt{\frac{2\pi^2 h_4}{\rho}}. \end{aligned} \tag{8.31}$$

However, it appears that a measurement of a lower corner frequency ρ has not been reported anywhere in the literature. Further, in analogy with the white-frequency Lorentzian spectrum, if it is assumed that $\rho = 8\pi^4 h_4$ then the linewidth becomes independent of the coefficient h_4, which does not seem plausible. Lastly, if ρ is assumed to be a cutoff independent of h_4 then the linewidth $W_4 \propto \sqrt{h_4}$ which is the same order of variation as the flicker frequency noise.

Vannicola [12] has worked out a relationship for the autocorrelation function of an oscillator's signal for the random-walk frequency case based on the method of stationary independent increments [11] as follows:

$$R_4(\tau) = \exp\left[-\frac{\sigma_4^2(3C_4|\tau|^2 + |\tau|^3)}{6}\right], \tag{8.32}$$

where $\sigma_4^2 = E\{\phi_4^2(t)\}$ is the drift variance of the random-walk frequency process having units of $\mathrm{rad}^2/\mathrm{s}^3$, and C_4 being an arbitrary constant multiplier having units of seconds. Incidentally $h_4 = \sigma_4^2$ [12]. Vannicola numerically evaluated this model to plot the total $S_4(f)$. In the following this model is analysed in detail and an expression for the linewidth is worked out.

In Appendix A the covariance of random-walk frequency noise modelled as integral Brownian motion has been derived. Using that result we have computed the

RF autocorrelation as follows:

$$R_4(\tau) = \exp\left[-\frac{h_4(3t|\tau|^2 + |\tau|^3)}{6}\right] = \exp\left[-\frac{h_4 t|\tau|^2}{2}\right]\exp\left[-\frac{h_4|\tau|^3}{6}\right]. \qquad (8.33)$$

Therefore, we have found the RF autocorrelation function to be non-stationary. C_4 in (8.32) is actually the running time variable. Our analysis shows that $R_4(\tau)$ is actually a dispersing function of time. It is apparent from (8.33) that the RF spectrum $S_4(f)$ is a convolution of a dispersing Gaussian function with $\mathcal{F}\left(\exp\left[-\frac{h_4|\tau|^3}{6}\right]\right)$, where $\mathcal{F}(.)$ denotes the Fourier Transform.

For short observation times the term $3t|\tau|^2$ will be negligible compared with $|\tau|^3$. That is, the dispersive effect appears only for relatively long observation times. To evaluate the Fourier Transform of the non-Gaussian part, i.e., $\mathcal{F}\left(\exp\left[-\frac{h_4|\tau|^3}{6}\right]\right)$, we first computed the Fourier Transform $\mathcal{F}\left(\exp\left[-\frac{|\tau|^3}{6}\right]\right)$ numerically, as shown in Fig. 8.5. In addition to the central peak, two sets of *satellite peaks* can be observed. The 3-dB line is also displayed and we can estimate the 3-dB linewidth as 0.33 Hz. Now, using the Scaling Property of the Fourier Transforms, we can conclude that the 3-dB linewidth of $\mathcal{F}\left(\exp\left[-\frac{|h_4^{1/3}\tau|^3}{6}\right]\right)$ is $0.33 \times h_4^{1/3}$. Except for the scaling factor this relation for the oscillator linewidth is identical to that in (8.27). Therefore we conclude that under frequency multiplication the short-term spectral linewidth increases as $N^{2/3}$.

The existence of satellite peaks has been confirmed by the measurements conducted in [97–99, 110]. The reason for their existence could be partially coherent feedback, or relaxation phenomena in the resonator lattice. The existence of satellite peaks might appear peculiar to some readers because it is well-known from Woodward's Theorem that the spectrum of the FM waveform is Gaussian in shape for high modulation indices [70]. We note that phase modulation due to random-walk frequency noise might constitutes low modulation indices which could explain the non-Gaussian spectral shape observed here.

As a sidenote, another phenomenon giving rise to satellite peaks is the non-Gaussian nature of the underlying phase noise statistics. In [111] it has been proved that non-Gaussian modulation processes can give rise to non-Gaussian spectra. Experimental observation of non-Gaussian spectra are reported in [112]. We emphasise however that the existence of satellite peaks in our analysis is due to random-walk frequency modulation having Gaussian statistics, as explained in Chapter 7.

We will now analyse (8.33) in detail for a medium-term observation time of 1

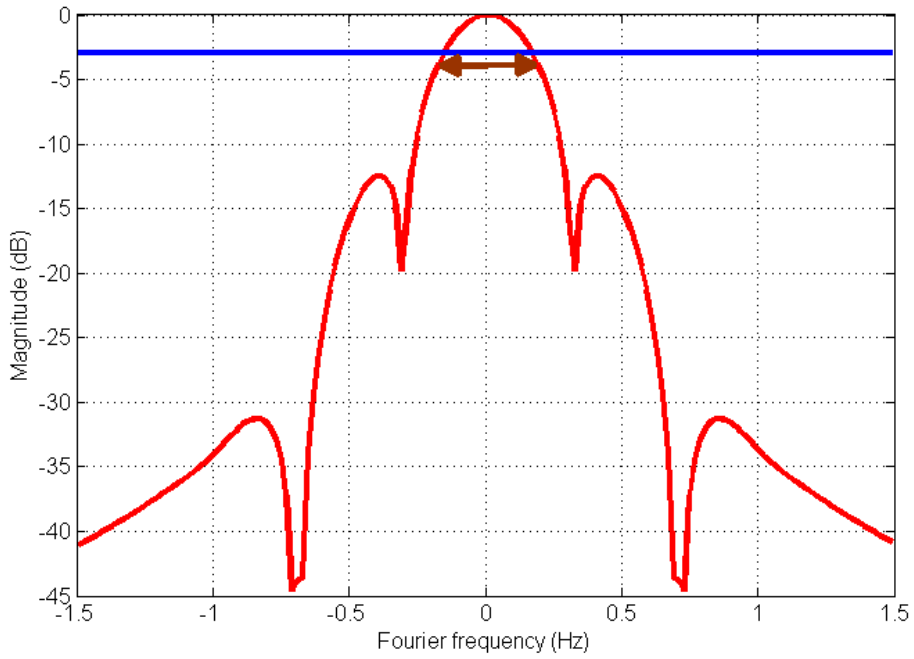

Figure 8.5: Non-Gaussian part of the spectrum of an oscillator having random-walk frequency noise. The 3-dB linewidth is marked with a double-arrow.

second. Setting $t = C_4 = 1$ (sec) we can write,

$$R_4(\tau) = \exp\left[-\frac{h_4|\tau|^2}{2}\right] \exp\left[-\frac{h_4|\tau|^3}{6}\right]. \tag{8.34}$$

For the Gaussian part the Fourier Transform is,

$$\mathcal{F}\left(\exp\left[-\frac{h_4|\tau|^2}{2}\right]\right) = \sqrt{\frac{2\pi}{h_4}} \exp\left[-\frac{\omega^2}{2h_4}\right], \tag{8.35}$$

so that the variance is $\sigma_\omega^2 = h_4$ and the 3-dB width of this component of the spectrum is,

$$\begin{aligned} W_{4_{Gaussian}} &= 2.355 \times \sigma_\omega/2\pi \quad \texttt{Hz} \\ &= 2.355 \times \frac{\sqrt{h_4}}{2\pi} = 0.375\sqrt{h_4}. \end{aligned} \tag{8.36}$$

To our knowledge, the closed-form solution to the convolution of the Gaussian and non-Gaussian parts is not available in the literature. In theory one only requires to compute the total linewidth of the convolved function and we have taken this up as future work. An approximation to the 3-dB width of the resulting spectrum is the *square root of the sum of squares* of the linewidths of the two symmetric functions

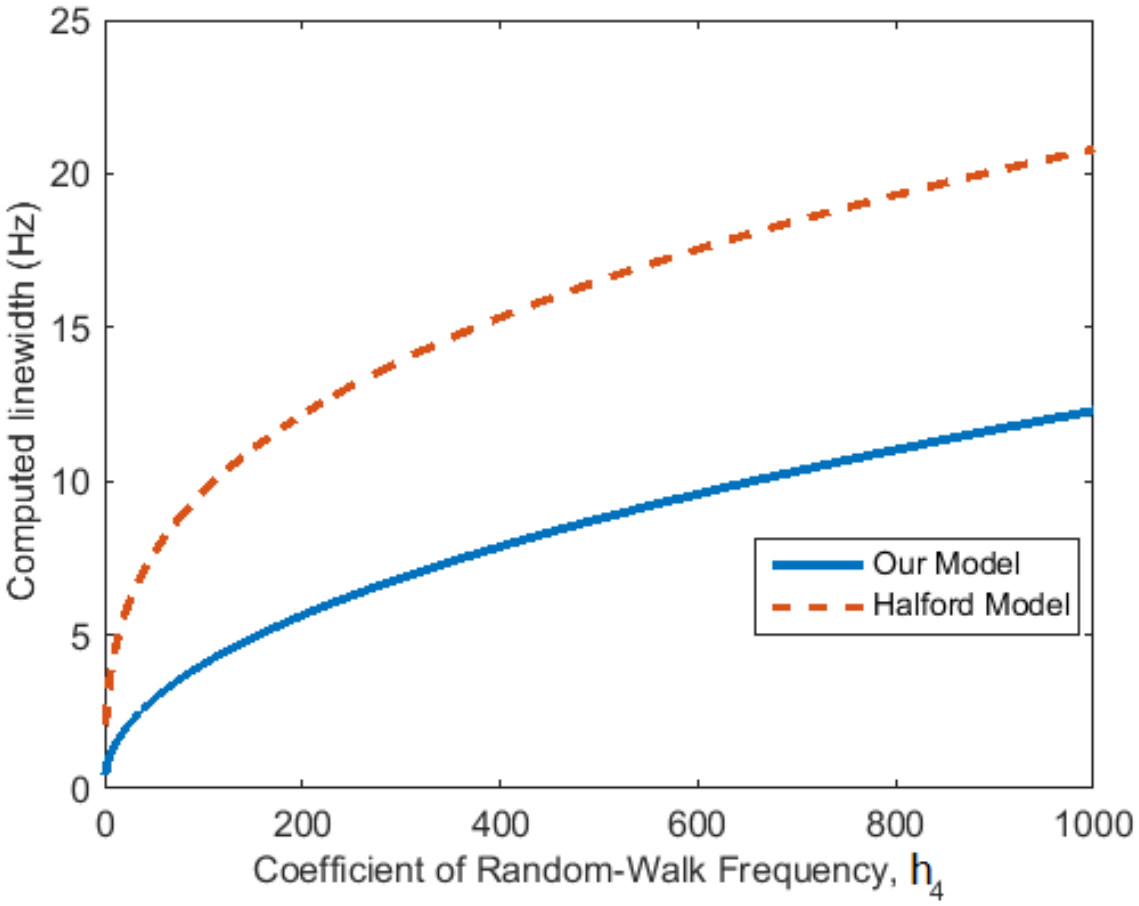

Figure 8.6: Comparison of the linewidth due to random-walk frequency noise predicted using Halford's model (top) and our model (bottom).

being convolved. Therefore, the final expression for the linewidth of an oscillator having random-walk frequency instability is,

$$\begin{aligned} W_4 &= \sqrt{\left(0.375\sqrt{h_4}\right)^2 + \left(0.33 \times h_4^{1/3}\right)^2} \\ &= \sqrt{0.14\ h_4 + 0.11\ h_4^{2/3}}. \end{aligned} \tag{8.37}$$

From (8.37) it can be noted that for $h_4 = 1$ both components of the linewidth are roughly equal. For smaller h_4 the non-Gaussian part will mostly determine the linewidth while for large h_4 the Gaussian part will dominate. The total spectral shape due to random-walk frequency noise will similarly depend on the level of the noise: for low h_4 the spectrum will resemble Fig. 8.5 while for high values of h_4 it will be Gaussian in shape.

Fig. 8.6 shows a comparison of Halford's linewidth (8.27) with (8.37). As can be witnessed, Halford's model overestimates the linewidth. From (8.37) it is apparent

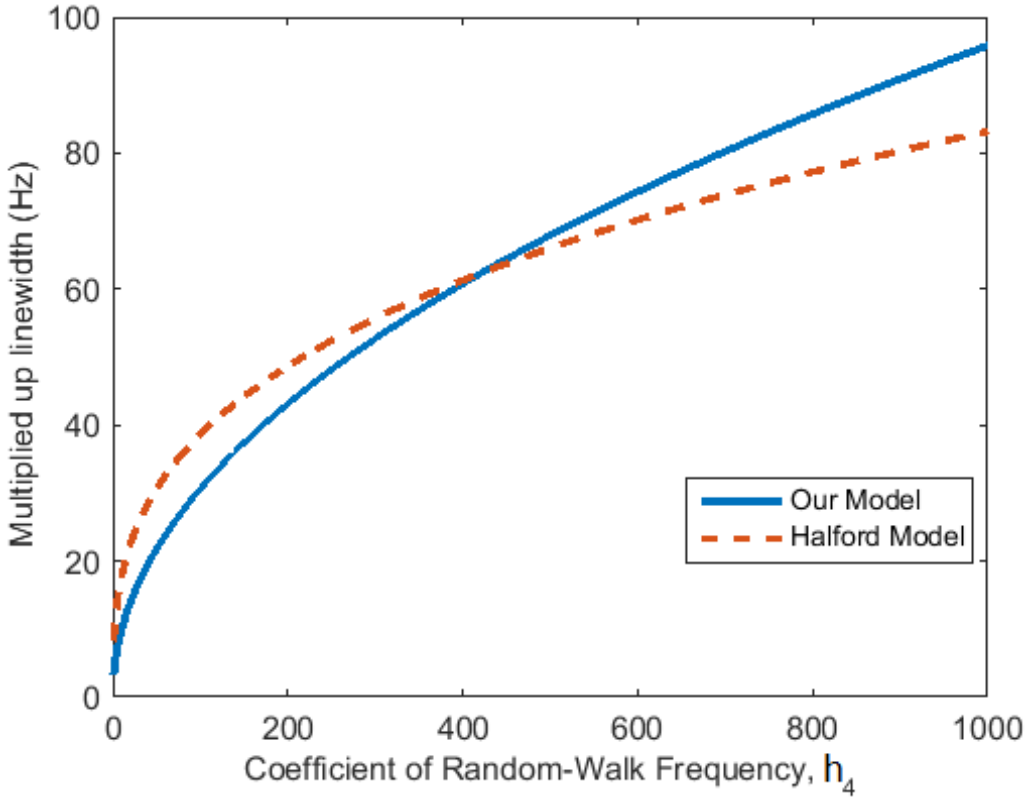

Figure 8.7: Comparison of the multiplied up linewidths due to random-walk frequency noise for $N = 8$

that under frequency multiplication by N the the linewidth becomes:

$$\begin{aligned} \widehat{W}_4 &= \sqrt{0.14\ N^2 h_4 + 0.11\ (N^2 h_4)^{2/3}} \\ &= \sqrt{0.14\ N^2 h_4 + 0.11\ N^{4/3} h_4^{2/3}}. \end{aligned} \tag{8.38}$$

Therefore, the linewidth is related to N and h_4 in a non-linear fashion, so a direct comparison with Halford's model is not possible: fixing one parameter allows to compare both for the other parameter. Assuming a frequency multiplication by $N = 8$ we get,

$$\widehat{W}_4 = \sqrt{9h_4 + 1.76h_4^{2/3}}. \tag{8.39}$$

A comparison of (8.39) with Halford's linewidth for $N = 8$ ($\widehat{W}_4 = 8.32h_4^{1/3}$) is presented in Fig. 8.7. The plot shows that Halford's model overestimates the linewidth for small h_4 and underestimates the linewidth for large h_4.

Finally we note that if the linewidth is measured using a delayed self-heterodyne system then the phase noise processes at the two inputs of the mixer add (assuming $\tau_d > \tau_c$ so that the two are uncorrelated). So h_4 in (8.37) is to be replaced by $2h_4$.

The resulting measured linewidth is,

$$\begin{aligned} W_{4(meas)} &= \sqrt{\left(0.375\sqrt{2h_4}\right)^2 + \left(0.33 \times (2h_4)^{1/3}\right)^2} \\ &= \sqrt{0.28\ h_4 + 0.173\ h_4^{2/3}}. \end{aligned} \tag{8.40}$$

Therefore, the Gaussian part increases by $\sqrt{2}$ while the non-Gaussian part increases by $\sqrt[3]{2}$. Using (8.37) and (8.40) the overall increase in the measured linewidth should be computed numerically as $W_{4(meas)}/W_4$.

In deriving (8.40), we assumed an observation time of 1 second. The general linewidth for $t = \tau_m$ can also be seen in Table 8.1. The linewidth is therefore proportional to $\sqrt{\tau_m}$. For measurement time much less or much greater than 1 second, the multiplied up linewidth will be different from Fig. 8.7.

8.5.6 The total linewidth

Table 8.1 summarises the relations for oscillator linewidth. The composite linewidth of an oscillator will be a function of the linewidths due to each frequency noise process. If the h_β for a given noise process is low then the RF spectrum due to that component of noise will be closer to a delta function [69] and will contribute less to the overall linewidth. Assuming the phase noise processes as being independent of each other, an approximation to the total $S_{RF}(f)$ can be found by convolving the individual power spectra [69,91]. The overall linewidth, therefore, will be the *square root of the sum of squares* of the individual 3-dB linewidths [68]. That is,

$$W_{total} \approx \sqrt{W_2^2 + W_3^2 + W_4^2}. \tag{8.41}$$

8.6 Oscillator linewidth as a measure of range resolution

In FMCW radar systems, the range profile is computed by computing the Fourier Transform of the IF signal measured over a finite observation time. The range resolution, therefore, is defined by the oscillator linewidth, W_{total}. In general, the range resolution is inversely proportional to both the frequency noise and the measurement time.

In coherent radars, the local oscillator signal is derived from the transmitted signal. An important thing to note is that all the phase and frequency noise processes

Noise Type	**Lineshape**	**Linewidth**	**Multiplied Linewidth**	**Measured Linewidth**
White Freq.	Lorentzian	πh_2	$N^2 \pi h_2$	$2\pi h_2$
Flicker Freq.	Gaussian	$\frac{2.355}{2\pi}\sqrt{\frac{h_3}{\pi}\left[1+\ln\left(\tau_m\sqrt{\frac{h_3}{2\pi^3}}\right)\right]}$	$\frac{2.355\ N}{2\pi}\sqrt{\frac{h_3}{\pi}\left[1+\ln\left(N\tau_m\sqrt{\frac{h_3}{2\pi^3}}\right)\right]}$	$\frac{2.355}{2\pi}\sqrt{\frac{h_3}{\pi}\left(4.3+\ln\frac{4.3h_3\tau_d^{2.1}}{\pi}\right)}$
RW Freq.	...	$\sqrt{0.14\ \tau_m h_4 + 0.11\ h_4^{2/3}}$	$\sqrt{0.14\ N^2\tau_m h_4 + 0.11\ N^{4/3} h_4^{2/3}}$	$\sqrt{0.28\ \tau_m h_4 + 0.173\ h_4^{2/3}}$

Table 8.1: Summary of oscillator linewidths due to the frequency noise processes.

decorrelate with range. Therefore, the actual measured linewidth will be much smaller than that predicted by the above results. In particular, all the frequency noise coefficients will have to be reduced by the decorrelation factor $4\sin^2(\pi f \tau_d)$ to get the correct resolution. Further work on this idea is still needed and is a part of our future work.

For non-coherent radar, the LO is independent of the transmitted/received signal. As such there is no phase coherence between the two, and the phase noise processes will not decorrelate with time delay. Therefore, even for short observation times the target spectrum will be broader, and will be defined by the sum of the linewidths on both signals due to white frequency noise. The resulting spectral shape is expected to be the convolution of two Lorentzian functions. For longer observation time, on the time-scale where the higher-order frequency noise processes can play their role, the target spectrum will be broader and be a function of the measurement time as well. The Allan Variance can be used to compute the aforesaid time-scales. Further work on this idea is also a part of our future work.

8.7 Conclusion

In this chapter the relationship of the linewidth of RF oscillators with the phase noise processes having power-law spectra was discussed. The relations for each phase noise process were dealt with individually along with the effect of frequency multiplication on the RF spectrum. The existing models of the RF spectra of oscillators were compared and their effectiveness in computing the linewidth was analysed. We developed a new model to compute the oscillator linewidth for the case of random-walk frequency noise. A comparison of the new model with Halford's classic method of estimating oscillator linewidth was presented at the source frequency as well as for the frequency multiplied signal. The linewidth due to the flicker frequency noise and random-walk frequency noise was found to increase with increasing measurement time. In the random-walk frequency case it was shown that the shape of the spectrum in addition to its width depends on h_4. The results presented here are also useful to predict the lineshape and width at the output of a PLL synthesiser employing frequency multiplication in the loop. Finally the relationship of oscillator linewidth with FMCW range resolution was discussed for the coherent and non-coherent radars. It was shown that in general the range resolution degrades with increasing frequency noise and increasing measurement time. Measurement results could not be presented due to the unavailability of expensive oscillator linewidth measurement equipment.

Chapter 9

Conclusion and Future Work

9.1 Conclusion

The present PhD Thesis focused on quantifying the impact of oscillator phase noise on the design of MMW CW radar systems. We have demonstrated how phase noise impacts the performance of radar systems using analysis, design of circuits, and data visualisation.

In a nutshell, this Thesis first presented phase noise modelling techniques for the whole radar system, and then focused on the detailed phase noise modelling of the important parts of a general radar system, including the frequency synthesiser, the analog-to-digital converter, and the phase measurement processor. Afterwards, the relationship of the oscillator linewidth with the phase noise processes was developed and analysed. The Thesis concluded with the presentation of a new generalised Brownian motion phase noise model for the RF spectrum of oscillators.

The system-level phase noise modelling provided guidelines on choosing the appropriate components to minimise the impact of phase noise for a given radar system design at hand. Techniques for modelling phase noise at various points in the system were presented. In Chapter 3 a relationship was derived to relate the phase noise sideband levels of two targets at different ranges. The relationship was validated through practical measurements obtained by a MMW FMCW radar system.

The frequency synthesiser was shown to be the most significant phase noise contributor. The inadequacy of modern PLL-based frequency synthesisers was demonstrated in the measurements, as they lead to raised phase noise sidebands around large targets, thus decreasing the signal-to-noise margin for weak target detection. A new low phase noise signal source was designed and implemented successfully in a commercial radar system. The results showed a huge improvement of 30 dB in

the phase noise sidebands, effectively solving the phase noise problem for the radar system under consideration. The effects of phase noise *decorrelation* with range were also studied in detail. The variation in the coherent sideband ripples was analysed and verified in the practical measurements presented in Chapter 4. The conclusion is that phase noise cancellation by the receiver's mixing process is a decreasing function of range. For a target at 50 meters, for example, the phase noise at the 100 kHz offset is 13.6 dB lower than at the transmitter. For a target at a range of 200 m, the cancellation is only 1.8 dB. The cancellation is exactly 0 dB for a target at 250 m. These calculation can be extended to other frequency offsets. This clearly shows that after a few hundred meters, the phase noise cancellation offers no help, and the radar designer must resort to reducing the phase noise in other parts of the system.

In addition to utilising linear phase noise models, the Thesis proceeded on to quantifying the non-linear phase noise effects. A phase noise model separating the carrier lineshape and the phase noise pedestal was described in Chapter 4. The modified Lorentzian function was presented as a new model of the phase noise pedestal. The idea of *coherence time* was used as a tool for the selection of radar signal sources and a novel equation was derived that gives an optimistic estimate of the coherence time for radar systems. Also, a novel minimum bound on the transmitter phase noise level was derived to prevent excessive distortion of target spectra.

New phase noise models were developed for the analog-to-digital conversion (ADC) process. The ADC process was shown to *time-decorrelate* the sampled signal when the sampling clock was locked to the reference oscillator of the transmitted signal. In the case of an independent sampling clock, a novel equation was derived for the jitter transfer from the sampling clock to the sampled radar signal. The effects of phase noise decorrelation were also taken into account in the developed model. A comparison method was developed to aid the selection of an appropriate sampling clock for a given radar application. The result of this modelling process was invaluable: it was shown that for a MMW radar having inherently high levels of phase noise, a relatively cheaper sampling clock can be employed in the radar system without an increase in the overall phase noise. For low-GHz (and even lower-frequency) radar systems, one needs to be more careful about the selection of the sampling clock: a cheap sampling clock might become the dominant phase noise contributor in the system. These design guidelines have been detailed in Chapter 5.

A significant contribution of this Thesis is the derivation of the mathematical bounds under which a single-channel radar system can measure the signal's phase unambiguously. Compared with an I/Q receiver, one-half of the hardware is saved

when a single-channel receiver is employed, which results in thousands to hundreds of thousands of pounds worth of savings depending on the scale at which a given radar system is employed. The bounds derived in Chapter 6 are really upper bounds on the target velocities, and are easily met in a wide variety of radar applications.

Chapter 7 presented a novel method of characterising the phase noise statistics using the integer and the fractional Brownian motion models. This constitutes a method alternative to the Correlation Theory method used by various authors [54, 90, 91, 102], and new results were derived for the phase noise spectra. In particular, a novel analysis of the RF spectrum due to random-walk phase noise was presented: it was found that the RF spectrum is non-Gaussian in shape, and exhibits non-stationary time-dispersion in addition to *satellite peaks*. We believe that these results are in agreement with measured oscillator RF spectra. These results depart from the conventional predictions of the Correlation Theory of the Gaussian spectral shape.

Continuing the non-linear analysis, a novel division of the phase spectrum in terms of the *coherence frequency*, the intermediate region, and the linear phase noise regime, was presented in Chapter 8. The three regions of the phase spectrum were related to the linewidth, the non-linear phase noise region, and the linear phase noise regions of the RF spectrum respectively. This relationship provides a clear insight into which phase noise processes affect which part of the RF spectrum. A review of the existing models of oscillator linewidth was presented and the effect of frequency multiplication on the linewidth was discussed for each phase noise process.

All of the above ideas helped to optimise the performance of the long-range radar system (LRS) designed by the Author for Navtech Radar Ltd. during the course of this work. The new results and techniques presented in this Thesis helped to maximise the performance of a market leading commercial radar sensor through better detection and tracking of weak targets.

9.2 Future Work

Several theoretical developments can be identified from the work in this Thesis that will be taken up as future work. Some of the research problems are as follows.

9.2.1 A real-exponent phase noise model

The integer power-law phase noise model was utilised throughout this thesis. In practice phase noise spectra appear frequently with non-integer exponents. A conventional analysis would decompose a non-integer exponent spectrum into two in-

teger power-law spectral components as follows. For a real exponent a between integers β and $\beta + 1$ one can write,

$$\frac{h_a}{f^a} = \frac{h_\beta}{f^\beta} + \frac{h_{\beta+1}}{f^{\beta+1}}, \tag{9.1}$$

where h_a would be available through a practical measurement while h_β and $h_{\beta+1}$ would be obtained using, for example, least-squares curve fitting. However, through the work in this Thesis we can envisage an alternative real-exponent phase noise model for oscillators. An outline is given as follows.

As shown in Chapters 7 and 8, white and flicker phase noise processes only contribute to sideband spectra. It was shown in Chapter 8 that for a general real exponent > 1 the modified Lorentzian spectrum converged, implying that any real exponent phase noise having power > 1 (i.e. greater than flicker phase noise) contributes to the linewidth of oscillators. Also, in Chapter 7 it was shown that the RF spectrum of oscillators is stationary for powers up to 3, and that the RF spectrum due to flicker frequency noise is independent of time. The analysis in Chapter 8, on the other hand, shows that the oscillator linewidth is indeed a function of time. This could be explained by noting that the RF spectrum in Chapter 7 is for the phase noise coefficient being *just under* exact flicker frequency noise. The linewidth broadening in Chapter 8 then must be for the phase noise coefficient being *just over* exact flicker frequency noise (i.e. exponent > 3). An evidence support this hypothesis is the fact that the linewidth due to random-walk frequency noise indeed broadens with time, so one can conclude that the phase noise processes with power $1/f^{3+}$ causes time-varying linewidth broadening. These observations can be used and developed further into a more complete model of phase noise. The developed models did not take into account any correlation between the individual phase noise processes. As a future work, this model can be extended to account for these correlations. A quantitative analysis of the origin of such correlations also seems appropriate in this regard.

9.2.2 Infrared Catastrophe

The statistical models of flicker phase and frequency noises are known to blow up at the origin (i.e. zero offset from the carrier). This is referred to as *Infrared Catastrophe* in the phase noise literature. It is noted that this phenomenon is in direct disagreement with practically measured oscillator spectra that always have a finite power level at the carrier frequency.

In this thesis, two methods of estimating the RF spectrum of oscillators were ex-

plored, namely, Correlation Theory (Chapter 8), and the Brownian motion models (Chapter 7). Chorti's analysis in [54, 91] shows that when using Correlation Theory, Infrared Catastrophe can only be avoided if both a lower and a higher cutoff frequency is assumed for the flicker noises. However either of the cutoffs do not have any physical justification or experimental validation to support them. Nossenson's analysis in [92] shows a Gaussian spectrum for near flicker of frequency noise, which is in agreement with Correlation Theory, but again blows up for exact flicker frequency. In addition Nossenson's model does not explain the $1/f^3$ sideband spectrum (instead the short-term spectrum comes out as $1/f^2$ using that analysis). The sideband spectrum for flicker phase noise is indeed $1/f$, however that model also blows up at the origin. Therefore, these two theories cannot satisfactorily solve the problem of Infrared Catastrophe.

We note that the finite carrier power must be due to the laws governing the oscillator, in particular the Law of Conservation of Energy. Therefore, an analysis of the oscillator's RF spectrum based on the Law of Conservation of Energy seems imperative. Non-linear models giving rise to *Jump Hysteresis* will be explored as a future work to model the flicker phase and frequency processes [113, 114]. Ignoring the amplitude noise and AM-FM coupling has hitherto been a widely used approximation in the phase noise literature. It has been pointed out in [113] that amplitude-frequency dependence, however small, cannot be ignored to successfully model the flicker noises.

9.2.3 Estimation of the Coherence Time

The idea of *Coherence Time* appeared in this Thesis as an important parameter defining the maximum range until a radar's transmitter remains self-coherent. As a future work the detailed relationship of the coherence frequency f_c with the phase noise processes will be derived. An outline is given as follows. f_c is defined by the equation:

$$\int_{f_c}^{\infty} S_\phi(f)df = 1 \ \mathtt{rad}^2, \tag{9.2}$$

where we note that the white-phase noise process is not considered in evaluating the integral. Depending on the level of the power distribution between the carrier and the sidebands in the RF spectrum, some of the phase noise processes are considered in the evaluation of (9.2) and others are not. Following is a general guideline on the inclusion of the phase noise processes.

First the integral in (9.2) should be computed using the flicker phase $(1/f)$

component only. If the integral is ≥ 1 then f_c can be estimated. However, if the integral turns out to be < 1 then the white frequency ($1/f^2$) component should also be considered in the integral. Repeat this procedure by adding the higher-order phase noise processes until the integral is equal to 1.

9.2.4 Estimation of the true range resolution

It is well-known that the fundamental range resolution in radar systems can be calculated as $\Delta R = c/2B$, where c is the speed of light and B is the spectral bandwidth of the transmitted waveform. The range *resolution* on the other is defined using the Rayleigh criterion, i.e. the minimum of one target's response being at the maximum (or peak) of an adjacent target's response. A measure of the range resolution is the 3-dB points of a target's response, which is conveniently described as the 3-dB linewidth of the transmitting oscillator. This has been the rationale behind our work on oscillator linewidth.

The phase noise processes cause spectral broadening, so the actual resolution of FMCW radar systems is less (i.e. coarser) than $c/2B$. As a future work, the correct relationship between the range resolution (or equivalently the linewidth) and the phase noise processes will be established. We have proven that the frequency noise processes contribute to the linewidth. However we note that the problem of Infrared Catastrophe mentioned in Section 9.2.2 needs to be solved before an accurate relationship can be derived. Nevertheless, a reduction in frequency noise in general does lead to sharper peaks in the radar response.

As mentioned earlier, a detailed future work on FMCW radar range resolution should include the effects of decorrelation and sub-coherence time delays in coherent radars, and also an estimation of the time-scale of flicker frequency and random-walk frequency noises using the idea of Allan Variance.

9.2.5 Signal averaging under frequency noise

Coherent integration was shown to improve the signal to phase noise performance in FMCW radar systems. However, practical experience has shown that in the limit of very large averages (thousands or more) the improvement in SNR slows down and then flattens off. Two causes of this phenomenon are worth further consideration:

1. When the sampling clock employed in the system is independent of the transmitted signal, it will inevitably drift with respect to the received/IF signal. So the points on the sinewaves being sampled will vary with time. For larger

observation times, the sampling clock will be sampling the signal with a time-varying frequency drift. These effects will render the averaging less effective.

2. The Allan Variance is a good way of visualising how the variance of an oscillator's signal changes with observation time. The variance drops for the white & flicker phase processes and the white frequency noise process. However, the two-sample Allan Variance plot flattens off for the case of flicker frequency noise. This gives an idea that further averaging will not decrease the variance/noise power of the signal. The Allan Variance curve then rolls up for the random-walk frequency case. This tends to suggest that averaging on this time-scale will actually result in degraded performance.

Appendix A

The Covariance of Integral Brownian Motion[1]

Integral Brownian Motion (iBm) can be modelled as follows [93,115]. Consider zero-mean white phase noise with variance σ^2 and covariance $\sigma^2\delta(t)$. The integral of white phase noise is the ordinary Brownian motion, Bm(t) (Wiener process) with zero-mean, variance $\sigma^2|t|$ and covariance $\sigma^2 \min(t, t+\tau)$. The integral of the Brownian motion process is the zero-mean integral Brownian motion process $\phi_4(t) = iBm(t)$ with variance,

$$\begin{aligned} \mathtt{var}\left[iBm(t)\right] &= \mathtt{var}\left[\int_0^t Bm(t)dt\right] \\ &= \int_0^t \int_0^s \mathtt{var}\left[Bm(\zeta)\right] d\zeta \; dt \\ &= \sigma^2|t|^3/3. \end{aligned} \tag{A.1}$$

For $t_2 > t_1 > 0$ the covariance of $\phi_4(t) = iBm(t)$ is,

$$\begin{aligned} R_{\phi_4}(t_1, t_2) &= E\left[\int_0^{t_1} Bm(\zeta)d\zeta \int_0^{t_2} Bm(\xi)d\xi\right] \\ &= \int_0^{t_2} \int_0^{t_1} E\left[Bm(\zeta)Bm(\xi)\right] d\zeta \; d\xi \\ &= \int_0^{t_2} \int_0^{t_1} \sigma^2 \mathtt{min}(\zeta, \xi) d\zeta \; d\xi \\ &= \sigma^2 t_1^2 \left(\frac{t_2}{2} - \frac{t_1}{6}\right). \end{aligned} \tag{A.2}$$

[1]The contents of this Appendix have been submitted for publication in [89].

Substituting $t_1 = t$ and $t_2 = t_1 + \tau$ ($\tau > 0$) and we get,

$$R_{\phi_4}(t, t+\tau) = \sigma^2 \left(\frac{t^3}{3} - \frac{\tau t^2}{2} \right). \tag{A.3}$$

For $\tau = 0$ (A.3) reduces to (A.1) as expected. Finally for $t_1 = t_2 = t + \tau$ we get,

$$R_{\phi_4}(t+\tau, t+\tau) = \sigma^2 \frac{(t+\tau)^3}{3}. \tag{A.4}$$

Appendix B

Development of the Long-Range System

As mentioned in Chapter 1, the research work in the thesis is based on the work done in developing a MMW long-range radar sensor (LRS) system under a collaboration between University of Bath and Navtech Radar Ltd.[1] The collaboration was funded in part by Innovate UK (formerly the Technology Strategy Board, UK) under the KTP[2] number 9308.

The KTP project has been a significant step in the understanding of the low-noise electronic design of radar systems. The LRS is envisaged to make accessible a large share of the European as well as the non-European market for long-range radars in the millimetre wave (MMW) frequency band[3]. An objective of the design work was to make the research relevant in the industrial-context, i.e., a theoretically optimum solution designed to achieve the goals of mass-production, reasonable cost, tight power budget, and compact form factor.

A fully working prototype of the long-range radar system (LRS) was developed earlier on during the present work. At the time of writing, production models of this system - the HDR300 series of radars - are being prepared to be shipped. A photograph of the HDR300 product is shown in Fig. B.1, which has been built as an extension of Navtech's AGS1600 products. The LRS project was about extended the operating range of the system beyond 1 km in strongly clutter environments. This required a higher-power transmitter as well as the signal processing hardware that could handle the increased data throughput for the extended range. Field trials

[1]Contact: Navtech Radar Ltd., Home Farm, Ardington, Wantage, OX12 8PD, UK.

[2]Knowledge Transfer Partnership

[3]The term *long-range radar* (LRR) in the context of MMW radar systems has recently been used for radar systems with a detection range of up to and beyond 250 meters.

Figure B.1: The HDR330 Long-Range Radar Sensor Product

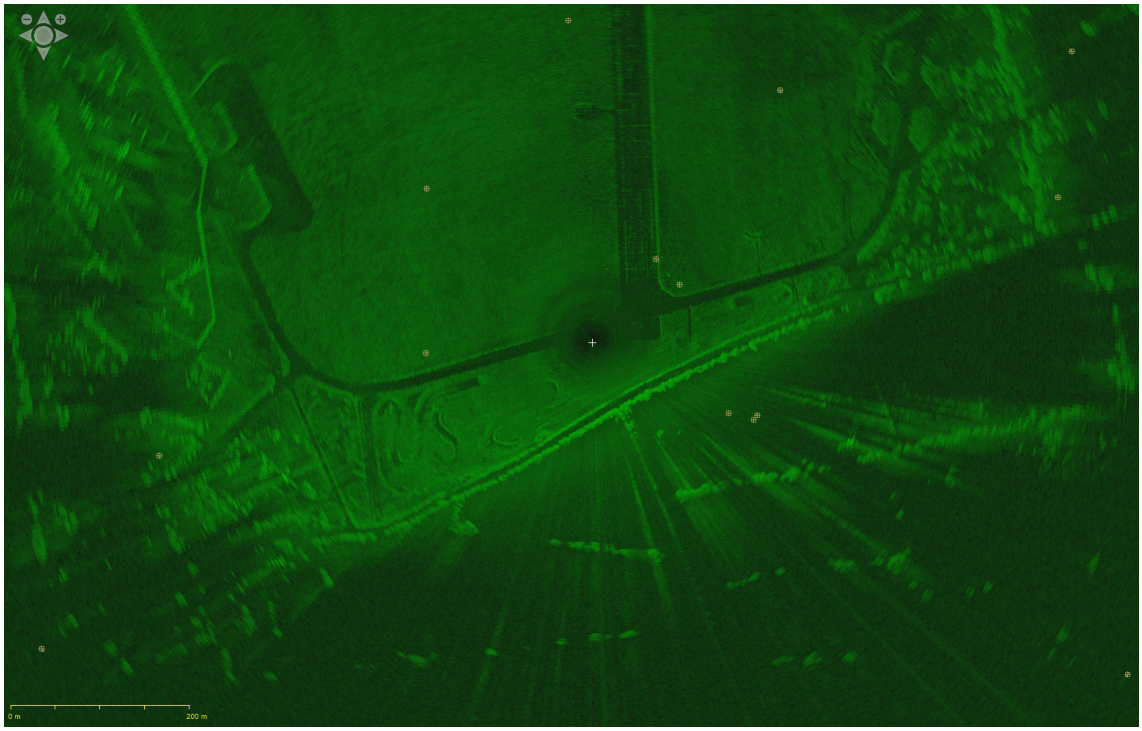

Figure B.2: PPI display of the radar using the PLL/VCO Synthesiser

of the developed radar system were been done at the White Waltham Airfield near London and the Abingdon Airfield in Oxfordshire. The maximum detection range for pedestrians (i.e. small targets) has been progressively increased up to 1.8 km over grass (i.e. strong clutter). This is a significant improvement over Navtech's AGS1600 product. In benign environments the new HDR330 systems can work up to 3 km.

A new low phase noise frequency synthesiser was developed for the LRS to reduce the phase noise sidebands that were originally raised further due to the high power transmitter being used. Fig. B.2 shows a PPI display of a part of Abindgon Airfield with the conventional PLL-based frequency synthesiser. The streaking is visible in the scene. Fig. B.3 shows a PPI display of a part of Abindgon Airfield with the low phase noise frequency synthesiser. As can be observed, the streaking has been reduced and the scene has better definition. This has led to better tracking performance for Navtech's radar systems.

In the following, a couple of features developed during the project are detailed that were also helpful in the research in this Thesis.

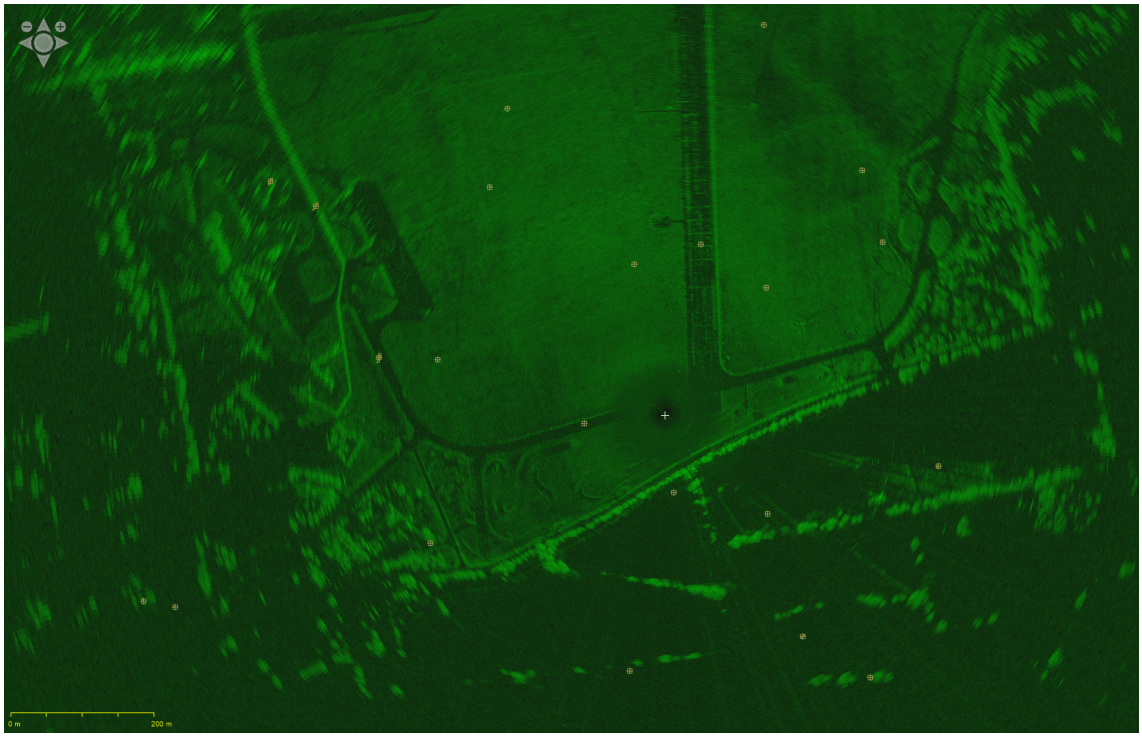

Figure B.3: PPI display of the radar using the low phase noise Synthesiser

B.1 Simulation software for generating target responses

A major step in modelling the phase noise in radar systems was the development of a simulation model in SciLab. Fig. B.4 shows screen shots of the software. The software takes the phase noise data of the VCO and the reference oscillator used in the frequency synthesiser, and compares both at the desired output frequency (9.5 GHz) in this case as shown in Fig. B.4a (top-left inset). Note the *cross-over* frequency which is the optimum loop bandwidth to minimise the overall phase noise. The loop bandwidth can be chosen to simulate the phase noise at the output of the synthesiser. The signal is passed through the transceiver chain, which in this case includes frequency multiplication on the transmitter side and homodyne mixing on the receiver side. Finally the FFT bandwidth is added to simulate the signal on the radar's display. Fig. B.4b shows another feature of the designed software that generates *phase noise masks* for the VCO and the reference oscillator to comply with.

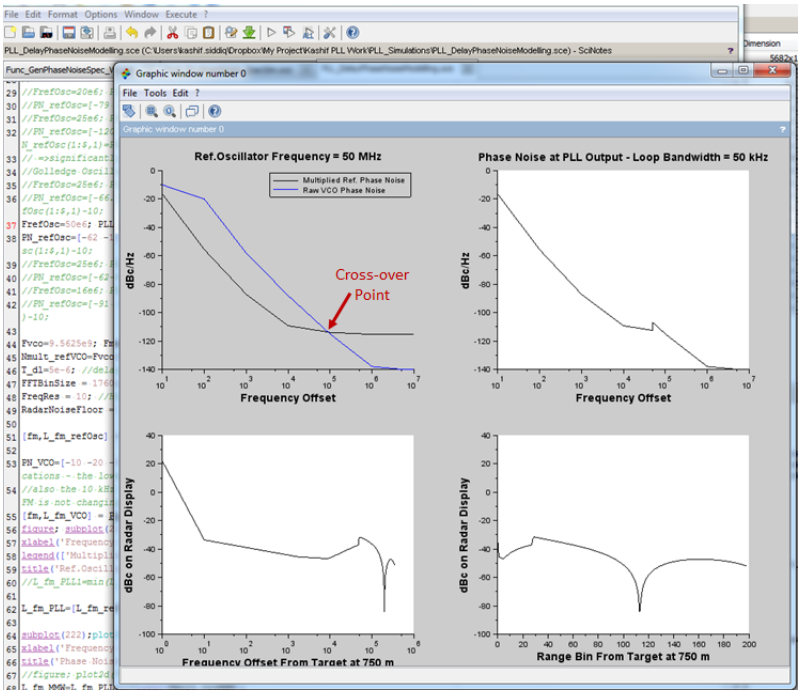

(a) Main software

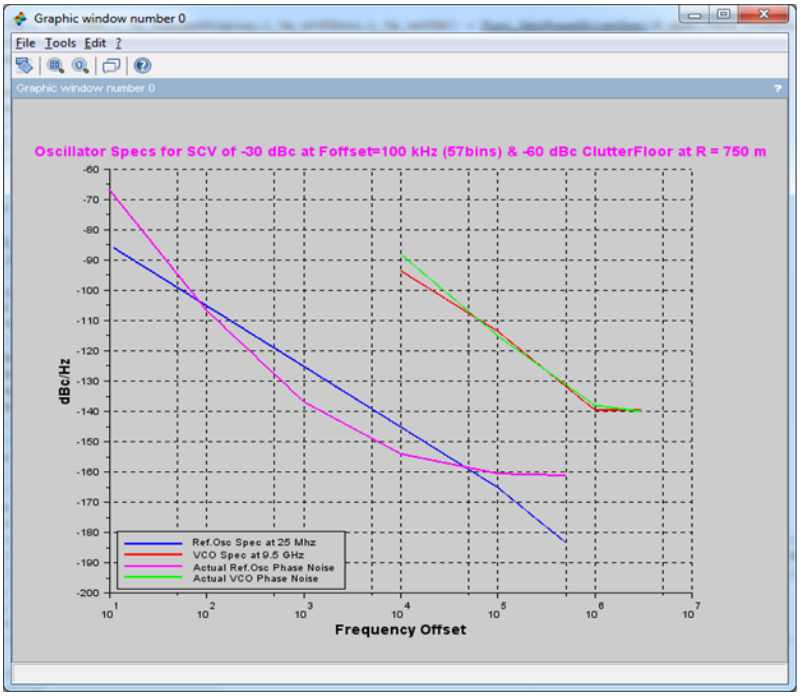

(b) Spec Simulation

Figure B.4: Phase Noise Simulation Software ©Kashif Siddiq

B.2 ADC data logging function

For the present work an additional software mode was developed for the LRS that allowed the ADC data to be stored directly on a hard-drive instead of being processed. Using this feature the raw data sampled by the ADC was used to test signal processing algorithms. Some of the plots in this thesis have utilised this functionality. The radar's processing chain was also modelled in SciLab so that the processed data produced by the radar system could be simulated.

Appendix C

Alternative Phase Noise Modelling Methodologies

The power-law phase noise model is only one of a large number of modelling methodologies used by researchers. Although the power-law model along with the RF spectral model has been used in the present thesis, it is appropriate to mention some of the important alternative phase noise models:

1. **Time-domain Models:** These methods apply novel statistical techniques to the time-domain data to extract information about the short- and long-term phase noise processes. These include the Allan Variance [107, 116], the phase and frequency Structure Functions [50, 67], the Multivariance Method [117, 118], and Lowest-Mode Estimator [119, 120].

2. **Models utilising oscillator topology:** These models use the circuit parameters of oscillator like the Quality Factor (Q) and the oscillator's topology [24, 102, 121–125].

3. **Models utilising oscillator material parameters:** These models use material parameters like carrier density, carrier mobility, relaxation phenomena, etc. to model quantum phase noise in lasers [23, 99, 126, 127].

4. **Time-series model:** In these, the oscillator signal is modelled using one of the conventional signal-processing models like the ARMA, ARIMA, ARFIMA, and Wiener Models [128, 129]. These techniques can be helpful for cancelling phase noise on a per-sweep basis (as opposed to averaging). In [61] a multi-rate filter model is presented for the generation of radar pulses having phase noise.

5. **Nonlinear Dynamical Models:** The models perform a Phase Plane Analysis on dynamical oscillator models based on the Fokker-Planck equation and the Langevin equation [14, 47, 108, 130, 131].

6. **Linear Time-Varying models** These models again use the Phase Plane Analysis but apply to the restricted class of linear time-varying (LTV) oscillators. An example is the Impulse Sensitivity Function model [48].

7. **Fractal Models** The multifractal model is described in [132]. It is interesting to note that the power-law model has also been used in other branches of science [7] including the science of turbulence, heart rates, and finance [132, 133]. An example is the Mandelbrot-Zipf's law used in linguistics [134].

8. **Signal Processing Techniques** Following are some of the signal processing methods available in the literature to reduce the effects of phase noise.

   - The Polynomial Phase transform (PPT) [135]
   - The Generalised Ambiguity Function (GAF) [136],
   - The Generalised Chirp Transform (GCT) [137],
   - The Extended Generalised Chirp Transform (EGCT) [138].

   In [139] a performance comparison has been made for the above-mentioned algorithms when applied to various applications (including radar).

References

[1] European Telecommunications Standards Institute, "Electromagnetic compatibility and Radio spectrum Matters (ERM)," *ETSI Standard EN 301 091*, ETSI, France, 2014.

[2] G. M. Brooker, "Mutual interference of millimeter-wave radar systems," *IEEE Transactions on Electromagnetic Compatibility*, vol. 49, no. 1, pp. 170–181, Feb 2007.

[3] D. K. Barton, *Radar System Analysis and Modeling (Artech House Radar Library)*. Artech House Publishers, 2004.

[4] M. A. Richards, *Fundamentals of Radar Signal Processing, Second Edition (McGraw-Hill Professional Engineering)*. McGraw-Hill Education, 2014.

[5] M. Skolnik, *Introduction to Radar Systems*. McGraw-Hill Education, 2002.

[6] J. B. Billingsley, *Low-Angle Radar Land Clutter: Measurements and Empirical Models*. William Andrew Publishing, 2002.

[7] R. F. Voss, "1/f (flicker) noise: A brief review," in *33rd Annual Symposium on Frequency Control. 1979*, May 1979, pp. 40–46.

[8] "IEEE Standard Definitions of Physical Quantities for Fundamental Frequency and Time Metrology - Random Instabilities," *IEEE Std 1139-1999*, 1999.

[9] D. Halford, J. Shoaf, and A. Risley, "Spectral Density Analysis: Frequency Domain Specification and Measurement of Signal Stability," *27th Annual Symposium on Frequency Control*, pp. 421–431, 1973.

[10] E. Rubiola, *Phase Noise and Frequency Stability in Oscillators (The Cambridge RF and Microwave Engineering Series)*. Cambridge University Press, 2010.

[11] J. Rutman, "Characterization of Phase Frequency Instabilities in Precision Frequency Sources: Fifteen Years of Progress," *Proc IEEE*, vol. 66, no. 9, 1978.

[12] V. C. Vannicola and P. K. Varshney, "Modeling of frequency random walk instability and effects on spectral spreading," in *ICC '82 - The Digital Revolution*, vol. 3, 1982.

[13] D. B. Leeson and G. F. Johnson, "Short-term stability for a doppler radar: Requirements, measurements, and techniques," *Proceedings of the IEEE*, vol. 54, no. 2, pp. 244–248, Feb 1966.

[14] E. E. Hegazi, J. Rael, and A. Abidi, *The Designer's Guide to High-Purity Oscillators (The Designer's Guide Book Series)*. Springer, 2004.

[15] M. Denny, *Blip, ping & buzz: Making Sense of Radar and Sonar*. Baltimore: Johns Hopkins University Press, 2007.

[16] W. Schottky, "ber spontane Stromschwankungen in verschiedenen Elektrizittsleitern (About spontaneous current fluctuations in various electricity conductors)," *Ann. der Phys.*, 57, 541, 1918.

[17] ——, "Zur Berechnung und Beurteilung des Schroteffektes (To calculate and assess the shot effect)," *Ann. der Phys.*, 68, 157, 1922.

[18] J. Johnson, "The Schottky Effect in Low Frequency Circuits," *Physical Review*, vol. 26, no. 1, pp. 71–85, 1925.

[19] W. Schottky, "Small-Shot Effect and Flicker Effect," *Physical Review*, vol. 28, no. 1, pp. 74–103, 1926.

[20] J. Johnson, "Thermal Agitation of Electricity in Conductors," *Nature*, vol. 119, no. 2984, pp. 50–51, 1927.

[21] J. B. Johnson, "Thermal Agitation of Electricity in Conductors," *Physical Review*, vol. 32, no. 1, pp. 97–109, 1928.

[22] H. Nyquist, "Thermal Agitation of Electric Charge in Conductors," *Physical Review*, vol. 32, no. 1, pp. 110–113, 1928.

[23] P. H. Handel, "Quantum approach to 1/f noise," *Physical Review A*, vol. 22, no. 2, p. 745, 1980.

[24] D. B. Leeson, "A simple model of feedback oscillator noise spectrum," *Proceedings of the IEEE*, vol. 54, no. 2, pp. 329–330, Feb 1966.

[25] R. S. Raven, "Requirements on master oscillators for coherent radar," *Proceedings of the IEEE*, vol. 54, no. 2, pp. 237–243, Feb 1966.

[26] S. J. Goldman, *Phase Noise Analysis in Radar Systems Using Personal Computers*. Wiley-Interscience, 1989.

[27] K. Siddiq, R. J. Watson, S. R. Pennock, P. Avery, R. Poulton, and B. Dakin-Norris, "Phase noise analysis in fmcw radar systems," in *Radar Conference (EuRAD), 2015 European*, Sept 2015, pp. 501–504.

[28] V. J. Arkesteijn, E. A. M. Klumperink, and B. Nauta, "Jitter requirements of the sampling clock in software radio receivers," *IEEE Transactions on Circuits and Systems II: Express Briefs*, vol. 53, no. 2, pp. 90–94, Feb 2006.

[29] B. Brannon, "Sampled systems and the effects of clock phase noise and jitter," *Analog Devices Appl. Note AN-756*.

[30] P. Smith, "Little known characteristics of phase noise," *Analog Devices Appl. Note AN-741*, Aug 2004.

[31] C. Azeredo-Leme, "Clock jitter effects on sampling: A tutorial," *IEEE Circuits and Systems Magazine*, vol. 11, no. 3, pp. 26–37, thirdquarter 2011.

[32] T. N. Guo, "Unique measurement and modeling of total phase noise in rf receiver," *IEEE Transactions on Circuits and Systems II: Express Briefs*, vol. 60, no. 5, pp. 262–266, May 2013.

[33] N. D. Dalt, M. Harteneck, C. Sandner, and A. Wiesbauer, "On the jitter requirements of the sampling clock for analog-to-digital converters," *IEEE Transactions on Circuits and Systems I: Fundamental Theory and Applications*, vol. 49, no. 9, pp. 1354–1360, Sep 2002.

[34] V. Manassewitsch, *Frequency Synthesizers: Theory and Design*. Wiley-Interscience, 2005.

[35] R. Undheim, "Design of a Linear FMCW Radar Synthesizer with Focus on Phase Noise," Master's thesis, Norwegian University of Science and Technology, 2012.

[36] U. L. Rohde, *Microwave and Wireless Synthesizers: Theory and Design*. Wiley-Interscience, 1997.

[37] B. Razavi, "Heterodyne phase locking: A technique for high-speed frequency division," *IEEE Journal of Solid-State Circuits*, vol. 42, no. 12, pp. 2887–2892, Dec 2007.

[38] F. M. Gardner, *Phaselock Techniques*. Wiley-Interscience, 2005.

[39] M. Pichler, A. Stelzer, P. Gulden, C. Seisenberger, and M. Vossiek, "Phase-Error Measurement and Compensation in PLL Frequency Synthesizers for FMCW Sensors - I: Context and Application," *IEEE Transactions on Circuits and Systems I: Regular Papers*, vol. 54, no. 5, pp. 1006–1017, May 2007.

[40] S. Scheiblhofer, M. Treml, S. Schuster, R. Feger, and A. Stelzer, "A versatile FMCW radar system simulator for millimeter-wave applications," in *2008 European Radar Conference*, Oct 2008, pp. 447–450.

[41] M. Ash and P. V. Brennan, "Transmitter noise considerations in super-nyquist fmcw radar design," *Electronics Letters*, vol. 51, no. 5, pp. 413–415, 2015.

[42] P. D. L. Beasley, "The Influence of Transmitter Phase Noise on FMCW Radar Performance," in *2006 European Radar Conference*, Sept 2006, pp. 331–334.

[43] A. G. Stove, "Linear FMCW radar techniques," *IEE Proceedings F - Radar and Signal Processing*, vol. 139, no. 5, pp. 343–350, Oct 1992.

[44] V. Kroupa, "Noise properties of pll systems," *IEEE Transactions on Communications*, vol. 30, no. 10, pp. 2244–2252, Oct 1982.

[45] Analog.com. ADISIMPLL software. [Online]. Available: https://form.analog.com/Form_Pages/RFComms/ADISimPll.aspx

[46] K. Siddiq, M. K. Hobden, S. R. Pennock, and R. J. Watson, "Phase noise in FMCW radar systems," *IEEE Transactions on Aerospace & Electronic Systems*, (Accepted subject to review) 2017.

[47] A. Demir, A. Mehrotra, and J. Roychowdhury, "Phase noise in oscillators: a unifying theory and numerical methods for characterization," *IEEE Transactions on Circuits and Systems I: Fundamental Theory and Applications*, vol. 47, no. 5, pp. 655–674, May 2000.

[48] A. Hajimiri and T. H. Lee, "A general theory of phase noise in electrical oscillators," *IEEE Journal of Solid-State Circuits*, vol. 33, no. 2, pp. 179–194, Feb 1998.

[49] E. Baghdady, J., B. Nelin, and R. Lincoln, "Short-Term Frequency Stability: Characterization, Theory, and Measurement," *Proceedings of the IEEE*, 1965.

[50] W. C. Lindsey and C. M. Chie, "Frequency Multiplication Effects on Oscillator Instability," *IEEE Transactions on Instrumentation and Measurement*, vol. IM-27, no. 1, 1978.

[51] F. L. Walls and A. DeMarchi, "RF Spectrum of a Signal after Frequency Multiplication: Measurement and Comparison with a Simple Calculation," *IEEE Transactions on Instrumentation and Measurement*, 1975.

[52] X. Zhang, B. J. Rizzi, and J. Kramer, "A new measurement approach for phase noise at close-in offset frequencies of free-running oscillators," *IEEE Transactions on Microwave Theory and Techniques*, vol. 44, no. 12, pp. 2711–2717, Dec 1996.

[53] D. Halford, "Infrared-Microwave Frequency Synthesis Design: Some Relevant Conceptual Noise Aspects," *Proc. Frequency Standard and Metrology Seminar*, Sep 1971.

[54] A. Chorti and M. Brookes, "Resolving near-carrier spectral infinities due to 1/f phase noise in oscillators," in *2007 IEEE International Conference on Acoustics, Speech and Signal Processing - ICASSP '07*, vol. 3, April 2007, pp. III–1005–III–1008.

[55] R. D. Weglein, "The Coherence of a Radar Master Oscillator," *40th Annual Frequency Control Symposium*, pp. 379–384, 1986.

[56] A. Aubry, A. D. Maio, V. Carotenuto, and A. Farina, "Radar Phase Noise Modeling and Effects-Part I: MTI Filters," *IEEE Transactions on Aerospace and Electronic Systems*, vol. 52, no. 2, pp. 698–711, April 2016.

[57] A. Aubry, V. Carotenuto, A. D. Maio, and A. Farina, "Radar Phase Noise Modeling and Effects-Part II: Pulse Doppler Processors and Sidelobe Blankers," *IEEE Transactions on Aerospace and Electronic Systems*, vol. 52, no. 2, pp. 712–725, April 2016.

[58] S. H. Talisa, K. W. O'Haver, T. M. Comberiate, M. D. Sharp, and O. F. Somerlock, "Benefits of Digital Phased Array Radars," *Proceedings of the IEEE*, vol. 104, no. 3, pp. 530–543, March 2016.

[59] W. Q. Wang, "GPS-Based Time Phase Synchronization Processing for Distributed SAR," *IEEE Transactions on Aerospace and Electronic Systems*, vol. 45, no. 3, pp. 1040–1051, July 2009.

[60] G. Liao and H. Li, "Estimation Method for InSAR Interferometric Phase Based on Generalized Correlation Steering Vector," *IEEE Transactions on Aerospace and Electronic Systems*, vol. 46, no. 3, pp. 1389–1403, July 2010.

[61] M. Brooker and M. Inggs, "Efficient Generation of f^{α} Noise Sequences for Pulsed Radar Simulation," *IEEE Transactions on Aerospace and Electronic Systems*, vol. 46, no. 2, pp. 737–744, April 2010.

[62] T. h. Chen, "FM/AM Noise Test Set for a Pulsed Doppler Radar," *IEEE Transactions on Aerospace and Electronic Systems*, vol. AES-19, no. 6, pp. 788–794, Nov 1983.

[63] M. Dudek, I. Nasr, D. Kissinger, R. Weigel, and G. Fischer, "The impact of phase noise parameters on target signal detection in FMCW-radar system simulations for automotive applications," in *Proceedings of 2011 IEEE CIE International Conference on Radar*, vol. 1, Oct 2011, pp. 494–497.

[64] C. Baktir, E. Sobaci, and A. Dnmez, "A guide to reduce the phase noise effect in FMCW Radars," in *2012 IEEE Radar Conference*, May 2012, pp. 0236–0239.

[65] E. Schlecht and I. Mehdi, "Effects of local oscillator phase noise on submillimeter-wave spectrometer performance," in *2014 39th International Conference on Infrared, Millimeter, and Terahertz waves (IRMMW-THz)*, Sept 2014, pp. 1–2.

[66] E. Bava, A. D. Marchi, and A. Godone, "Spectral analysis of synthesized signals in the mm wavelength region," *IEEE Transactions on Instrumentation and Measurement*, vol. 26, no. 2, pp. 128–132, June 1977.

[67] W. C. Lindsey and C. M. Chie, "Theory of oscillator instability based upon structure functions," *Proceedings of the IEEE*, vol. 64, no. 12, pp. 1652–1666, Dec 1976.

[68] M. J. O'Mahony and I. D. Henning, "Semiconductor laser linewidth broadening due to 1/f carrier noise," *Electronics Letters*, vol. 19, no. 23, pp. 1000–1001, November 1983.

[69] L. B. Mercer, "1/f frequency noise effects on self-heterodyne linewidth measurements," *Journal of Lightwave Technology*, vol. 9, no. 4, pp. 485–493, Apr 1991.

[70] B. Joss, L. G. Bernier, and F. Gardiol, "RF Spectrum of the Oscillator Signal Under Non-Stationary Phase Instabilities," in *40th Annual Symposium on Frequency Control. 1986*, May 1986, pp. 300–305.

[71] K. Kikuchi and T. Okoshi, "Dependence of semiconductor laser linewidth on measurement time: evidence of predominance of 1/f noise," *Electronics Letters*, vol. 21, no. 22, pp. 1011–1012, October 1985.

[72] M. Pichler, A. Stelzer, P. Gulden, C. Seisenberger, and M. Vossiek, "Phase-Error Measurement and Compensation in PLL Frequency Synthesizers for FMCW Sensors - II: Theory," *IEEE Transactions on Circuits and Systems I: Regular Papers*, vol. 54, no. 6, pp. 1224–1235, June 2007.

[73] C. Wagner, R. Feger, A. Haderer, A. Fischer, A. Stelzer, and H. Jager, "A 77-GHz FMCW radar using a digital phase-locked synthesizer," in *2008 IEEE MTT-S International Microwave Symposium Digest*, June 2008, pp. 351–354.

[74] F. Herzel, A. Ergintav, and Y. Sun, "Phase Noise Modeling for Integrated PLLs in FMCW Radar," *IEEE Transactions on Circuits and Systems II: Express Briefs*, vol. 60, no. 3, pp. 137–141, March 2013.

[75] C. Wagner, A. Stelzer, and H. Jager, "Estimation of FMCW radar system performance using measurement data of a 77-GHz transmitter," in *2006 Asia-Pacific Microwave Conference*, Dec 2006, pp. 1701–1704.

[76] R. A. Habel, M. Pelletier, F. Chenier, M. Lecours, and G. Y. Delisle, "Design of a high resolution millimeter wave FM-CW radar," in *Proceedings of Canadian Conference on Electrical and Computer Engineering*, Sep 1993, pp. 51–54 vol.1.

[77] M. Vossiek, P. Heide, M. Nalezinski, and V. Magori, "Novel FMCW radar system concept with adaptive compensation of phase errors," in *1996 26th European Microwave Conference*, vol. 1, Sept 1996, pp. 135–139.

[78] A. Frischen, J. Hasch, and C. Waldschmidt, "FMCW ramp non-linearity effects and measurement technique for cooperative radar," in *2015 European Radar Conference (EuRAD)*, Sept 2015, pp. 509–512.

[79] J. B. Hagen, *Radio-Frequency Electronics: Circuits and Applications*. Cambridge University Press, 2009.

[80] L. Richter, H. Mandelberg, M. Kruger, and P. McGrath, "Linewidth determination from self-heterodyne measurements with subcoherence delay times," *IEEE Journal of Quantum Electronics*, vol. 22, no. 11, pp. 2070–2074, Nov 1986.

[81] M. K. Hobden, "77GHz FMCW Radar Head Design Study: A Survey of Monostatic and Bistatic Architectures," *E2V Technologies Tech. Report 2006/007*, Jan 2006.

[82] K. Siddiq, R. J. Watson, S. R. Pennock, P. Avery, R. Poulton, and S. Martins, "Analysis of sampling clock phase noise in homodyne FMCW radar systems," in *2016 IEEE Radar Conference (RadarConf)*, May 2016.

[83] M. Shinagawa, Y. Akazawa, and T. Wakimoto, "Jitter analysis of high speed sampling systems," in *VLSI Circuits, 1989. Digest of Technical Papers., 1989 Symposium on*, May 1989, pp. 95–96.

[84] K. Siddiq, M. K. Hobden, R. J. Watson, S. R. Pennock, and S. Martins, "On phase measurement in FMCW radar systems," in *Sensor Signal Processing for Defence (SSPD)*, Submitted 2017.

[85] D. G. Tucker, "The synchrodyne and coherent detectors," *Wireless Engineer*, July 1952.

[86] S. Haykin, *Communication systems*, 4th ed. John Wiley & Sons, 2001.

[87] M. Kronauge and H. Rohling, "New chirp sequence radar waveform," *Aerospace and Electronic Systems, IEEE Transactions on*, vol. 50, no. 4, pp. 2870–2877, October 2014.

[88] M. A. Richards, *Fundamentals of radar signal processing*. McGraw-Hill, 2005.

[89] K. Siddiq, R. J. Watson, S. R. Pennock, and S. Martins, "A generalised Brownian motion model of RF spectral dispersion due to phase noise," in *Radar Conference (EuRAD), 2017 European*, (Accepted) 2017.

[90] G. V. Klimovitch, "Near Carrier Oscillator Spectrum due to Flicker and White Noise," *IEEE International Symposium on Circuits and Systems*, 2000.

[91] A. Chorti and M. Brookes, "A Spectral Model for RF Oscillators With Power-Law Phase Noise," *IEEE Transactions on Circuits and Systems–I: Regular Papers*, vol. 53, no. 9, 2006.

[92] N. Nossenson and B. Z. Bobrovsky, "Analysis of direct spectrum measurement of a sinusoidal signal impaired by either fractional gaussian phase noise or fractional brownian phase motion," *IEEE Transactions on Ultrasonics, Ferroelectrics, and Frequency Control*, vol. 56, no. 11, pp. 2351–2362, November 2009.

[93] V. V. Uchaikin, *Fractional Derivatives for Physicists and Engineers: Volume I Background and Theory.* Springer, 2013.

[94] B. B. Mandelbrot and J. W. V. Ness, "Fractional brownian motions, fractional noises and applications," *SIAM Review*, vol. 10, no. 4, pp. 422–437, 1968.

[95] S. Nadarajah, "A generalized normal distribution," *Journal of Applied Statistics*, vol. 32, no. 7, pp. 685–694, 2005.

[96] J. A. Barnes, "Noise and Time and Frequency - A Potpourri," *42nd Annual Frequency Control Symp.*, 1988.

[97] J. S. Cohen, F. Wittgrefe, M. D. Hoogerland, and J. P. Woerdman, "Optical spectra of a semiconductor laser with incoherent optical feedback," *IEEE Journal of Quantum Electronics*, vol. 26, no. 6, pp. 982–990, Jun 1990.

[98] B. Daino, P. Spano, M. Tamburrini, and S. Piazzolla, "Phase noise and spectral line shape in semiconductor lasers," *IEEE Journal of Quantum Electronics*, vol. 19, no. 3, pp. 266–270, Mar 1983.

[99] P. Spano, S. Piazzolla, and M. Tamburrini, "Phase noise in semiconductor lasers: A theoretical approach," *IEEE Journal of Quantum Electronics*, vol. 19, no. 7, pp. 1195–1199, Jul 1983.

[100] K. Siddiq, M. K. Hobden, S. R. Pennock, and R. J. Watson, "The linewidth of oscillators with power-law phase noise," *IEEE Transactions on Circuits and Systems II: Express Briefs*, (Submitted) 2017.

[101] P. R. Shepherd, N. Faulkner, E. Vilar, and P. Bradsell, "Relation between power spectrum and phase spectrum of oscillators," *Electronics Letters*, vol. 18, no. 14, pp. 614–615, July 1982.

[102] G. V. Klimovitch, "a Nonlinear Theory of Near Carrier Phase Noise in Free Running Oscillators," *Third IEEE International Caracas Conference on Devices, Circuits and Systems*, 2000.

[103] W. R. Attkinson, L. Fey, and J. Newman, "Spectrum analysis of extremely low frequency variations of quartz oscillators," *Proceedings of the IEEE*, vol. 51, no. 2, pp. 379–379, Feb 1963.

[104] X. Chen, "Ultra-Narrow Laser Linewidth Measurement," Ph.D. dissertation, Virginia Polytechnic Institute and State University, 2006.

[105] T. Okoshi, K. Kikuchi, and A. Nakayama, "Novel method for high resolution measurement of laser output spectrum," *Electronics Letters*, vol. 16, no. 16, pp. 630–631, July 1980.

[106] F. C. Ndi, J. Toulouse, R. K. Pattnaik, C. McIntosh, and A. Yeniay, "Influence of dispersion properties of the delay line in self heterodyne linewidth measurements," in *Optical Fiber Communication Conference and Exhibit, 2001. OFC 2001*, vol. 3, March 2001, pp. WDD25–WDD25.

[107] D. W. Allan, "Statistics of Atomic Frequency Standards," *Proc IEEE*, vol. 54, no. 2, pp. 221–230, 1966.

[108] A. Demir, "Phase noise in oscillators: DAEs and colored noise sources," in *Computer-Aided Design, 1998. ICCAD 98. Digest of Technical Papers. 1998 IEEE/ACM International Conference on*, Nov 1998, pp. 170–177.

[109] F. Herzel, "An analytical model for the power spectral density of a voltage-controlled oscillator and its analogy to the laser linewidth theory," *IEEE Transactions on Circuits and Systems I: Fundamental Theory and Applications*, vol. 45, no. 9, pp. 904–908, 1998.

[110] J. H. Midgley, "Comments on "Optical spectra of a semiconductor laser with incoherent optical feedback"," *IEEE Journal of Quantum Electronics*, vol. 30, no. 8, pp. 1964–1965, Aug 1994.

[111] N. Blachman and G. McAlpine, "The Spectrum of a High-Index FM Waveform: Woodward's Theorem Revisited," *IEEE Transactions on Communication Technology*, vol. 17, no. 2, pp. 201–208, April 1969.

[112] A. Mecozzi, S. Piazzolla, A. Sapia, and P. Spano, "Non-gaussian statistics of frequency fluctuations in line-narrowed semiconductor lasers," *IEEE Journal of Quantum Electronics*, vol. 24, no. 10, pp. 1985–1988, Oct 1988.

[113] M. K. Hobden, "The Behaviour of the Self Excited Oscillator," *Horological Science Newsletter*, no. 2012-3, pp. 17–22, July 2012.

[114] H. Tong, *Non-Linear Time Series: A Dynamical System Approach (Oxford Statistical Science Series, 6)*. Oxford University Press (UK), 1993.

[115] A. Papoulis and S. U. Pillai, *Probability, Random Variables and Stochastic Processes*. McGraw-Hill Europe, 2002.

[116] J. A. Barnes, A. R. Chi, L. S. Cutler, D. J. Healey, D. B. Leeson, T. E. McGunigal, J. A. Mullen, W. L. Smith, R. L. Sydnor, R. F. C. Vessot, and G. M. R. Winkler, "Characterization of frequency stability," *IEEE Transactions on Instrumentation and Measurement*, vol. IM-20, no. 2, pp. 105–120, May 1971.

[117] F. Vernotte, E. Lantz, J. Groslambert, and J. J. Gagnepain, "A new multivariance method for the oscillator noise analysis," in *Frequency Control Symposium, 1992. 46th., Proceedings of the 1992 IEEE*, May 1992, pp. 284–289.

[118] ——, "Oscillator noise analysis: multivariance measurement," *IEEE Transactions on Instrumentation and Measurement*, vol. 42, no. 2, pp. 342–350, Apr 1993.

[119] J. E. Deeter and P. E. Boynton, "Techniques for the estimation of red power spectra. I - Context and methodology," *Astrophysics Journal*, vol. 261, pp. 337–350, Oct. 1982.

[120] J. E. Deeter, "Techniques for the estimation of red power spectra. II Evaluation of alternative methods," *Astrophysics Journal*, vol. 281, pp. 482–491, Jun. 1984.

[121] U. Rohde, et. al., "Searching for low phase-noise synthesizers," in *Microwaves & RF*, Nov January 2014.

[122] J. Everard and K. Ng, "Ultra-low phase noise crystal oscillators," in *2007 IEEE International Frequency Control Symposium Joint with the 21st European Frequency and Time Forum*, May 2007, pp. 1246–1250.

[123] J. Everard, "Low phase noise oscillators: Theory and application," in *2009 IEEE International Frequency Control Symposium Joint with the 22nd European Frequency and Time forum*, April 2009, pp. 338–343.

[124] A. A. Abidi and R. G. Meyer, "Noise in relaxation oscillators," *IEEE Journal of Solid-State Circuits*, vol. 18, no. 6, pp. 794–802, Dec 1983.

[125] D. Murphy, J. J. Rael, and A. A. Abidi, "Phase noise in lc oscillators: A phasor-based analysis of a general result and of loaded q," *IEEE Transactions on Circuits and Systems I: Regular Papers*, vol. 57, no. 6, pp. 1187–1203, June 2010.

[126] C. Henry, "Theory of the linewidth of semiconductor lasers," *IEEE Journal of Quantum Electronics*, vol. 18, no. 2, pp. 259–264, Feb 1982.

[127] F. N. Hooge, "1/f noise sources," *IEEE Transactions on Electron Devices*, vol. 41, no. 11, pp. 1926–1935, Nov 1994.

[128] A. N. Morabito, "Estimation and Mitigation of Phase Noise in a Coherent Distributed Passive Radar System," Ph.D. dissertation, University of Washington, 2008.

[129] A. N. Morabito, J. D. Sahr, Z. M. P. Berkowitz, and L. E. Vertatschitsch, "Phase noise analysis in distributed coherent noise radar systems," in *2008 International Radar Symposium*, May 2008, pp. 1–4.

[130] P. Maffezzoni, "Frequency-shift induced by colored noise in nonlinear oscillators," *IEEE Transactions on Circuits and Systems II: Express Briefs*, vol. 54, no. 10, pp. 887–891, Oct 2007.

[131] P. Maffezzoni and D. D'Amore, "Analysis of phase diffusion process in oscillators due to white and colored-noise sources," *IEEE Transactions on Computer-Aided Design of Integrated Circuits and Systems*, vol. 30, no. 10, pp. 1574–1578, Oct 2011.

[132] B. B. Mandelbrot, *Multifractals and 1/f noise: Wild self-affinity in physics.* New York: Springer, 1998.

[133] ——, *The Fractal Geometry of Nature*. W. H. Freeman and Co., 1983.

[134] M. A. Montemurro, "Beyond the Zipf-Mandelbrot Law in Quantitative Linguistics," in *Physica A: Statistical Mechanics and its Applications*, 2001, pp. 567–578.

[135] S. Peleg and B. Friedlander, "The discrete polynomial-phase transform," *IEEE Transactions on Signal Processing*, vol. 43, no. 8, pp. 1901–1914, Aug 1995.

[136] A. Wojtkiewicz et al., "A novel approach to signal processing in fmcw radar," in *Intl. Conf. Microwaves, Radar & Wireless Communications, MKON-2000, Wroclaw, Poland*, June 2000.

[137] G. Bonmassar and E. L. Schwartz, "Space-variant fourier analysis: the exponential chirp transform," *IEEE Transactions on Pattern Analysis and Machine Intelligence*, vol. 19, no. 10, pp. 1080–1089, Oct 1997.

[138] P. Samczyski, "Extended generalized chirp transform for signal parameter estimation in bistatic passive pulse radars," in *2013 14th International Radar Symposium (IRS)*, vol. 1, June 2013, pp. 155–160.

[139] B. Boashash, "Estimating and interpreting the instantaneous frequency of a signal. II. Algorithms and applications," *Proceedings of the IEEE*, vol. 80, no. 4, pp. 540–568, Apr 1992.

VITA

Mr Kashif Siddiq obtained his Bachelors and Masters in Electrical Engineering from the National University of Sciences & Technology (NUST) in 2004 and 2007 respectively. He worked at the Microwave Engineering Research Labs at the College of E&ME, NUST, from 2004 to 2007. In 2007 he joined the National University of Computer & Emerging Sciences as a Lecturer and was promoted to Assistant Professor of Electrical Engineering a year later, a post he held until 2012. In 2013 he joined Navtech Radar Ltd., UK, as a Radar Engineer. Between 2014 and 2016 Mr Siddiq worked as a KTP Associate with the University of Bath and Navtech Radar Ltd. Since 2016, he has been working as a Senior Radar Engineer with Navtech Radar Ltd.

Mr Siddiq registered with the UK Engineering Council as a Chartered Engineer in 2016. In 2015 Mr Siddiq, along with the team members at Navtech, jointly won the Design Team of the Year award at the British Engineering Excellence Awards. Also in 2015 he was nominated by Innovate UK for the Business Leader of the Future award. On the academic front, Mr Siddiq stood first in his Masters by scoring a CGPA of 4.0/4.0. He won a gold medal for the best undergraduate final year project in 2004. He also won a gold medal and was placed on the roll-of-honour for standing first in high school.